

EVALUATION OF COMPRESSED SENSING IN SYSTEMS

UWB WITH NBI

BY
SALEH AHMED ALAWSH

A Thesis Presented to the
DEANSHIP OF GRADUATE STUDIES

KING FAHD UNIVERSITY OF PETROLEUM & MINERALS

DHAHRAN, SAUDI ARABIA

In Partial Fulfillment of the
Requirements for the Degree of

MASTER OF SCIENCE

In

TELECOMMUNICATION ENGINEERING

April 2013

KING FAHD UNIVERSITY OF PETROLEUM & MINERALS

DHAHRAN, SAUDI ARABIA

DEANSHIP OF GRADUATE STUDIES

This thesis, written by **SALEH AHMED ALAWSH** under the direction of his thesis advisor and approved by his thesis committee, has been presented and accepted by the Dean of Graduate Studies, in partial fulfillment of the requirements for the degree of **MASTER OF SCIENCE IN TELECOMMUNICATION ENGINEERING**.



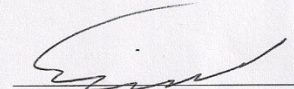
Dr. Ali Al-Shaikhi
Department Chairman



Dr. Ali H. Muqaibel
(Advisor)



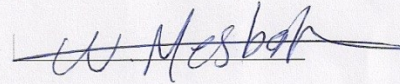
Dr. Salam A. Zummo
Dean of Graduate Studies



Dr. Samir Al-Ghadhban
(Member)

24/4/13

Date



Dr. Wessam Mesbah
(Member)

© SALEH AHMED ALAWSH

2013

III

Dedication

Dedicated to

My

Parents

Brothers

Sisters

Wife and Children {Salem & Haneen}

ACKNOWLEDGMENTS

First and foremost thanks to Allah for giving me strength, patience and ability to accomplish this research.

My deep acknowledgement for my parents who spent their time prays and asks Allah to help me during my study.

I would like to express my thankful for my advisor Dr. Ali Hussein Muqaibel for his guidance and support in my thesis. I appreciate his incredible patience, his continued guidance, and encouragement all through my graduate studies. During my research with Dr. Ali Muqaibel, I've increased my knowledge in the area of interest. Actually no words can express my appreciation for my advisor.

I would like to give special acknowledgment to the King Fahd University of Petroleum & Minerals, Hadhramout University for Science & Technology and Hadhramout Establishment for Human Development for supporting my study.

I would like to acknowledge the Deanship of Scientific Research (DSR) at King Fahd University of Petroleum & Minerals (KFUPM) for funding and supporting this work through project No. SB121014.

I would like to extend my appreciation to my committee members Dr. Samir Al-Ghadhban and Dr. Wessam Mesbah for their suggestions and valuable comments.

Special thanks to my brothers, sisters, wife and children for being there whenever I needed them. I would like to acknowledge all my friend especially at KFUPM campus who share with me my happiness and life out of my country.

No words could satisfy my thanks for Engineer Abdullah Ahmed Bugshan for his continuous encouragement and support. During my study, I always find him wherever needed. He used to give us much of his valuable time to set and solve problems.

Saleh Ahmed Yaslam Alawsh

Table of Contents

ACKNOWLEDGMENTS	V
LIST OF TABLES	XI
LIST OF FIGURES	XII
ABSTRACT.....	XIV
ملخص الرسالة.....	XVII
CHAPTER 1 INTRODUCTION AND MOTIVATION	1
1.1 Introduction	1
1.2 Organization of the Thesis	2
1.3 Thesis Contribution	3
1.4 Technical Background.....	5
1.4.1 Ultra Wideband Signals.....	5
1.4.2 Narrowband Interference Signals	9
1.4.3 Compressive Sensing.....	10
1.5 Literature Review	10

1.5.1 Narrowband Interference Mitigation in UWB Systems	11
1.5.2 Compressed Sensing Based UWB Systems	16
1.5.3 Compressed Sensing Based UWB Systems with Narrowband Interference Mitigation	18
CHAPTER 2 UWB-CS SYSTEM MODEL AND NBI.....	21
2.1 Introduction	21
2.2 UWB Channel Model.....	22
2.3 Matching Pursuit	24
2.4 Narrowband Interference Modeling	27
2.4.1 Unlicensed Narrowband Interference.....	27
2.4.2 Licensed Narrowband Interference	29
2.5 Summary and Concluding Remarks.....	31
CHAPTER 3 MITIGATION OF NARROWBAND INTERFERENCE IN SYSTEMS WITH CHANNEL TRAINING	33
3.1 Introduction	33
3.2 UWB Transmitter Configuration	35

3.3 Interference Configuration	38
3.4 Receiver Configuration	39
3.4.1 Compressive Measurements	41
3.4.2 Data Detection	44
3.5 Simulation and Results	47
3.6 Chapter Summary	63
CHAPTER 4 MITIGATION OF NARROWBAND INTERFERENCE IN BLIND SYSTEMS.....	65
4.1 Introduction	65
4.2 UWB Transmitter Configuration	66
4.3 Interference Configuration	70
4.4 UWB Receiver Configuration	70
4.4.1 Analog Front-End	72
4.4.2 DSP Back-End	76
4.5 Simulation and Results	84
4.6 Chapter Summary	97

CHAPTER 5 CONCLUSION AND FUTURE WORK.....	100
5.1 Summary of Conclusions	100
5.2 Future Work	103
APPENDIX.....	105
REFERENCES.....	114
VITAE.....	120

LIST OF TABLES

Table 1-1 Emission limits for indoor and outdoor systems in EIRP [Nik09].....	7
Table 2-1 IEEE802.1.4a channel model classification	23
Table 2-2 Comparison between different NB services	31
Table I-1 Abbreviations	105
Table I-2 List of Variables	108

LIST OF FIGURES

Figure 1-1 The main topics of the research	5
Figure 1-2 FCC spectral mask for UWB indoor communication systems	6
Figure 1-3 Time and frequency domains for the Gaussian, first, and second derivative Gaussian pulses	8
Figure 1-4 FCC spectral mask for UWB indoor communication systems with narrowband systems	9
Figure 1-5 Autocorrelation receiver (AcR).....	12
Figure 1-6 System architecture of CS based-UWB system [Zha09]	17
Figure 2-1 Block diagram of the proposed system model	22
Figure 2-2 The impulse response and the power delay profile of CM1	24
Figure 2-3 Matching Pursuit for signal structure estimation	26
Figure 3-1 Block diagram for the I-UWB system	36
Figure 3-2 Implemented I-UWB signaling scheme	37
Figure 3-3 I-UWB receiver with GLRT detector	40
Figure 3-4 Distribution of pulses transmitted over time – Frames and chips are synchronized for all users	47
Figure 3-5 Flowchart for the main steps of the UWB system with training.....	50
Figure 3-6 The BER as a function of $Np1$ and $Np2$	52
Figure 3-7 The BER as a function of $Np1$ and $Np3$	53
Figure 3-8 The BER as a function of $Np2$ and $Np3$	55
Figure 3-9 BER with different frame number.....	56
Figure 3-10 The BER as a function of the interference threshold	57
Figure 3-11 System performance for different NBI	58

Figure 3-12 The performance for licensed NBIs	60
Figure 3-13 System performance when 0, 2, 3, 5, 10, 15, 20 and 25 users are active.....	61
Figure 3-14 Throughput of DS-TH coding for different number of interfering users.....	62
Figure 4-1 Signal paths taken by the UWB-IR and the NBI signals	67
Figure 4-2 Hanning window in time and frequency domain	68
Figure 4-3 Hanning modulated pulse and its power spectrum	69
Figure 4-4 Frame format for the bursty data transmission	70
Figure 4-5 Correlator receiver with digital notch filter	72
Figure 4-6 Time and frequency domain representations of the BPF	73
Figure 4-7 Frequency domain for different test functions selected randomly	75
Figure 4-8 The location of the k^{th} nonzero samples	81
Figure 4-9 Flow chart for the main steps of the blind system	85
Figure 4-10 Performance of a partial band interferer for different burst size.....	87
Figure 4-11 Performance for different UWB modulated pulses jammed by a partial band interferer.....	89
Figure 4-12 Performance of a partial band interferer with different bandwidth.....	90
Figure 4-13 Performance of 2 partial bands interferer with different bandwidth.....	91
Figure 4-14 BER Performance as a function of the NBI's bandwidth.....	92
Figure 4-15 BER performance in the presence of licensed NBIs.....	94
Figure 4-16 BER performance when changing the bandwidth of the UWB modulated pulse	96
Figure 4-17 BER performance for one partial band interferer with different baud rate...	97

ABSTRACT

Full Name : Saleh Ahmed Alawsh

Thesis Title : EVALUATION OF COMPRESSED SENSING IN UWB SYSTEMS
WITH NBI

Major Field : Telecommunication Engineering

Date of Degree : April 2013

Ultra-wideband (UWB) radios are expected to be the next generation of transmission system that can support high data rate and power-constrained applications such as wireless sensor and body area networks. Because of their large bandwidth, two problems arise, namely the high speed analog-to-digital-conversion (ADC) required at the receiver side and the coexistence with other narrowband systems that share the same part of the spectrum. The two problems can be reduced using compressive sensing (CS). Narrowband interference (NBI) sources can be licensed or unlicensed signals with different center frequencies and different bandwidths. In this thesis, both trained and blind systems have been examined in mitigating the effect of the NBI in UWB system using CS as well as reduce the speeds of the ADC.

In trained systems, three training pilot groups are required. The system is first trained to estimate the NBI with no UWB transmission, then the UWB signal space is estimated and finally the channel impulse response is extracted. This research optimizes UWB systems with CS to mitigate the effect of NBI through efficient assignments of pilot symbols among the required training. Extensive simulation is conducted to investigate the

optimum distribution of the pilot symbols that enhances the system's bit-error-rate (BER) performance. Based on this investigation, a better understanding of the effect of the NBI's characteristics on UWB systems with CS is drawn. Furthermore, the impact of the number and the type of the NBI sources is also evaluated. The impact of multiple users on the system behavior is considered. It is shown that the number of pilot symbols in the third group is directly proportional to the performance; hence once the minimum number of pilot symbols for first two groups is met, the extra symbols should be assigned to get information about the channel.

In blind UWB systems, we investigate the problem in bursty application such as wireless sensor network. The receiver does a joint decoding of the time of arrival and the data bits using quadratic programming (QP). A correlator receiver combined with digital notch filter is applied. The basis functions in the correlators are designed to be highly frequency selective through windowing technique. Hence only few measurements are corrupted by the interferer. In this part, we study the performance of different licensed and unlicensed NBIs and we extend the mitigation technique to suppress the effect of multiple NBIs. The work discusses the system behavior under different NBI's and UWB signal bandwidths. Furthermore, the thesis evaluates the effect of the burst size, the type of the modulated window and the baud rate on the performance. For a partial band jammer, slight enhancement is achieved when doubling the bandwidth. In the dual-band jammer case, the enhancement due to the mitigation against the jammers is evident. For the considered scenarios, we demonstrate that the BER is a strong function of the NBI's bandwidth while it is a weak function of the pulse shape. As the UWB signal's bandwidth increases, the

number of the notched measurements lessens and we preserve the important information about the transmitted pulse.

ملخص الرسالة

الاسم الكامل: صالح أحمد العوش

عنوان الرسالة: تقييم لتقنية الاستشعار عن الضغط على الأنظمة فائقة عرض النطاق مع نظام التداخل الضيق

التخصص: هندسة الاتصالات

تاريخ الدرجة العلمية: ابريل ٢٠١٣

ينظر إلى أنظمة الاتصالات اللاسلكية فائقة عرض النطاق (UWB) لتكون الجيل المستقبلي لنظام نقل البيانات، حيث أنها تتميز بقدرتها على إرسال البيانات لا سلكيا بسرعة هائلة. وتطبيقاتها تتمثل في أجهزة الاستشعار اللاسلكية وشبكات الاتصالات المتعددة. بسبب كبر النطاق الترددي، تظهر هناك مشكلتان وهما: محول الاشارات التناظريه الى الاشارات الرقمية (ADC) ذو السرعة العاليه والمطلوب في جهة المستقبل و تواجد اشارات الفائقة عرض النطاق مع الأنظمة الضيقة الأخرى التي تعمل وتتشرك بنفس المجال الترددي. كلا المشكلتان نستطيع ان نقل تأثيرهما باستخدام تقنية الاستشعار عن الضغط (CS). مصادر التداخل الضيقة ممكن ان تكون اما مرخصه (ذات تردد ثابت) او غير مرخصه (باي تردد) بمركز ترددي مختلف ونطاق ترددي ايضا مختلف. في هذه الأطروحه، تم فحص طريقتين في الانظمه المدربه والانظمه العمياء (غير مدربه) لتخفيف التداخل المسبب من النظام ذو النطاق الترددي الضيق على النظام الفائق العرض الترددي باستخدام تطبيق استشعار الضغط وايضاً لتخفيض سرعة محول الاشارات (ADC).

في الانظمه المدربه، نحتاج لثلاث مجموعات تجريبية لتدريب النظام. بداية يقوم النظام فائق العرض بالتدريب لتخمين مصدر التداخل الضيق بدون ان يقوم بارسال اي معلومات، ثم يتم تخمين فضاء اشارة النطاق الفائق العرض، وفي النهاية يتم استخلاص معلومات عن قناة الاتصال. هذا البحث يقوم بتحسين اداء النظام الفائق العرض بخوارزميات تكنولوجيا استشعار الضغط بحيث نحد ونخفف من تأثير التداخل الناشئ عن النظام ذو النطاق الضيق. وتشمل عملية التحسين توزيع فعال للرموز على مجموعات الرموز المستخدمه للتدريب للحصول على افضل اداء. بداية سوف نقوم بمحاكاة النظام لمدته طويله من اجل معرفة افضل توزيع لمجموعات الرموز المستخدمه لتحسين أداء النظام بناء على دراسة معدل نسبة الخطأ (BER) بناء على هذا التحقيق، سيتم رسم فهم افضل عن تأثير خواص مصدر التداخل على النظام الفائق العرض بتكنولوجيا استشعار الضغط. وعلاوة على ذلك، سيتم ايضا تقييم أثر عدد ونوع مصادر التداخل ذات النطاق الضيق الممكن تواجدها. سنحاول ايضا دراسة اداء النظام في حالة تواجد مجموعه من المستخدمين للنطاق فائق العرض. يظهر البحث ان عدد الرموز المستخدمه في المجموعه الثالثه يتناسب طرديا مع أداء النظام، لذلك عند الحصول على العدد الكافي من الرموز في المجموعتين الاولى والثانيه فان الرموز الاخرى الاضافيه يجب تخصيصها لاستخلاص معلومات اكثر عن قناة الاتصال.

في الأنظمة العمياء (غير المدربة) تم بحث المشكله في التطبيقات التي ترسل بياناتها بشكل متقطع كشبكات الاستشعار اللاسلكية. المستقبل في هذه الأنظمة يقوم بفك التضمين اولا يخمن وقت وصول المعلومات المتقطعة ثم يقوم بتقدير البيانات المرسله باستخدام برمجة الدرجة الثانية (QP). في هذه الأنظمة يتم استخدام مستقبل ذو اشارات معينه مع مرشح الشق (notch) الرقمي. هذه الاشارات المستخدمه يتم تصميمها بحيث تكون ذات انحدار عالي في المجال الترددي من خلال ضربها بنافذه معينه. تصميم الاشارات بهذا الشكل يضمن لنا ان مصدر التداخل سوف يتألف عدد قليل من القياسات فقط. في هذا الجزء, سندرس أداء النظام الفائق العرض تحت تأثير مصادر تداخل مختلفه سواءً كانت مرخصه او غير مرخصه, كذلك سنقوم بتطوير ومد تقنية تخفيف التداخل لتكون قادره على الحد من تأثير مصدري تداخل في آن واحد. هذا العمل, يناقش سلوك النظام الفائق العرض تحت تأثير مصادر تداخل ضيقه ذات مدى ترددي مختلف. كذلك كيفية تأثر النظام عندما نقول باستخدام مجال ترددي مختلف لارسال البيانات الفائقة العرض. علاوة على ذلك, الأطروحه تقيم تأثير عوامل أخرى على أداء النظام مثل حجم البيانات المتقطعه، وشكل النبضه المستخدمه و معدل ارسال الرموز. في حالة وجود مصدر تداخل واحد, بناءً على النتائج فقد تحصلنا على تحسن بسيط باستخدام عند إلغاء تأثير مصدر التداخل مقارنةً مع اهماله. بينما عند وجود مصدري تداخل فان الفرق كبير وواضح. النتائج للسيمايوهات التي بحثها تبين ان معدل نسبة الخطأ (BER) يتأثر بشكل كبير بالمجال الترددي لمصدر التداخل المؤثر، بينما يكون التأثير قليل جدا عند استخدام نبضات مختلفه لتشكيل البيانات المرسله للنطاق الفائق العرض. النتائج ايضاً تشير الى انه كلما زاد المجال الترددي للاشارة فائقة العرض او مجال النبضه فان عدد القياسات التي يتم حذفها بسبب وجود مصدر التداخل يقل، وفي هذه الحاله نحفظ بمعظم البيانات المهمه التي تشكل النبضه المرسله.

CHAPTER 1 INTRODUCTION AND MOTIVATION

1.1 Introduction

Ultra Wide-Band (UWB) technology is a promising a cutting edge in delivering high data rate for short range wireless communication systems. It is suitable for applications which need low power such as multi-hop wireless networks. Recently, UWB technology became a good candidate for short-range indoor high-resolution positioning systems. UWB signals have the ability to trade bandwidth for a reduced transmission power. This can be achieved by sending a very short pulse duration which means very large bandwidth. UWB signals include not only carrier-less base-band signals, such as Impulse Radio (IR) or non-sinusoidal pulses, but also wide-bandwidth signals with carriers, such as Multi-Band Orthogonal Frequency Division Multiplexing (MB-OFDM).

Because of their large bandwidth, UWB signals may encounter some problems especially with high sampling rate required at the receiver side. Reducing the complexity of UWB receiver is an important issue. Moreover, coherence existence with other narrowband systems is a major concern which needs to be addressed through a proper mechanism. Compressive Sensing (CS) is a promising signal processing solution which can reduce the sampling requirements as well as avoid the interference with narrowband systems.

Narrowband Interference (NBI) signals may have two scenarios. One of them is overlaying the UWB spectrum over a licensed narrowband signal. The other is the intentional jamming where someone share part of the UWB spectrum in order to disturb the existence transmission [Sti06]. Because of the power constraint of UWB signals, the

mitigation of the NBI over UWB system is a challenging task. Although, both narrowband and UWB systems may affect each other [Dow04], [Nik09], our interest is on mitigation of the NBI effect on UWB systems. When the narrowband signals are very strong, they will interfere with UWB signal and may degrade the system performance [Wan10a].

This thesis utilizes CS as a mean to mitigate NBI in UWB systems. The mitigation is studied in both trained and blind systems. CS is used to detect and remove NBI effects as well as reduce the sampling rate at the receiver side. The Bit Error Rate (BER) performance in both systems is examined by applying different NBIs, with different center frequencies and bandwidths.

1.2 Organization of the Thesis

The thesis is organized as follows. Chapter 1 presents a brief introduction to UWB systems, narrowband systems, and compressive sensing technique. Details are given in how to generate UWB pulses as well as UWB systems pros and cons. The issue of spectrum sharing between UWB systems and different narrowband systems is also discussed. Chapter 2 is preserved for channel modeling and narrowband interferers modeling. In addition, compressive sensing framework and how it is utilized to reconstruct sparse signals are illustrated with details. The IEEE802.11.4a UWB channel model is discussed briefly in this chapter. Chapter 2 also presents different interferers models. Chapter 3 discusses the mitigation problem in training UWB systems. Those systems use pilot symbol assisted modulation combined with direct sequence spread

spectrum and time hopping for signaling. The mitigation process focuses on the detection and elimination of the most significant NBI components in the Discrete Cosine Transform (DCT) or Discrete Fourier Transform (DFT) domain. Chapter 4 studies the mitigation of the narrowband interference in blind systems. The center frequency of the interfering source and the bandwidth of UWB signal as well as other factors play an important role in the mitigation process. Chapter 5 concludes the thesis with summary of findings, the recommendation for future.

There are two tables in the appendix. One of them is dedicated for all the abbreviations mentioned in the thesis. All the variables used in this work and their indications are listed in the other table.

1.3 Thesis Contribution

Both trained and blind systems have been investigated for mitigating the NBI in UWB system using compressive sensing. The NBI sources were assumed to be licensed and unlicensed signals with different center frequencies and different bandwidths.

- In trained systems, three training pilot groups are required. We investigated the effect of each **pilot group symbols** and obtained the **distribution** that optimizes the BER performance. We've shown that the first and the last pilot group symbols are very important. Communications can be achieved without using the second group. Though, the performance can be enhanced if we make use of the second pilot group symbols. The study also shows that the third group is the most dominant one. Hence extra symbols should be assigned to estimate the channel.

- Moreover, the trained system performance is further examined in the presence of **multiuser interference** when other users share the same channel. Throughput of the system is evaluated in the presence of multiuser interference in addition to the NBI.
- In blind UWB systems, we extended the mitigation technique in [Oka09b] to mitigate the effect of **two NBIs**. For the considered SIR, we concluded that the 2 partial bands NBI has less effect on the performance than the partial band jammer since the power at the effecting bands are so low compared with that of the partial band NBI.
- We examine the effect of the **NBI's bandwidth** and the **UWB signal's bandwidth** on system performance. Those parameters are related to the mitigation process. For the considered scenarios, we've demonstrated that the BER is a strong function of the NBI's bandwidth and of the UWB signal's bandwidth. In addition, we've studied different parameters that may affect the system performance such as the **burst size, the type of the modulated window and the baud rate**. Our study shows that sending the information using large burst size outperforms sending it using small burst size since the probability of making an error in one bit decreases as the burst size increases. We also prove that the BER is a weak function of the considered modulated window. Additionally, the performance is highly affected when the NBI's center frequency is shifted to the center frequency of the transmitted pulse.

1.4 Technical Background

Compressive sensing is a promising signal processing technique used to reduce the sampling rate at the receiver as well as reduce the effect of the NBI on the UWB systems. As depicted in Figure 1-1, the thesis includes three main topics, UWB, NBI and CS. This section provides the reader with technical background related to UWB signals, NBI, and CS techniques.

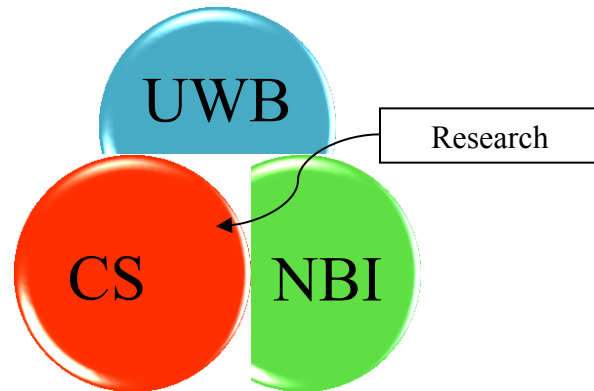


Figure 1-1 The main topics of the research

1.4.1 Ultra Wideband Signals

UWB signals are usually defined as any signal that occupies bandwidth greater than 500 MHz or has a fractional bandwidth, B_f , greater than 0.2. The fractional bandwidth is defined as the ratio between the signal bandwidth (BW) and its center frequency f_c as given by:

$$B_f = \frac{BW}{f_c} = \frac{f_H - f_L}{(f_H + f_L)/2} \quad (1-1)$$

where f_L is the lower band, and f_H is the upper band in the frequency spectrum at -10 dB points [Nik09]. The approved bands for indoor and outdoor UWB communications have a Power Spectral Density (PSD) lower than part 15 FCC limits which is -41.3 dB/MHz in the range of 3.1-10.6 GHz [Ale07], [Li09], [Zha06] as shown in Figure 1-2.

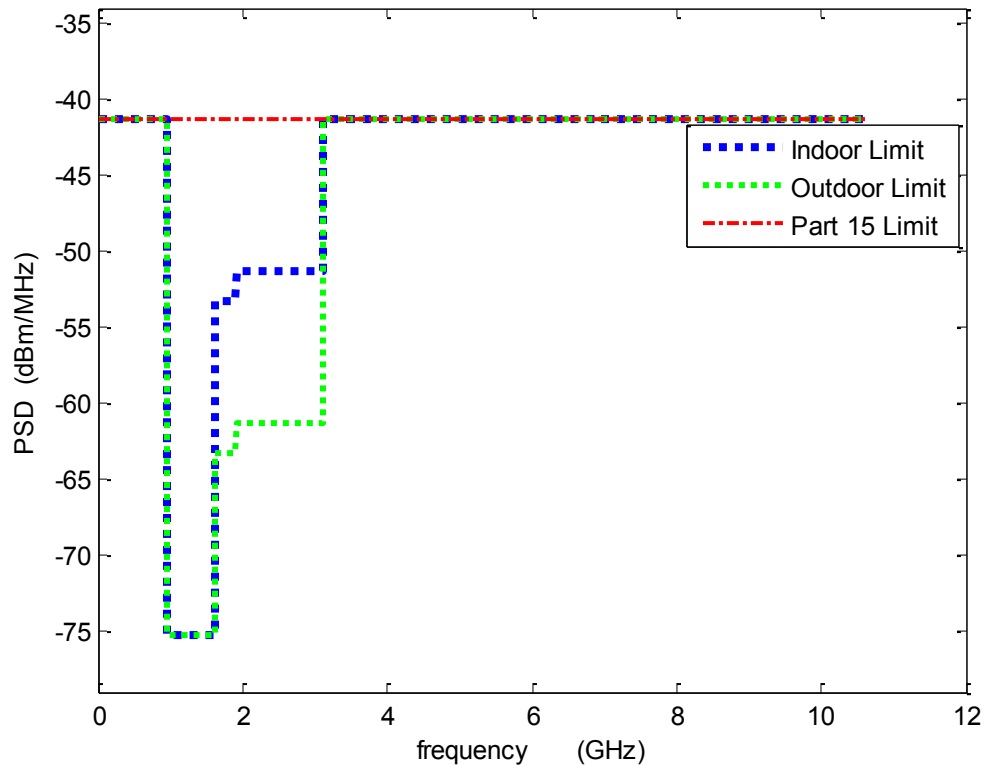


Figure 1-2 FCC spectral mask for UWB indoor communication systems

UWB signals have the ability to trade bandwidth for a reduced transmission power. The idea is based on sending a very short pulse duration which improves the immunity to multipath. The bandwidth is very large and according to Shannon theorem the data rate will also be large. UWB systems are proposed for many applications such as wireless sensor networks with low cost and low complexity [Li09], [Oka09a], [Ovt09], [Zha09].

One of the benefits of low-power spectral density is a low probability of detection. Therefore UWB signals are suitable for military applications. Another benefit is the long battery life/ lighter batteries for UWB devices.

Table 1-1 also depicts the corresponding Effective Isotropic Radiated Power (EIRP), and the frequencies for the indoor and the outdoor UWB systems.

Table 1-1 Emission limits for indoor and outdoor systems in EIRP [Nik09]

Emission limit for UWB	Indoor	Outdoor
Frequency (GHz)	EIRP (dBm/MHz)	EIRP (dBm/MHz)
0.96-1.61	-75.3	-75.3
1.61-1.9	-53.3	-63.3
1.9-3.1	-51.3	-61.3
3.1-10.6	-41.3	-41.3

The choice of the UWB waveforms depends on many factors. The most common waveform is the Gaussian pulse and its higher derivatives. The higher derivatives are more favorable because of their low DC content. The time and the frequency domain for the first, and the second derivatives Gaussian pulses are shown in Figure 1-3. Orthogonal Hermite or modified Hermite pulses, Legendre pulses and Prolate spheroidal functions are also among several proposed UWB waveforms [Nik09]. The Gaussian pulse is expressed mathematically as:

$$p(t) = \frac{1}{\sqrt{2\pi\sigma^2}} e^{-\frac{t^2}{2\sigma^2}} \quad (1-2)$$

The first and the second derivative of the Gaussian pulse are

$$p'(t) = \frac{dp(t)}{dt} = \frac{-t}{\sigma^2\sqrt{2\pi\sigma^2}} e^{-\frac{t^2}{2\sigma^2}} \quad (1-3)$$

$$p''(t) = \frac{d^2p(t)}{dt^2} = \frac{1}{\sigma^2\sqrt{2\pi\sigma^2}} \left[\frac{t^2}{\sigma^2} - 1 \right] e^{-\frac{t^2}{2\sigma^2}} \quad (1-4)$$

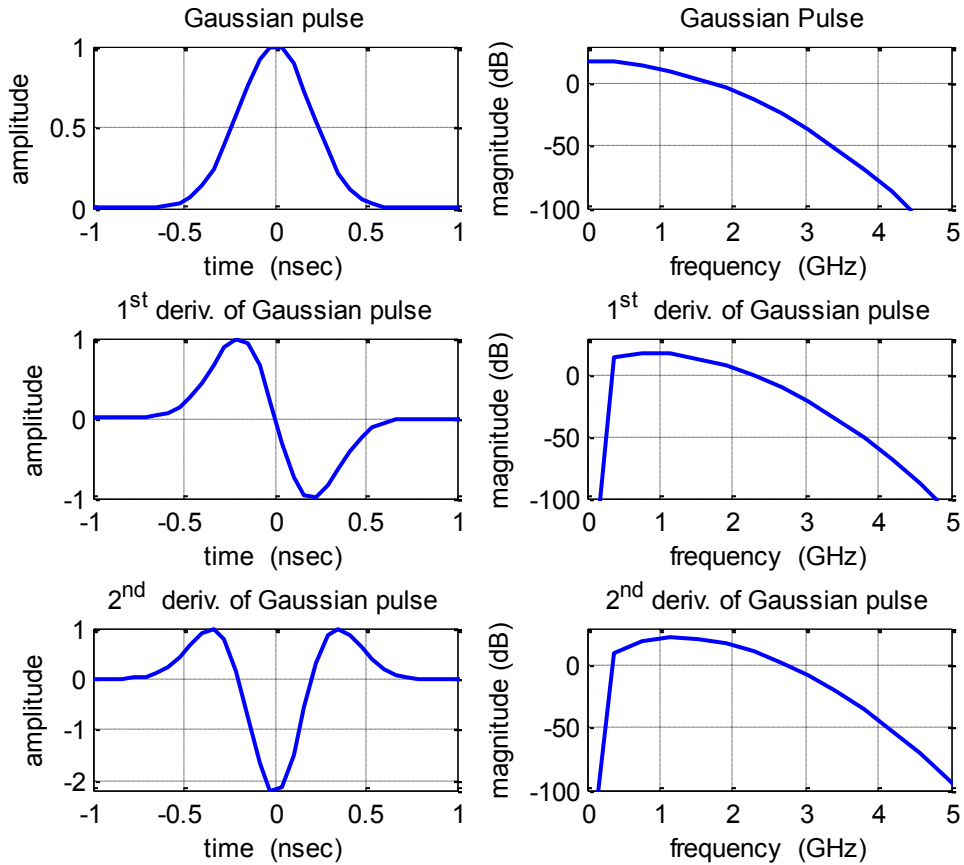


Figure 1-3 Time and frequency domains for the Gaussian, first, and second derivative Gaussian pulses

The energy of such pulses extends over large bandwidth. Figure 1-3 shows the Gaussian pulse in time and frequency domains where the amplitudes are normalized. The

corresponding first and second derivative Gaussian pulses are also plotted in both domains. The graph as well indicates that there are low DC components for the Gaussian derivative pulses. In the remaining chapters the second derivative Gaussian pulse is used unless otherwise is specified.

1.4.2 Narrowband Interference Signals

There are many systems that share the UWB frequency spectrum, see Figure 1-4. Those systems can be categorized into two types. Systems having fixed or assigned frequency range are called licensed systems. Systems which don't have assigned frequency spectrum are known as unlicensed systems. The licensed systems are the most important interference sources for the UWB signals including WiMAX, WLAN, and Bluetooth.

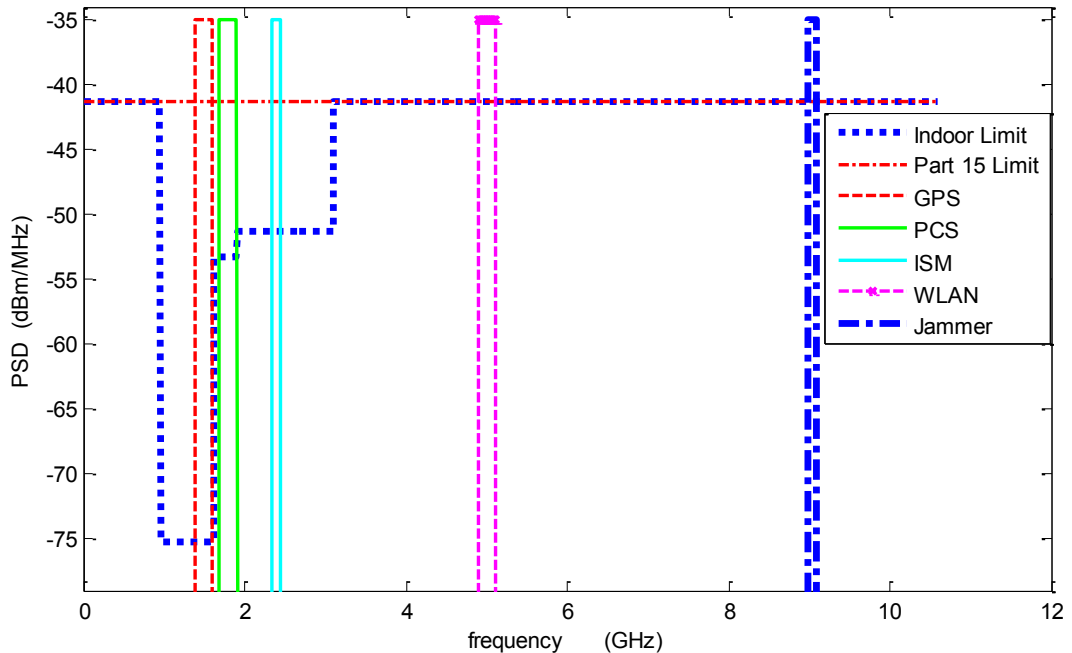


Figure 1-4 FCC spectral mask for UWB indoor communication systems with narrowband systems

Figure 1-4 illustrates many narrowband systems that share the UWB spectrum including, GPS, Personal Communications Service (PCS), the Industrial, Scientific, and Medical band (ISM), WLAN, and intentional jammers. Bluetooth and IEEE802.11b WLAN are two standards which use the 2.4 GHz (ISM) band.

1.4.3 Compressive Sensing

According to the sampling theorem, the minimum required sampling frequency for accurate detection is twice the maximum frequency of the transmitted signal. When acquiring a high frequency signal, a very high speed ADC is needed. Those ADCs are difficult to design [Zha09]. The problem becomes worse with channel distortion and Inter-Symbol Interference (ISI) which appears when a high data rate goes over a frequency selective channel in such case an equalizer is employed. High data rate requirements will definitely affect the receiver design i.e. more complex Digital Signal Processing (DSP) components are required [Ale07].

CS technique has been used to reduce the speed of ADC into a sub-Nyquist rate in UWB systems which can be designed and implemented. This could be achieved if the UWB signal is sparse i.e. has few nonzero terms [Gom10], [Gom11], [Wan07a], [Wan08], [Zha09], [Zha10]. More details about CS are provided in Chapter 2 Section 2.3.

1.5 Literature Review

This section provides a literature review for the most relevant works in the field of interest. This section is divided into three subsections. The first subsection summarizes

and provides works related to the mitigation of NBI in UWB systems. The second subsection goes through others studying the utilization of CS to UWB systems. The last subsection investigates works that address the problem of NBI in UWB systems based on CS.

1.5.1 Narrowband Interference Mitigation in UWB Systems

Since UWB systems have a wide bandwidth; they may coexist with other licensed or unlicensed narrowband systems. Researchers proposed different mechanism for peaceful coexistence between UWB and narrowband systems.

Generally, wideband systems like Direct Sequence (DS) systems are capable of interference suppression. The degree of the suppression may not be satisfactory when the spreading gain is limited and a very strong NBI is presented. Wang et al., in [Wan10a], proposed DS-UWB system as an extension to the code aided interference suppression which uses the linear minimum mean-square error algorithm for multiuser detection [Poo97]. A considerable enhancement in the NBI suppression capability is achieved by introducing a new type of spreading sequence method. In case of very high data rate application, inter-chip interference is present because of the non-sharply peak autocorrelation of the sequence. Consequently an equalizer needs to be implemented which increases the receiver complexity. For such application, the equalizer needed was avoided with spreading sequence that has sharply peak autocorrelation [Wan10b].

The performance of DS pulse amplitude modulation UWB system with IEEE802.11a WLAN as NBI source was studied by [Li09], [Zha06].

The negative impact of NBI can be reduced by proper pulse shaping. In [Li09], nonlinear chirp pulses were used to create UWB pulses and decrease the NBI. The pulses are flexible in the design and have low complexity.

Another method to reject the NBI is based on Singular Value Decomposition (SVD) [Zha06]. To reduce the complexity of SVD, the input data is segmented to several groups, every group is rearranged in special way where the matrix dimension is reduced. At the end, SVD is applied on every matrix; consequently the complexity is reduced without clearly penalizing the BER.

Data can be used to modulate a polarity of the “data” pulse with respect to a “reference” pulse. In Auto-Correlation Receiver (AcR) shown in Figure 1-5, the received reference signal is delayed and then correlated with the data signal. The amount of the delay in an AcR is matched to the delay between reference and data pulse at the transmitter. The overall system is usually referred to as Transmitted-Reference (TR) AcR.

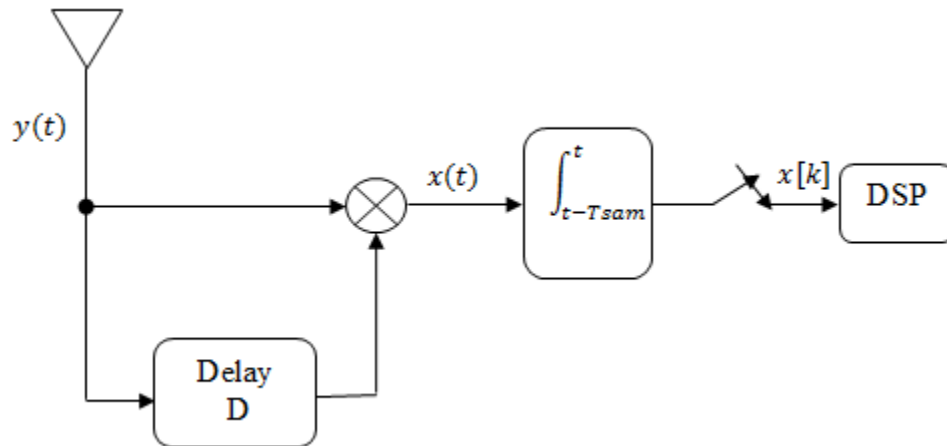


Figure 1-5 Autocorrelation receiver (AcR)

Although no channel estimation is required, the receiver front-end is open to undesirable noisy signals. On the darker side also, AcR suffers from ISI when the data rate is increased. Compared with coherent receiver, it is robust against the multipath propagation at low complexity. A data model; proposed by [Wit05]; was applied effectively for detection and NBI alleviation by combining several AcR channels linearly.

Narrowband interference suppression in [Dow04] is accomplished by a modified feedback loop mechanism. In this approach, feedback delay can be controlled to extract information from a number of previous transmitted pulses. The Signal-to-Interference Ratio (SIR) was improved as the number of involved pulses increased giving a cleaner pulse.

Dang and Van Der Veen, in [Dan06], investigated the mitigation problem in high data rate application. By oversampling, the transmitted symbols can be detected by gathering the energy of all the multipath arrivals. At certain range of SIR, it is possible to mitigate the NBI, though the model becomes invalid when the NBI is too strong. In this case, the NBI needs to be filtered before entering the AcR.

In [Ale07], NBI mitigation is achieved through a system made of two stages, namely: an adaptive NBI cancellation and a linear combiner. The scheme uses a canceller circuit based on feed forward approach. The interference is filtered out through tunable analog Band-Pass Filter (BPF) and subtracted from the received signal before the correlator. The output of the correlator is feedback to the canceller which adjusts the canceller parameters until minimal interference is observed. In case of too strong NBI or a second

interferer is presented, a linear combiner is used to reject any leakage. The AcR uses a method based on SVD to identify the spectral location of the NBI. In [Ale09], a method of threshold comparator based on the SVD of a reduced rank of the received data matrix is used for NBI detection. Then an approach analogous to DFT calculation is followed for the NBI center frequency identification.

Filtering is also used by other researchers for NBI cancellation [Sti06], [Ovt09]. A technique based on multicarrier called amplitude-phase adaptive sine-modulated/cosine-modulated filter bank equalizer was applied by [Sti06]. It was used to mitigate the distortion on an OFDM sub-channel by a NBI located at an OFDM adjacent sub-channel. Ovtcharov et al., in [Ovt09], proposed a scheme using complex adaptive digital filtering. The filter monitors the NBI's frequency regularly based on the least mean square algorithm to adjust its frequency to match the center frequency of the NBI. The approach can eliminate the NBI effects; however the performance becomes worse for SIR greater than 0 dB because the NBI filter introduces amplitude and phase distortion.

Apart from filtering, the NBI problem is solved as well by introducing a pulse that meets the Federal Communication Committee (FCC) spectrum mask and has spectral nulls at frequencies of NBI in the UWB spectrum [Wan06], [Wan07], [Zha11]. The transmitted pulse for this approach is represented by a coded based Gaussian monocycle pulse where the value of each code bit gives the weighting coefficient of each monocycle pulse. The resulting pulse is the sum of weighted and overlapping Gaussian monocycles. Thus the shape of the resulting spectrum is determined by both the Fourier transform of the basic Gaussian monocycle pulse and the spectrum of the intended codeword. Even though, a

set of multi-variables nonlinear equations has to be solved to get the codeword. The approach can be applied for different modulation techniques such as pulse position modulation, and OFDM-UWB and IR UWB [Wan06], [Wan07].

In [Zha11], the FCC mask was realized through combining multiple Gaussian derivative pulses (1st-15th) with proper scaling. The resulting pulse is added to a similar one with a certain time delay. The final resultant pulse meets the FCC PSD, bandwidth mask, and has multiple nulls to mitigate the NBI at certain frequencies. The nulls can be controlled by changing the time delay. The pulses designed in [Wan06] and [Wan07] are suitable only for single NBI whereas in [Zha11], they have the ability to suppress multiple NBI with low implementation cost and low power.

The NBI can be reduced by exploiting the UWB signals immunity to the multipath effect based on interference Selection Diversity (SD) in Single-Input-Multiple-Output (SIMO) system. In contrast to the conventional SD, the receiver selects the weakest signal and feeds it to the demodulator. Since UWB signal power over all antennas is almost constant, while the interfering power varies independently from one antenna to another when the multipath angle spread is high [Ibr07], any increase in the received power is related to a superior NBI power. Better performance was realized through doubling the number of receiving antennas. In addition, this approach doesn't need fast ADC, synchronization and knowledge of the location or the statistical characteristics of the NBI signal.

We have discussed several methods to solve the NBI problem. Given that our promised solution is the CS; we concentrate on the literature that exploits CS for UWB systems.

1.5.2 Compressed Sensing Based UWB Systems

Even when no interference is assumed, compressive sensing techniques are used to reduce the sampling rate to sub-Nyquist rate and hence results in low ADC requirements. Researchers on UWB systems used CS in training systems [Jin12], [Wan07a], [Wan07b], [Wan08] while others applied it for blind systems [Oka09a], [Oka09b]. For the case of impulse radio (I-UWB), CS was applied by many researchers [Oka09a], [Oka09b], [Oka09c], [Wan07a], [Wan08], [Zha09], [Zha10]. Other researchers applied CS for UWB systems in bursty applications such as wireless sensor networks [Jin11], [Jin12], [Oka09a], [Oka09b], [Oka09c].

A serial system structure; shown in Figure 1-6; was proposed by [Zha09]. The system is suitable for I-UWB communications, which is sparse in time domain. An UWB signal is transmitted by supplying a sparse bit stream through an UWB pulse generator and a pre-coding filter. After the channel, a low-rate ADC samples the received signal which is then processed by a recovery algorithm.

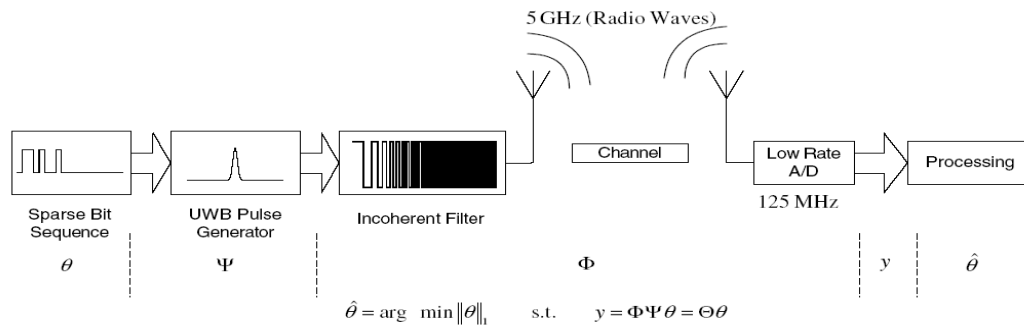


Figure 1-6 System architecture of CS based-UWB system [Zha09]

Based on the CS UWB Single-Input-Single-Output (SISO) system in [Zha09], a 2×2 Multiple-Input-Multiple-Output (MIMO) system was proposed by [Zha10]. The method in [Zha10] is different from the method in [Zha09] in that the UWB channel was modeled with pulse distortion. Though, the total samples/sec at the receiver is almost the same, the sampling rate is reduced at each receiver branch compared with [Zha09] system.

A CS based Maximum Likelihood Sequence Estimation (MLSE) correlator receiver was proposed in [Oka09a]. It consists of an analog front-end which contains a bank of correlators with test functions, low ADC, and DSP back-end based on a computationally efficient Quadratic Program (QP) reconstruction. The number of correlators is smaller than the required by Shannon-Nyquist sampling theorem.

To support burst applications [Jin11], [Jin12] suggested the use of a pre-coding filter followed by UWB pulse generator.

Generalized Likelihood Ratio Test (GLRT) detector based on compressive measurements, where the received signal was projected onto a random digital basis, was

derived by [Wan07a]. CS was applied for channel estimation. The complexity of the system was reduced by taking advantage of the sparsity of the received signal [Wan07b]. Two compressive measurements were applied. The first one was based on random basis as in [Wan07a], while the other was constructed based on the subspace signal structure estimated by Matching Pursuit (MP) algorithm. For training, pilot symbol assisted modulation was used to provide information about the channel [Wan07a], [Wan07b], and to estimate the signal structure [Wan07b].

1.5.3 Compressed Sensing Based UWB Systems with Narrowband Interference Mitigation

Applying CS technique, as we've mentioned, was mainly used to reduce the sampling rate. Few researches have investigated the possibility of NBI mitigation in UWB systems by utilizing CS. Similar studies utilized CS in NBI mitigation for OFDM systems. An algorithm based on CS technique was proposed in [Gom10], [Gom11] to estimate and mitigate the NBI signals undergoing fast and frequency-selective fading channels in OFDM systems. Before channel estimation, NBI is estimated and cancelled. Both references studied the case of asynchronous jamming where the NBIs and the desired signals do not coincide (some frequency offset).

Wang et al. in [Wan08] extended the subspace detection method in [Wan07b] to NBI mitigation in which the NBI subspace is estimated from random measurements when the UWB signal is absent. The coefficients of the NBI signal were estimated using Basis Pursuit Denoising (BPDN) algorithm. Once the UWB symbols are detected, both null

subspace of the NBI and UWB subspace -estimated by BPDN- are used to construct the compressive measurement matrix. For signaling purpose, pilot symbol assisted modulation combined with direct sequence spread spectrum coding and time-hopping (DS-TH) coding was suggested. The pilot symbols were divided into three groups in order to: estimate the NBI subspace; estimate the UWB signal subspace; and provide information about the channels.

Combining the correlator receiver [Ok09a] with digital notch filter was applied to NBI suppression when strong NBI was present from licensed systems like WiMAX [Oka09b]. The NBI affects only small part of the CS measurements by setting the test functions to be highly frequency selective at the correlators. During the QP reconstruction, a ‘digital notch’ was employed which discovers and drops those affected measurements with only few numbers of correlators. An approach -in between [Oka09b] and [Wan08] was also used for NBI elimination [Jin12]. The proposed system used a training sequence in the first burst and didn’t transmit any information. Then a method similar to that in [Wan08] was used to detect the coefficients of the NBI.

For CS based UWB systems, no additional hardware are required to detect and mitigate the NBI subspace as well as no ISI was assumed (low pulse rate). The NBI signals in are sparsely characterized in the DCT [Wan08]. Though in [Oka09b], the baud rate might be close to the Nyquist rate with imperfect timing. The basis functions are sinusoidal waveforms which are sparse in frequency domain.

In light of the literature survey, the thesis branches into two main directions. The former branch is the mitigation of NBI in training UWB systems. The latter is the mitigation in blind UWB systems.

CHAPTER 2 UWB-CS SYSTEM MODEL AND NBI

2.1 Introduction

This chapter provides the required technical background related to UWB channel modeling, CS technique, and NBI modeling. The UWB IEEE802.11.4a channel model is introduced first. The ability of CS technique to detect and reconstruct unknown signals from far few numbers of measurements is explained in the next subsection. There are many CS algorithms with different complexity; including Basis Pursuit (BP), Matching Pursuit (MP), Orthogonal Matching Pursuit (OMP), and Basis Pursuit Denoising (BPDN). The chapter covers the details of MP algorithm because it is the one that will be used in this work. In this chapter we introduce different models required to evaluate the proposed NBI mitigation techniques. Important properties of interferers are explained. We focus on the types that are used in the simulation in the coming chapters.

The block diagram of the proposed system, shown in Figure 2-1, involves an UWB system and a NB system. Thermal noise is added at the UWB receiver. The channel model for the UWB transmitter is different than the NBI channel. In the coming sections, UWB channel, MP algorithm, and NBI modeling are explained in details.

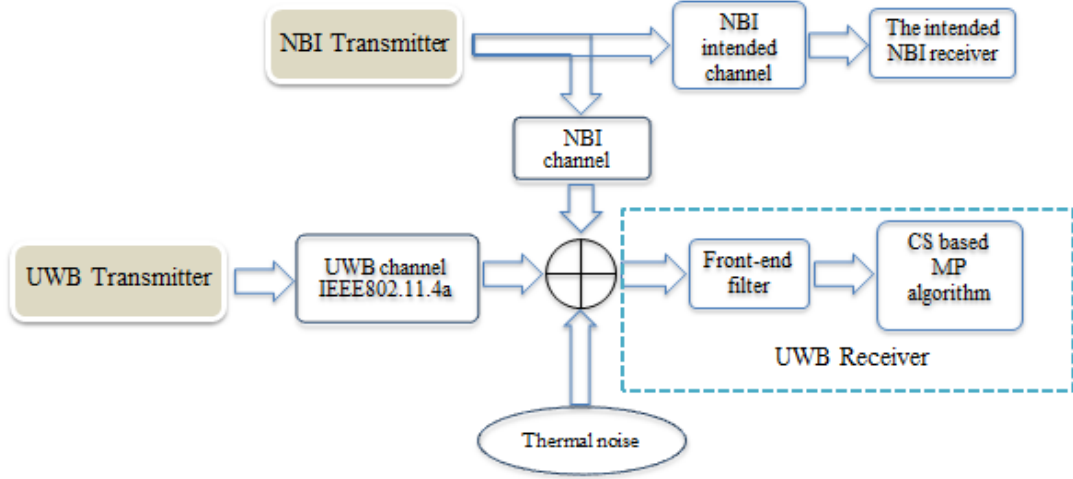


Figure 2-1 Block diagram of the proposed system model

2.2 UWB Channel Model

The used UWB channel model is the one proposed by the IEEE 802.11.4a working group [Mol06]. The model is proposed by modifying the conventional model for Saleh-Valenzuela (S-V) model [Sal87]. It is applicable for different environments such as indoor residential, indoor office, industrial, outdoor, and open outdoor environments. The multipath components arrive as clusters according to Poisson distribution, and each path in a certain cluster also arrives with the same distribution. Thus the inter-arrival times for the clusters and the paths within the clusters are exponentially distributed. The impulse response of the channel can be expressed as:

$$h(t) = \sum_{l=0}^L \sum_{k=0}^{K_l} a_{l,k} \delta(t - T_l - \tau_{l,k}). \quad (2-1)$$

where L is the number of clusters, K_l is the number of multipath components within the l^{th} cluster, $a_{l,k}$ is the multipath gain coefficient of the k^{th} component in the l^{th} cluster,

T_l is the delay of the l^{th} cluster which is defined as the Time Of Arrival (TOA) of the first arriving multipath component within the l^{th} cluster, and $\tau_{l,k}$ is the delay of the k^{th} multipath component relative to the l^{th} cluster arrival time, T_l . The two dimensional model can be reduced into one dimensional discrete model including a mixed Poisson distribution for ray arrival times:

$$h(t) = \sum_{l=0}^{L-1} \alpha_l \delta(t - \tau_l) \quad (2-2)$$

where α_l, τ_l are the attenuation and the delay of the l^{th} path. The channel model was already implemented using Matlab in [Mol06], and the thesis uses it directly.

Table 2-1 IEEE802.1.4a channel model classification

LOS	Environment	NLOS	Environment
CM-1	Residential	CM-2	Residential
CM-3	Office	CM-4	Office
CM-5	Outdoor	CM-6	Outdoor
CM-7	Industrial	CM-8	Industrial
		CM-9	outdoor

Channel models in IEEE 802.15.4a are classified as in the Table 2-1. Each model is applicable for a specific environment. Odd numbered channels represent line-of-sight scenarios, while even numbered channels are for non-line-of-sight (NLOS).

Channel Model#1 (CM1) is used throughout the thesis. A representative simulated impulse response and power delay profile for CM1 is plotted in Figure 2-2. The path strength of the multipath after 150 nanosecond excess delay is negligible.

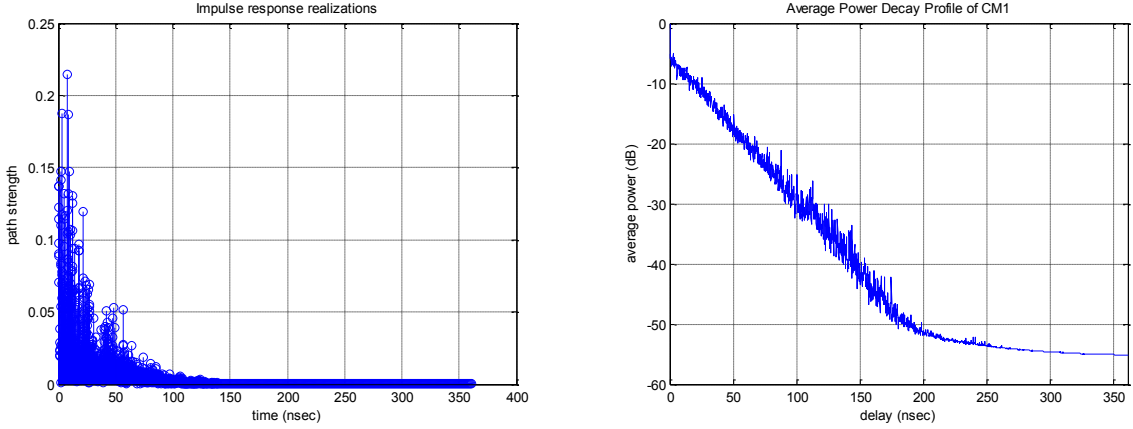


Figure 2-2 The impulse response and the power delay profile of CM1

2.3 Matching Pursuit

Let $\mathbf{x} \in \mathbb{R}^N$ be a vector of length $N \times 1$, most of its elements are zeros and there are K nonzero elements in \mathbf{x} . Assume also that Ψ is a basis matrix of dimension $N \times N$. The vector \mathbf{x} can be represented by a linear combination as:

$$\mathbf{x} = \sum_{n=1}^N \theta_n \psi_n = \Psi \boldsymbol{\theta} \quad (2-3)$$

where $\boldsymbol{\theta} = [\theta_0, \theta_1, \dots, \theta_{N-1}]$ is $N \times 1$ vector of constant coefficients. The signal \mathbf{x} is called K -sparse or it is sparse in the Ψ -domain. By utilizing the CS, the sparse signal \mathbf{x} can be reconstructed from M measurements where $N \gg M$ by projecting \mathbf{x} onto a measurement matrix Φ with $M \times N$ dimension as:

$$\mathbf{y} = \Phi \mathbf{x} \quad (2-4)$$

$$\mathbf{y} = f \boldsymbol{\theta} \text{ where } f = \Phi \Psi \quad (2-5)$$

The CS technique has proven that a major factor for accurate reconstruction process is the incoherence between Φ and Ψ [Can06], [Zha9], [Zha10].

Through an optimization problem of the l_1 -norm the coefficients of the vector Θ can be recovered from the vector \mathbf{y} using the following formula:

$$\hat{\theta} = \underset{\tilde{\theta}}{\operatorname{argmin}} \|\tilde{\theta}\|_1 \text{ subject to } \mathbf{y} = f\tilde{\theta} \quad (2-6)$$

where $\hat{\theta}$ is the recovered vector. Linear programming such as BP or MP and OMP is used to solve the problem [Zha09].

In this work among many CS algorithms, MP is used. Matching Pursuit algorithm is simple and efficient. However, it isn't optimal because it doesn't take the noise effect into account. For the sparse signal, $\mathbf{x} = \mathbf{H}\boldsymbol{\theta}$ which is K -sparse on basis Ψ , where $\boldsymbol{\theta}$ is a vector with $K \times 1$ nonzero elements, and \mathbf{H} is a subspace matrix of dimension $N \times K$ that is constructed from the basis Ψ with $N \gg K$. The location of columns that construct the subspace matrix \mathbf{H} from the basis Ψ is unknown, which can be achieved using MP algorithm.

Given the measurement vector, $\mathbf{y} = \Phi\mathbf{x}$, the target of the algorithm is to extract the K largest columns correlated to \mathbf{y} from a combined dictionary $\mathbf{V} = \Phi\Psi$. Figure 2-3 summarizes the main steps for the MP algorithm. The process works iteratively with T_0 maximum number of iterations. It starts by an initialization states for the sparse vector $\hat{\theta}$ and starts a counter, i , for the number of iterations. In each turn, the algorithm goes over all \mathbf{V} columns, and searches for the most correlated column vector with \mathbf{y} then

removes it from \mathbf{y} giving a residual error vector, e_t . After each iteration, K can be approximated by observing the magnitude of the current residual. The subspace matrix $\hat{\mathbf{H}}$ is constructed by examining the number of the significant elements of $\hat{\boldsymbol{\theta}}$ when the threshold value, T_0 , becomes smaller than the ratio between residual vector and the measurement vector [Wan07b].

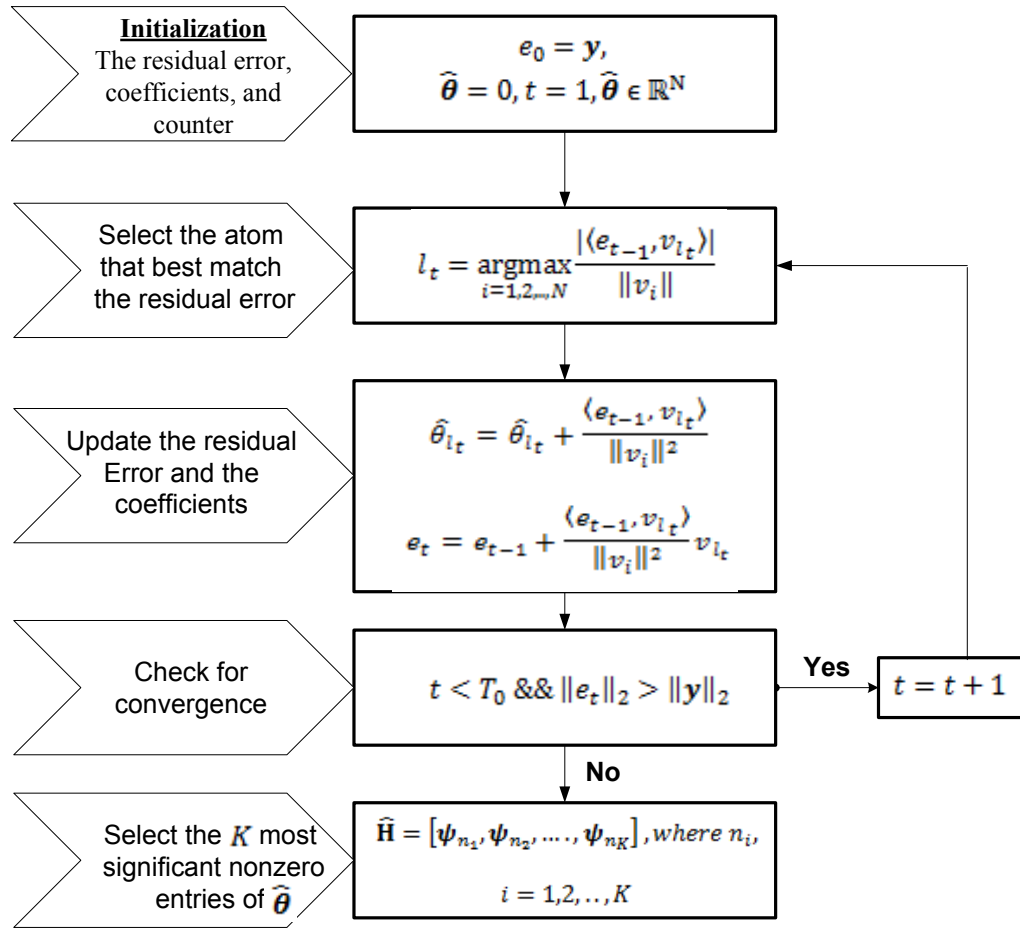


Figure 2-3 Matching Pursuit for signal structure estimation

Compressive sensing is used to estimate the coefficients of NBI in trained UWB systems. This can be done by exploiting the fact that the NBI has sparse representation in the DCT

domain. Furthermore, CS is applied to estimate and construct the subspace measurement matrix in which a sparse UWB signal lies. In blind UWB systems, the test functions in the correlator receiver are sparse in the frequency domain. The transmitted waveform contains only K nonzero samples i.e. it is K -sparse, therefore NBI is effectively eliminated. For I-UWB receivers, CS is also used to reduce the sampling rate at the receiver side far below the Nyquist rate.

2.4 Narrowband Interference Modeling

As the main objective of this work is to mitigate the NBI effect on UWB systems, it is very important to know the characteristics of those NBIs. The bandwidth and the center frequency of a UWB signal is denoted by Ω_U, f_{cU} respectively, while Ω_I, f_{cI} are the bandwidth and the center frequency of NBI signal and $\Omega_U \gg \Omega_I$. The performance is not affected when the interferer operates out of the band of interest. We are only interested in the jammers overlaying the UWB signal's bandwidth.

This section discusses different NBIs, such as single-tone, multi-tone and partial-band interference models [Che09]. Furthermore, we discuss some licensed NBIs like WiMAX, WLAN, and Bluetooth.

2.4.1 Unlicensed Narrowband Interference

The unlicensed narrowband interferers or jammers don't have fixed center frequency or bandwidth. A single tone jammer can be considered as the simplest form of interference, where a sinusoidal signal with a certain single frequency, f_I , lays within the UWB

signal's bandwidth. The extreme case occurs when the frequency of the jammer coincides with the center frequency of the UWB signal. The time domain expression of the tone jammer, $v(t)$, and its autocorrelation function, $R_v(\tau)$, are expressed as:

$$v(t) = a \cos(2\pi f_1 t) \quad (2-7)$$

$$R_v(\tau) = \frac{a^2}{2} \cos(2\pi f_1 \tau) \quad (2-8)$$

The average power of the jammer is $v = R_v(\tau = 0) = \frac{a^2}{2}$. The PSD of single tone interferer is the Fourier transform of its autocorrelation which is expressed as:

$$S_v(f) = \frac{a^2}{4} [\delta(f - f_1) + \delta(f + f_1)] \quad (2-9)$$

On the other hand, multi-tone interferer is constructed by adding more than one tone interference signal. Assuming N_v equal power tones, the multi-tone jammer can be defined as:

$$v_i(t) = \sum_{l=1}^{N_v} \sqrt{\frac{2}{N_v}} \cos(2\pi f_l t + \phi_l) \quad (2-10)$$

When the phase of the individual tones is random and independent, this type of interference has Gaussian distribution when $N_v \gg 1$ according to the central limit theorem.

Partial-band interference spreads its power, v , over a specific frequency band, so it affects a partial band of the total UWB signal bandwidth. The PSD of the partial-band jammer is given by:

$$S_v(f) = \begin{cases} \frac{v}{\Omega_I}, & |f - f_{cI}| \leq \Omega_I \\ 0, & \text{otherwise} \end{cases} \quad (2-11)$$

2.4.2 Licensed Narrowband Interference

The licensed narrowband interferers or jammers have fixed or assigned frequency range. WiMAX and IEEE802.11a WLAN are OFDM based systems where the available bandwidth divides into smaller sub-bands. The data transmitted in each sub-band utilizes different modulation techniques. The IEEE802.11b standard and Bluetooth operate over the 2.4 GHz ISM band.

WiMAX is a primary NB service based on the IEEE802.16-2004 standard. It operates in the band of 2-66 GHz over an adaptable channel bandwidth ranging from 1.25 MHz up to 20 MHz which can be any integer multiple of 1.25 MHz, 1.5 MHz, 1.75 MHz, 2 MHz, and 2.75 MHz. The modulation adaptively changes according to the channel conditions. With different coding rate, the system may provide data rate up to 75 Mbps.

Another OFDM based system is the IEEE802.11a WLAN which works in the 5.2 GHz spectrum with 20 MHz channel bandwidth. It uses adaptive modulation and coding which changes according to the channel conditions. Hence the system data rate might reach up to 54 Mbps [Bel03].

The IEEE802.11b WLAN has a bandwidth around 22 MHz and operates in the 2.4 GHz band as illustrated in Figure 1-4. WLAN simulates an implementation of the Direct Sequence Spread Spectrum (DSSS) system that provides 1 Mbps, 2 Mbps, 5.5 Mbps, and 11 Mbps payload data rates. The modulation of the system changes from DBSK to combinations of DQPSK, QPSK and complementary code keying (CCK) [Lan01], [Syd02].

Bluetooth operates in the 2.4 GHz ISM band. It transmits signals with small power around 1mW, therefore it is applicable for short-range technology. Frequency Hopping Spread Spectrum (FHSS) is used in Bluetooth. Bluetooth uses 1600 hop/sec to switch over 79 channels to avoid interfering with other systems operating in the same band. Each channel has a bandwidth of 1 MHz starting at 2.402 GHz and finishing at 2.48 GHz. Though the bandwidth is large, the common Bluetooth devices provides data rate of only 1 Mbps using Gaussian frequency shift keying (GFSK) [Lan01], [Syd02].

Table 2-2 illustrates comparisons between the NB services. It focuses mainly on the most important characteristics such as modulation and coding, the operating frequency band, bandwidth, and the maximum data rate supported by each service. It will be difficult to consider all possible NB systems. The discussion here provides guidelines for the chosen frequencies and bandwidths.

Table 2-2 Comparison between different NB services

NB service	WiMAX	IEEE802.11a	IEEE802.11b	Bluetooth
		WLAN	WLAN	
Technique	OFDM	OFDM	DSSS	FHSS
Modulation, coding rate	1/2 BPSK, 1/2, 3/4(QPSK, 16-QAM), 2/3, 3/4 64-QAM	1/2, 3/4 (BPSK, QPSK, 16-QAM) 2/3, 3/4 64-QAM	DBPSK, DQPSK, QPSK, CCK	GFSK
Spectrum GHz	2-11	5.2	2.4	2.4
Bandwidth MHz	20	20	22	
Maximum data rate Mbps	75	54	11	1

2.5 Summary and Concluding Remarks

This chapter provided the technical background required for mitigation of NBI in UWB CS based systems. The UWB IEEE802.11.4a channel model was present where we mainly focus on CM1 [Mol06] which we use in the simulation in Chapter 3 and Chapter 4. Among many CS algorithms the work concentrates on the MP algorithm.

Different unlicensed and licensed NBIs were discussed in this chapter. For the unlicensed NBI, the center frequency and the bandwidth of the jammers can be located anywhere in the UWB signal's spectrum. Licensed NB services are governed by standards.

In the next chapter, we will use MP algorithm to estimate the sparse components of the NBI in the DCT domain. Additionally, the basis or the subspace of the transmitted UWB signal will be constructed by the same algorithm. The algorithm aims to extract the sparse elements from a reduced set of measurements using a pre-defined dictionary. A dictionary, as we will see later, is a matrix that is built up from the signal of interest. Each column in this dictionary is a scaled and shifted version of the signal of interest. Matching Pursuit can be also used to estimate the columns from the designed dictionary that fully construct the sparse signal.

CHAPTER 3 MITIGATION OF NARROWBAND INTERFERENCE IN SYSTEMS WITH CHANNEL TRAINING

3.1 Introduction

In frequency selective channels, I-UWB pulses are distorted because of their wide bandwidth. When such pulses are sent over multipath environment, which cause ISI, the receiver must deal with timing problems carefully. The timing becomes so complex in multiple access techniques where there are many users sending on the same channel. It is even worse when an interferer shares part of the transmission bandwidth. The presence of interference degrades the system performance. Most UWB system achieves synchronization and proper channel estimation by sending a training sequence [Jin12], [Wan07a], [Wan07b], [Wan08]. Some systems are designed to work in the presence of NBI [Wan08] and some are designed to work in the presence of both NBI dense ISI [Jin12].

Training can be achieved by inserting a known data stream in the beginning of each frame or by sending pilot symbols at regular intervals during the whole transmission time. Many operations required at the receiver side such as channel estimation, synchronization, and data detection could be easily achieved when the received signal contains a training sequence. However, part of the transmitted data will be used as an overhead. Hence there is a tradeoff between the system performance and the throughput. Mitigation of narrowband interference can make use of the transmitted training sequence.

The main objective of this chapter is to mitigate the effect of interference on trained UWB systems based on CS technique. Narrowband interference signals may have sparse representation in the DCT domain. Our interest is to suppress the most significant components of the NBI signal in the DCT domain. The utilized system model is the one proposed by [Wan08]. In this research, the optimum pilot symbols distribution is investigated as well as the effect of each pilot group symbols is also studied. Moreover, we evaluate the performance of the receiver in [Wan08] in the presence of multiuser interference. The same signaling scheme (DS-TH) is used for multiple access.

When a random measurement matrix is applied in CS, the captured energy of the received UWB signal by a compressive detector may not be enough [Wan07a]. The performance can be enhanced if the UWB signal structure is employed in the construction of the projection matrix [Wan07b]. When structure is employed in designing the projection matrix, few measurements are required to get most of the received UWB signal energy. This is because the received UWB signal is sparse and located in low dimensional subspace. In addition, NBI can be represented as a sparse signal in the DCT domain. Since the length of the representation is limited, the coefficients in the DCT domain decay fast. Our interest is to suppress the most significant ones.

In this chapter, the construction of an UWB transmitter is explained first. Pilot symbol assisted modulation combined with DS spread spectrum and TH is applied for signaling purpose. Modeling of the interference source is discussed next. The UWB receiver design follows with two subsections, namely compressive measurements and data detection. The coefficients of the NBI and UWB signal structure are estimated during the first and

second stage of the pilot symbols respectively using MP algorithm. At the end of the chapter, simulation and results are discussed. How CS is applied to achieve the two jobs? This question is answered in the receiver configuration section.

3.2 UWB Transmitter Configuration

The proposed model has an UWB signal path and an interfering signal path, see Figure 3-1. The UWB transmitter consists of data symbols, DS code, TH code, and UWB pulse generators. The NBI transmitter comprises of a NBI symbols generator, followed by a modulation block. The transmitted UWB signal is convolved with the channel impulse response before being received. The received signal is also corrupted by NBI signal and thermal noise. The noisy signal goes through an ideal BPF that has bandwidth and center frequency matched to those of the intended signal to be received.

The system model is an I-UWB system in which binary symbols are represented by a sequence of pulses. The transmitted pulse, $\phi_U(t)$, can have different shapes. Unless otherwise specified we use the second derivative of the Gaussian pulse which has duration time T_{pulse} and unit energy. One binary symbol is transmitted through repeating $\phi_U(t)$ pulses in N_f frames. Hence the duration time for one symbol, T_s , is $T_s = N_f T_f$, where T_f is the frame duration. Each frame is further divides into N_c chips, and each chip has T_c duration.

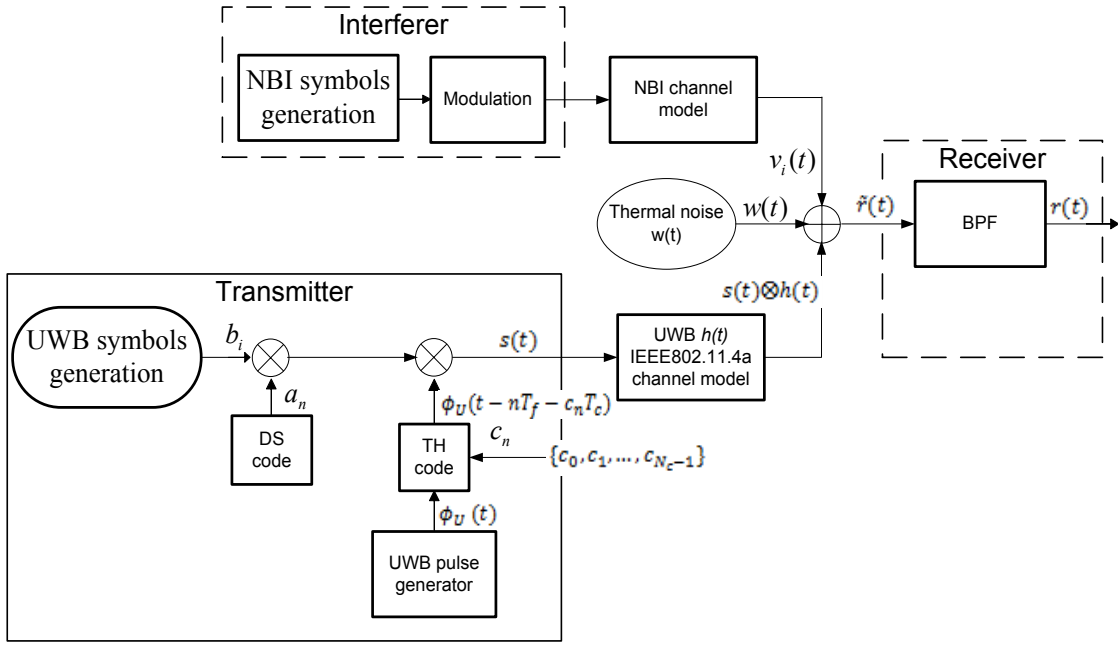


Figure 3-1 Block diagram for the I-UWB system

For signaling purpose, pilot symbol assisted modulation merged with direct sequence spread spectrum (DS) and time hopping (TH) is used. There are N_d symbols in each burst including N_p pilot symbols and N_s data modulated symbols, therefore $N_d = N_p + N_s$. The pilot symbols are divided into three groups, namely N_{p1} , N_{p2} and N_{p3} . The first group symbols are used to estimate the NBI signal subspace, the second group symbols are applied to estimate the UWB signal subspace; and the last group symbols gives information about the channel. During the first pilot symbols, zeros are sent, while ones are sent during the other two. Figure 3-2 represents the signaling scheme for the transmitted signal. Within each frame, the pulse is hopped and appeared in certain chips according to the TH code c_n . It also illustrates the format for one symbol time where the pulse appears in three different positions.

The transmitted signal for one burst can be represented mathematically as:

$$s(t) = \sum_{n=0}^{N_d N_f - 1} a_n b_{\lfloor n/N_f \rfloor} \sqrt{E} \phi_U(t - nT_f - c_n T_c) \quad (3-1)$$

where the DS code is $a_n \in \{\pm 1\}$, $b_{\lfloor n/N_f \rfloor}$ is the binary transmitted symbols, the TH code is $c_n \sim U[0, N_c - 1]$ and E is the energy of the transmitted signal. As we have mentioned before $b_i = 0$ for $i \in [0, N_{p1} - 1]$, $b_i = 1$ for $i \in [N_{p1}, N_p - 1]$, and $b_i = \pm 1$ with equal probability for $i \in [N_p, N_d - 1]$.

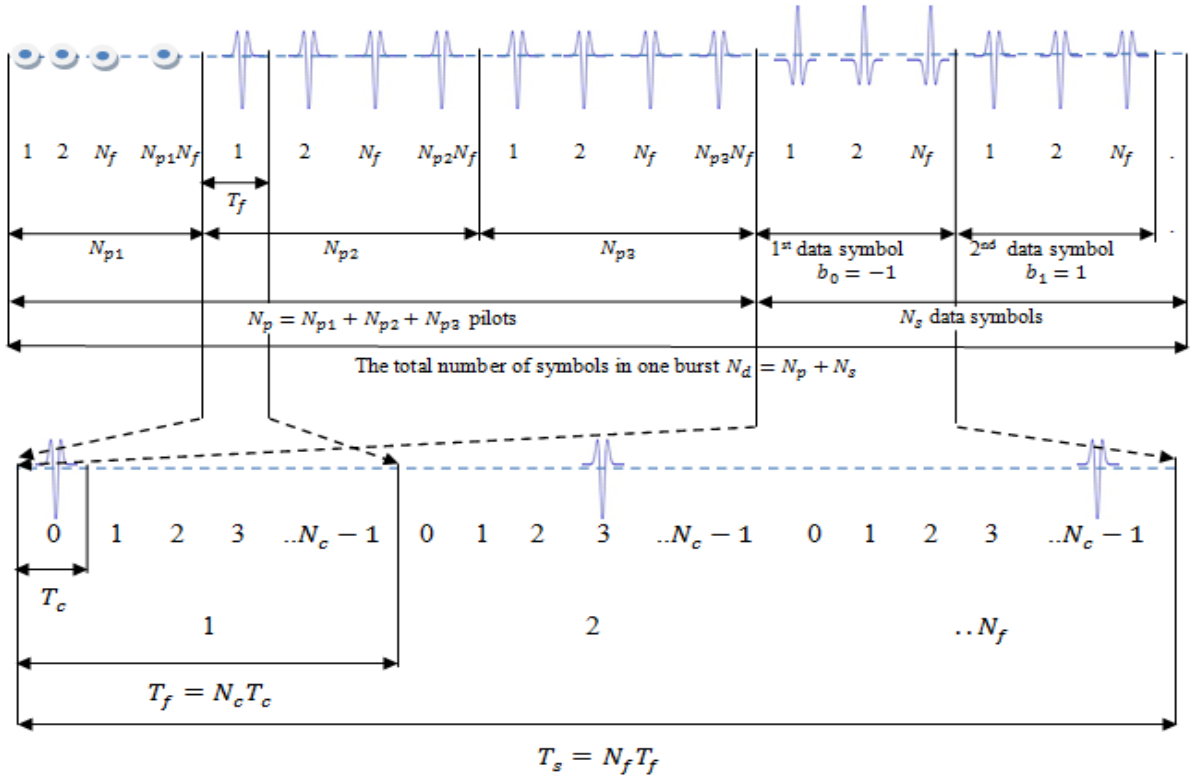


Figure 3-2 Implemented I-UWB signaling scheme

The none-periodicity introduced by the TH code gives a smooth shape for the frequency spectrum and avoids any spectral lines in the transmitted signal. The TH code also

minimizes the interference between users in multiple access technique, where each user has a unique TH code.

The transmitted signal then passes through a multipath communication channel, $h(t)$, having T_{med} maximum excess delay time with L paths, where α_l and τ_l are the attenuation, and delay associated with l^{th} path.

$$h(t) = \sum_{l=0}^{L-1} \alpha_l \delta(t - \tau_l) \quad (3-2)$$

To ignored ISI, the chip duration is fixed such that it is greater than the transmitted pulse duration plus the maximum excess delay of the channel ($T_c > T_{pulse} + T_{med}$). Although the UWB channel could have a large number of paths, only few paths are selected which contains most of the UWB channel's energy, see Figure 2-2. Since there are many insignificant paths, UWB channels can be modeled as sparse channels due to the large transmission bandwidth.

3.3 Interference Configuration

The interference source, $v(t)$, consists of two main blocks as in Figure 3-1. The first block generates the NBI symbols, and then the modulation is performed in the second block. The channel models for the intended UWB signal and the interferer in Figure 3-1 may be the same or may be different. When they are the same, the IEEE802.11.4a model is used with different realizations [Oka09b]. Some researchers used different channel for the interferer such as fast and frequency selective channel [Gom10], [Gom11], or frequency nonselective slow fading channel [Ibr07]. The interfering signal could be

passed through a perfect channel and used additively like AWGN to jam the receiver [Wan08]. When more than one NBI are present, the interference signal, $v_i(t)$ for $i = 1, 2, \dots, N_v - 1$, is modeled as the sum of N_v interferers.

3.4 Receiver Configuration

There are three main stages employed at the receiver side. The effect of the NBI is suppressed by designing a measurement matrix that uses the estimated NBI as a null subspace. In the first stage, the received signal is projected into a random measurement matrix. Since no UWB symbols are transmitted, the NBI's coefficients are estimated using CS. Subsequently, these coefficients are used to obtain the NBI signal subspace. In the next stage, the UWB signal subspace is constructed by making use of the projection matrix of the estimated NBI subspace through CS. Finally, a measurement matrix that combines the estimated null subspace of the NBI and the constructed UWB signal subspace is designed. This matrix has the ability to collect most of the received UWB signal energy as well as suppress the NBI if present.

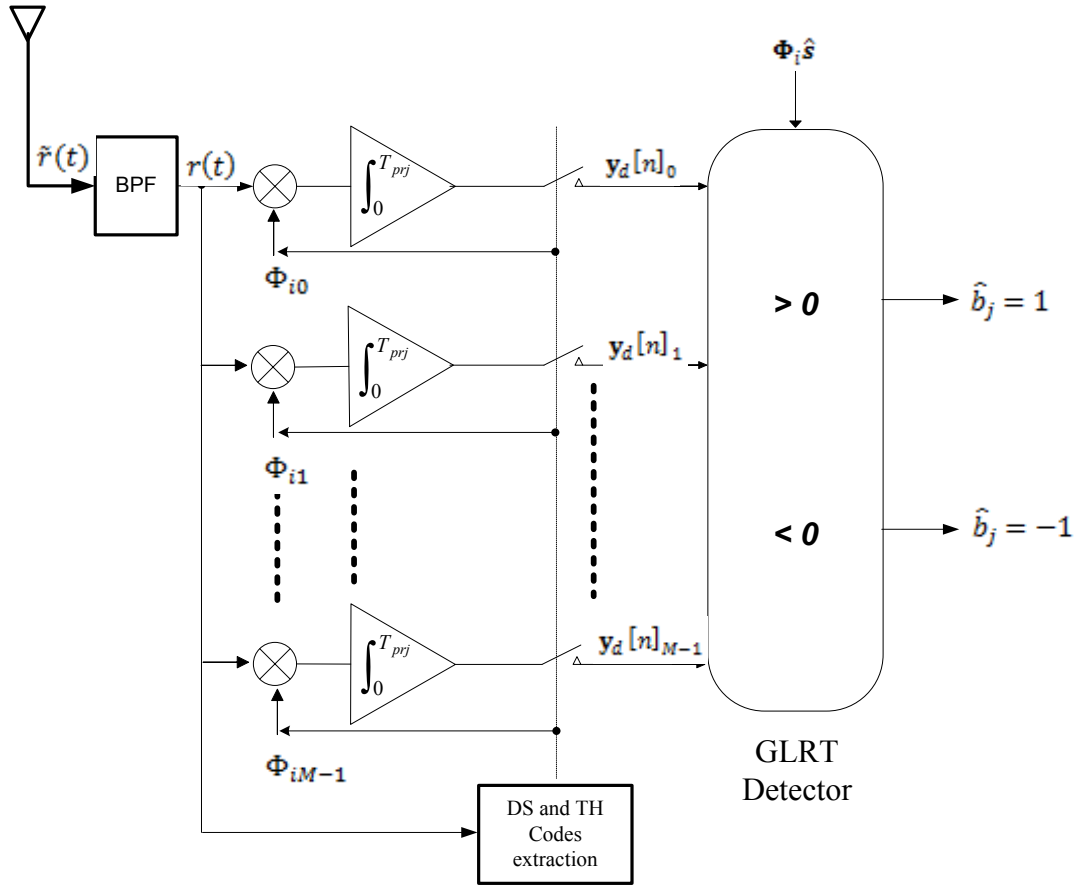


Figure 3-3 I-UWB receiver with GLRT detector

The receiver basically consists of BPF, M mixer-integrators, and generalized likelihood ratio test (GLRT) detector. The received UWB signal is contaminated by white Gaussian noise $w(t)$ with two sided power spectral density (PSD), $\frac{N_0}{2}$, and narrowband interference, $v(t)$. The filter has one-sided bandwidth, Ω , center frequency, f_c , and it affects only the noise. The output noise becomes $\tilde{w}(t)$, whereas the desired and interfering signals aren't distorted. The received signal at the output of the BPF is:

$$r(t) = \int_0^t h(t - \tau)s(\tau)d\tau + v(t) + \tilde{w}(t) \quad (3-3)$$

3.4.1 Compressive Measurements

The received signal is processed by three different measurement matrices; denoted by $\Phi_i, i = 1,2,3$, each of dimension $M \times N$. They are constructed to achieve the mitigation and demodulation requirements.

Full knowledge of the direct sequence code, a_n , and the time hopping code, c_n , is assumed at the receiver side. M Mixer-integrators are employed to get the compressive measurements, with integration period, T_{prj} , set as $T_{Pulse} + T_{med} \geq T_{prj} \geq T_{Pulse}$. The compressive measurements for the n^{th} frame have to be started at $t = c_n T_c + (n - 1)T_f$, and ended at $t + T_{prj}$. At this time the mixer-integrators are sampled at the same time, and then they reset to zero to be ready for the next frame.

The sampling frequency should fulfill the relation $f_s = 2 \times (f_c + \frac{\Omega}{2})$, hence the data has length of $N = T_{prj} f_s$. Since we use CS technique for two purposes which are ADC speed reduction and signal reconstruction, the sampling frequency becomes large because the transmitted signal is in the order of GHz. Actually, we don't sample at rate f_s because only the projected data goes through the ADC.

3.4.1.1 NBI Subspace Estimation

During the first pilot group symbols, the received signal get multiplied by Φ_1 which has independent and identically distributed (i.i.d.) Bernoulli distribution [Wan08]. In this stage, no UWB symbols are transmitted and the subspace of the NBI signal can be estimated. After multiplication by the direct sequence code, the compressive

measurements of the received n^{th} frame during the first pilot symbols, $\mathbf{y}_1[n]$, can be written as:

$$\mathbf{y}_1[n] = a_n \mathbf{\Phi}_1 \mathbf{r}[n] = a_n \mathbf{\Phi}_1 \mathbf{v}[n] + a_n \mathbf{\Phi}_1 \mathbf{w}[n], \quad n = 0, \dots, N_{p1} N_f - 1 \quad (3-4)$$

where $\mathbf{r}[n]$ is the sampled received signal of the n^{th} frame of size $N \times 1$. The digitized NBI and the digitized noise are $\mathbf{v}[n]$ and $\mathbf{w}[n]$ respectively, both of size $N \times 1$. The output $\mathbf{y}_1[n]$ is a vector of size $M \times 1$. The previous equation can be rewritten as:

$$\mathbf{y}_1[n] = a_n \mathbf{\Phi}_1 \mathbf{C} \zeta[n] + a_n \mathbf{\Phi}_1 \mathbf{w}[n] \quad (3-5)$$

where $\mathbf{C} = [\mathbf{c}_0, \mathbf{c}_1, \dots, \mathbf{c}_{N-1}]$ is the inverse DCT matrix, and $\zeta[n]$ is the DCT representation of $\mathbf{v}[n]$. The estimated NBI coefficients, $\hat{\zeta}[n]$, can be obtained in this stage based on $\mathbf{y}_1[n]$ because the NBI has sparse representation in the DCT domain. Matching Pursuit (MP) algorithm [Wan07b] is used to estimate those coefficients.

Suppose that $\tilde{\zeta}$ is defined as $\tilde{\zeta} = \sum_{n=0}^{N_{p1} N_f - 1} |\hat{\zeta}[n]|$, and $\zeta_{max} = \max\{\tilde{\zeta}_0, \tilde{\zeta}_1, \dots, \tilde{\zeta}_{N-1}\}$. The NBI subspace can be approximated as $\mathbf{C}_v = [\mathbf{c}_{n_0}, \mathbf{c}_{n_1}, \dots, \mathbf{c}_{n_J}]$, where $n_j \in \{i \mid |\zeta_i| > \mu \zeta_{max}\}$. The most significant coefficients of the NBI in the DCT domain are suppressed by controlling the interference threshold, μ . If we assign very large value for μ , the constructed NBI subspace won't suppress the interference effect. If it is too small, we will do unnecessary suppression for the zero coefficients since the NBI is sparse. The projection matrix of the NBI subspace signal is constructed as:

$$\mathbf{P}_v^\perp = \mathbf{I}_N - \mathbf{C}_v (\mathbf{C}_v^T \mathbf{C}_v)^{-1} \mathbf{C}_v^T \quad (3-6)$$

3.4.1.2 UWB Subspace Estimation

The received signal is then multiplied by the second measurement matrix, Φ_2 , during the second group pilot symbols [Wan07a], [Wan07b], [Wan08]. The UWB signal structure or subspace is estimated in this stage. During the second pilot symbols, the compressive measurements will be:

$$\begin{aligned} \mathbf{y}_2[n] &= a_n \Phi_2 \mathbf{r}[n] = \Phi_2 \mathbf{s} + a_{n+\Delta N} \Phi_2 \mathbf{v}[n + \Delta N] + a_{n+\Delta N} \Phi_2 \mathbf{w}[n + \Delta N], \\ n &= 0, \dots, N_{p2}N_f - 1 \end{aligned} \quad (3-7)$$

where $\Delta N = N_{p1}N_f$, and $\mathbf{s}_{N \times 1}$ is the digitized noise free received signal $h(t) \otimes \phi_U(t)$ within T_{prj} , where \otimes represents the convolution. The second measurement matrix is constructed as; $\Phi_2 = \Phi_1 \mathbf{P}^{\perp}$, consequently $\Phi_2 \mathbf{v}[n + \Delta N] \approx 0$. As a result, the effect of the NBI is suppressed. The UWB signal subspace is constructed from $\mathbf{y}_2[n]$ using MP algorithm. Averaging the second compressive measurement to reduce the noise is done using:

$$\bar{\mathbf{y}}_2 = \frac{1}{N_{p2}N_f} \sum_{n=0}^{N_{p2}N_f-1} \mathbf{y}_2[n] \quad (3-8)$$

Because of the multipath channel, the received UWB signal is a shifted and scaled version of the transmitted UWB pulse, $\phi_U(t)$. A dictionary, Ψ_c , can be designed such that each column is a time shifted version of $\phi_U(t)$. Let Ψ_u be the sampled form of Ψ_c with a rate of f_s . Each column of Ψ_u is normalized to have a unit energy. The j^{th} column is given by:

$$\Psi_{uj}(n) = \phi_U(n/f_s - j/f_s), n = 0, 1, \dots, f_s T_{prj} - 1 \quad (3-9)$$

Only K paths with the largest gains out of the total UWB channel paths are considered. This gives the received signal sparse representation (K -sparse). As a result, the UWB signal structure can be represented as $\mathbf{s} = \mathbf{H}_u \boldsymbol{\theta}_u$ where \mathbf{H}_u is a matrix of dimension $N \times K$ constructed from K relevant column vectors of Ψ_u , and $\boldsymbol{\theta}_u$ is a $K \times 1$ vector of non-zero coefficients. Given Ψ_u, Φ_2 and \mathbf{y}_2 , MP algorithm [Wan07b] can be used to estimate the K vectors from Ψ_u that construct the UWB signal subspace $\hat{\mathbf{H}}_u$.

3.4.2 Data Detection

Finally, the third group pilot symbols and the data modulated symbols are multiplied by the third measurement matrix Φ_3 . This matrix has the ability to collect most of the received UWB signal energy as well as suppress the NBI if present. The construction of Φ_3 utilizes the NBI and UWB subspaces using the formula [Wan07b], [Wan08]:

$$\Phi_3 = \mathbf{G}(\tilde{\mathbf{H}}_u^T \tilde{\mathbf{H}}_u)^{-1} \tilde{\mathbf{H}}_u^T \quad (3-10)$$

where \mathbf{G} is an i.i.d. random matrix of dimension $M \times N$, and $\tilde{\mathbf{H}}_u = \mathbf{P}_v^\perp \hat{\mathbf{H}}_u$. The compressive measurements multiplied by a_n during both the third pilot group symbols and the data modulated symbols are given respectively by:

$$\mathbf{y}_3[n] = \Phi_3 \mathbf{s} + a_{n+\tilde{\Delta}N} \Phi_3 \mathbf{v}[n + \tilde{\Delta}N] + a_{n+\tilde{\Delta}N} \Phi_3 \mathbf{w}[n + \tilde{\Delta}N], n = 0, \dots, N_{p3} N_f - 1 \quad (3-11)$$

$$\mathbf{y}_{d|j}[n] = b_j \Phi_3 \mathbf{s} + a_{n+\hat{\Delta}N} \Phi_3 \mathbf{v}[n + \hat{\Delta}N] + a_{n+\tilde{\Delta}N} \Phi_3 \mathbf{w}[n + \hat{\Delta}N], n = 0, \dots, N_f - 1 \quad (3-12)$$

where $\tilde{\Delta}N = (N_{p1} + N_{p2})T_f$, $\hat{\Delta}N = (N_p + j)N_f$, and $b_j \in \{\pm 1\}$ is the data modulated with $j = 0, 1, \dots, N_s - 1$. The term $\Phi_3 \mathbf{s}$ gives information about the channel and it can be obtained from $\mathbf{y}_3[n]$ within the same burst. Averaging $\mathbf{y}_3[n]$ over multiple frames is used as a template to demodulate the transmitted symbols. The maximum likelihood estimation of $\Phi_3 \mathbf{s}$ is given by:

$$\Phi_3 \hat{\mathbf{s}} = \frac{1}{N_{p3}N_f} \sum_{n=0}^{N_{p3}N_f-1} \mathbf{y}_3[n] = \Phi_3 \mathbf{s} + a_{n+\tilde{\Delta}N} \bar{\mathbf{w}} \quad (3-13)$$

where $\bar{\mathbf{w}} = \frac{1}{N_{p3}N_f} \sum_{n=0}^{N_{p3}N_f-1} \mathbf{v}[n + \tilde{\Delta}N] + \mathbf{w}[n + \tilde{\Delta}N]$ is a vector of length $N \times 1$ compromises of the sum of a WGN with variance $\frac{N_0\Omega}{N_{p3}N_f}$ and the residual NBI which can be also modeled as Gaussian noise [Wan07a],[Wan08].

Since the transmitter sends $b_j \in \{\pm 1\}$ with equal probability, two hypotheses must be distinguished by the detector:

$$\begin{aligned} \mathcal{H}_0 : \mathbf{y}_{d|j}[n] &= -\Phi_3 \mathbf{s} + a_{n+\hat{\Delta}N} \Phi_3 \mathbf{v}[n + \hat{\Delta}N] + a_{n+\hat{\Delta}N} \Phi_3 \mathbf{w}[n + \hat{\Delta}N], (b_j = -1), \\ n &= 0, 1, \dots, N_f - 1 \end{aligned} \quad (3-14)$$

$$\begin{aligned} \mathcal{H}_1 : \mathbf{y}_{d|j}[n] &= \Phi_3 \mathbf{s} + a_{n+\hat{\Delta}N} \Phi_3 \mathbf{v}[n + \hat{\Delta}N] + a_{n+\hat{\Delta}N} \Phi_3 \mathbf{w}[n + \hat{\Delta}N], (b_j = 1), \\ n &= 0, 1, \dots, N_f - 1 \end{aligned} \quad (3-15)$$

The statistics of the GLRT detector is defined as:

$$T(\mathbf{y}_{d|j}) = (\Phi_3 \mathbf{s} + \Phi_3 \zeta_p)^T (N_0 \Omega \Phi_3 \Phi_3^T)^{-1} (b_j \Phi_3 \mathbf{s} + \Phi_3 \zeta_d) \quad (3-16)$$

where $\zeta_p = \frac{1}{N_{p_3 N_f}} \sum_{n=0}^{N_{p_3 N_f}-1} \mathbf{w}[n + \hat{\Delta}N] + \mathbf{v}[n + \hat{\Delta}N]$, and $\zeta_d = \frac{1}{N_f} \sum_{n=0}^{N_f-1} \mathbf{w}[n + \tilde{\Delta}N] + \mathbf{v}[n + \tilde{\Delta}N]$.

The detector estimates $\hat{b}_j = 1$ if $T(\mathbf{y}_{d|j}) > 0$; otherwise $\hat{b}_j = -1$. The first bracket in the previous equation is the average of $\mathbf{y}_3[n]$ over $N_{p_3 N_f}$ frames used as a template, whereas the last bracket represents the average of the measurement vector during the data transmission over N_f frames.

Suppose that there are $m = 1, 2, \dots, N_u$ secondary users in addition to the primary user. The users transmit their information at the same time with the intended one and there is no delay of propagation, see Figure 3-4. Each user has its own DS code, TH code, and data. Therefore, collision or interference occurs if the TH codes are matched. This may amplify the intended pulse, reduce its level or make it zero depend on the DS code, the information of the interfering users, the number of users as well as the TH codes relative to the current transmitted pulse of the intended user. The k^{th} user has transmitted waveform over a burst represented by:

$$s^k(t) = \sum_{n=0}^{N_a N_f - 1} a_n^k b_{[n/N_f]}^k \sqrt{E} \phi_U(t - nT_f - c_n^k T_c) \quad (3-17)$$

where a_n^k and c_n^k are the DS, and the TH codes for the k^{th} user. The other parameters are similar to those related to the intended user.

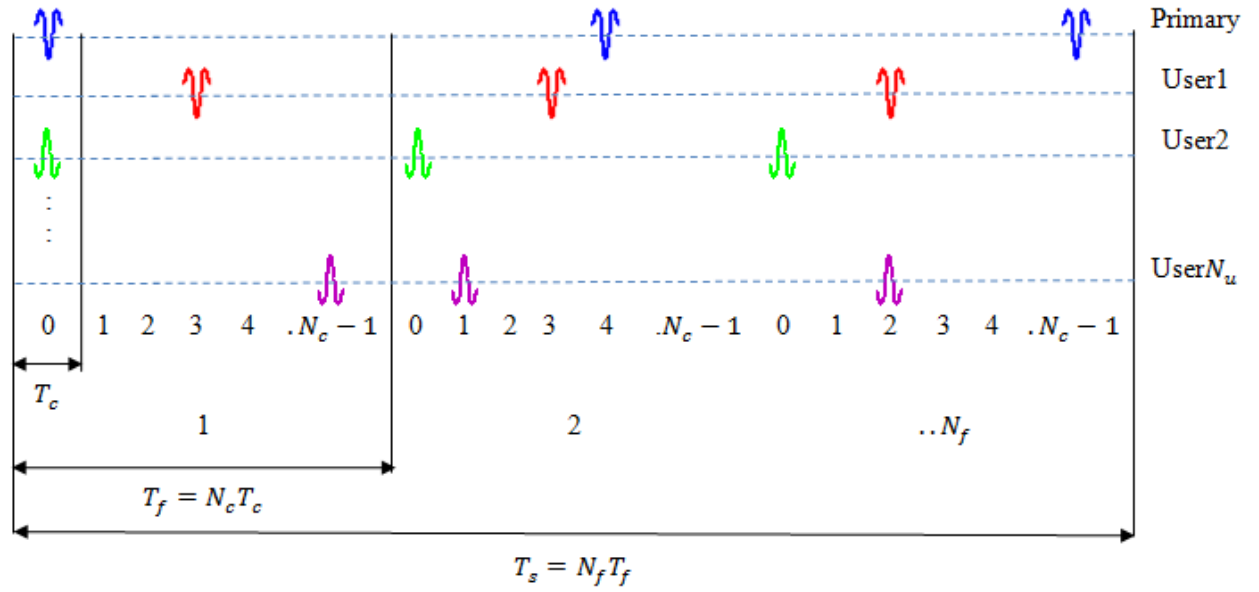


Figure 3-4 Distribution of pulses transmitted over time – Frames and chips are synchronized for all users

In a network, the average number of bits that are transmitted successfully or average rate of successful bit delivery is known as the throughput. In multiuser systems, the throughput decreases as the number of users increases. Throughput can be represented mathematically using the following formula:

$$\text{Throughput} = (1 - \text{BER})R_s \quad (3-18)$$

where R_s is the symbol rate in bps. In the simulation, the throughput is calculated for different number of the secondary users N_u .

3.5 Simulation and Results

In this section the mitigation of NBI in trained UWB systems is evaluated. The diagram in Figure 3-5 depicts the main steps that are used to investigate the mitigation process based on CS. As we've mentioned the transmission sequence contains the three groups of

pilot symbols, and the data modulated symbols. DS-TH is used for signaling where each symbol is repeated in N_f frames at different chips. The signal then goes through an IEEE802.11.4a channel. The NBI system also generates its own symbols, and sends them over an NBI channel.

At the receiver side, the received UWB signal is captured using BPF. The measurement is taken using three measurement matrices. First the corrupted received signal at the BPF's output is multiplied by Φ_1 which has Bernoulli distribution. This measurement vector is used to estimate the NBI subspace using CS. Second, the received signal is multiplied by Φ_2 which is constructed according to the estimated NBI subspace. Based on this measurement vector, the UWB signal subspace is estimated using CS. Third, the received signal is multiplied by Φ_3 that has the ability to null out the NBI and collect the UWB's signal energy. After averaging over the third group pilot symbols, the measurement vector now is used as a template in the demodulation process. Again the received signal is multiplied by Φ_3 but the measurement vector is applied as the input to the GLRT detector with previous template. Finally, the detector does the decision process.

An investigation of the pilot symbols distribution is considered in the first part of the simulation. Then we fix the distribution of the pilot symbol and study different related parameters such as the number of frames per symbol, N_f , and the interference threshold, μ . After that, the performance of the system is evaluated under the effect of different unlicensed and licensed NBIs. Finally, the system is tested in the presence of both NBI and multiuser interference. In addition, system throughput is examined under the effect of multiuser interference as well as NBI's effect.

To investigate the best distribution of pilot symbols in the presence of NBI, the following parameters are selected. The transmitted signal is the second derivative Gaussian pulse with duration $T_{pulse} = 0.75$ ns and center frequency, $f_{cU} = 3$ GHz. The bandwidth of the receiver BPF is 8 GHz; hence the sampling frequency is $f_s = 16$ GHz. The IEEE802.11.4a Channel Model 1 (CM1) [Mol06] which represents residential line-of-sight (LOS) environment is used. One thousand symbols ($N_d = 1000$) are transmitted over many realizations randomly generated from CM1. The mean root square delay spread is about 17 nanosecond, and the channel response is normalized to have unit energy. The projection time covers the whole received multipath arrivals. The sampling rate is reduced to $\frac{M}{N} = 20\%$ through CS, where N is the length of the received signal. The chip duration is $T_c = 32$ ns, and the number of chips is $N_c = 25$. The frame duration is $T_f = T_c N_c = 800$ ns, and the number of frames per symbol is $N_f = 5$, therefore $T_s = T_f N_f = 4$ μ s. The delivered data rate is $R_s = 250$ kbps. The total number of pilot symbols is $N_p = 45$ and interference threshold, $\mu = 10^{-2}$.

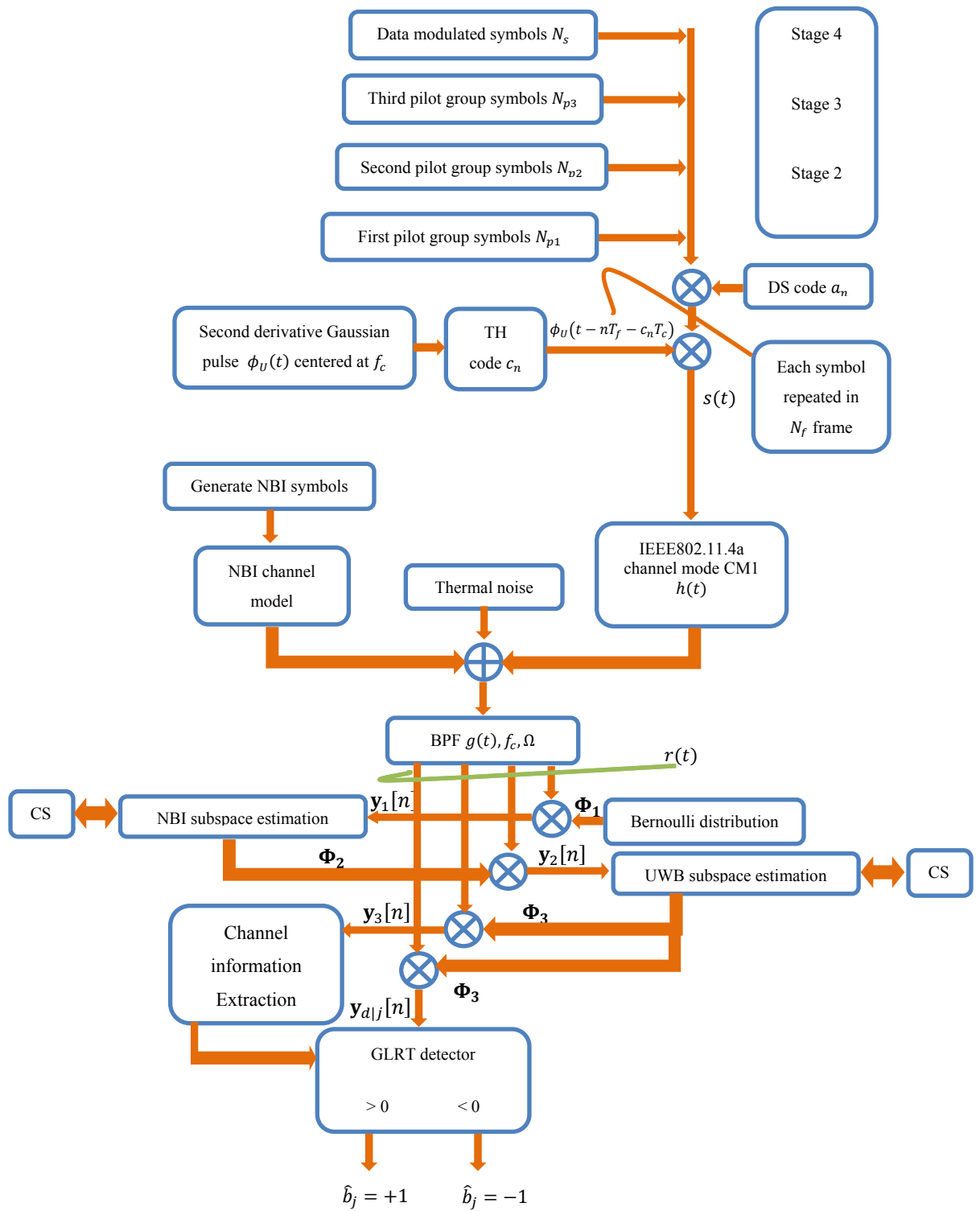


Figure 3-5 Flowchart for the main steps of the UWB system with training

The performance is evaluated for $\text{SNR} = -21$ dB and $\text{SIR} = -20$ dB. All those parameters are fixed in the simulation unless stated otherwise. The signal power is calculated over the whole time spanned by the multipath arrivals and the noise is added over the total duration time. The added noise will only have effect during the signaling time. This is why communication can be achieved at relatively low SNR.

In the following, we consider three different cases. In every case, we fix one pilot at a time and trade off the remaining two to keep N_p constant. The fixed pilot is assigned moderate value. The results are depicted in three figures. The figures are divided into two subplots. The difference between the subplots is in the center frequency of the NBIs. The center frequencies of the NBIs are either $f_{c11} = f_{c12} = 1.6$ GHz or $f_{c11} = f_{cU} = 3$ GHz, $f_{c12} = 1.6$ GHz. Each subplot contains three different NBIs with different bandwidth combinations. Three different bandwidth combinations are investigated: $(\Omega_{11} = 20$ MHz, $\Omega_{12} = 10$ MHz), $(\Omega_{11} = 40$ MHz and $\Omega_{12} = 20$ MHz) and $(\Omega_{11} = 100$ MHz $\Omega_{12} = 50$ MHz). For fair comparison all interferers are adjusted to have the same power. The results are illustrated in terms of BER as a function of N_{p1} or N_{p2} . Note as the number of symbols in one group increase the other will decrease to keep $N_p = 45$.

First, the number of pilot symbols in the third group, $N_{p3} = 10$, is fixed to evaluate the number of pilots required for subspaces estimation for the NBI and UWB signals, see Figure 3-6. The BER curves as function of N_{p1} can be divided into three different regions. For values of N_{p1} between 0 and 5 there is a gradual improvement in the system performance. From 5 to 15 symbols the tradeoff between N_{p1} and N_{p2} has a minimal

effect on the performance. As we increase N_{p1} more than 15 the performance starts to degrade at a slow pace. The symbols in N_{p1} are necessary to reduce the NBI's effect, however communication can still be achieved at $N_{p2} = 0$.

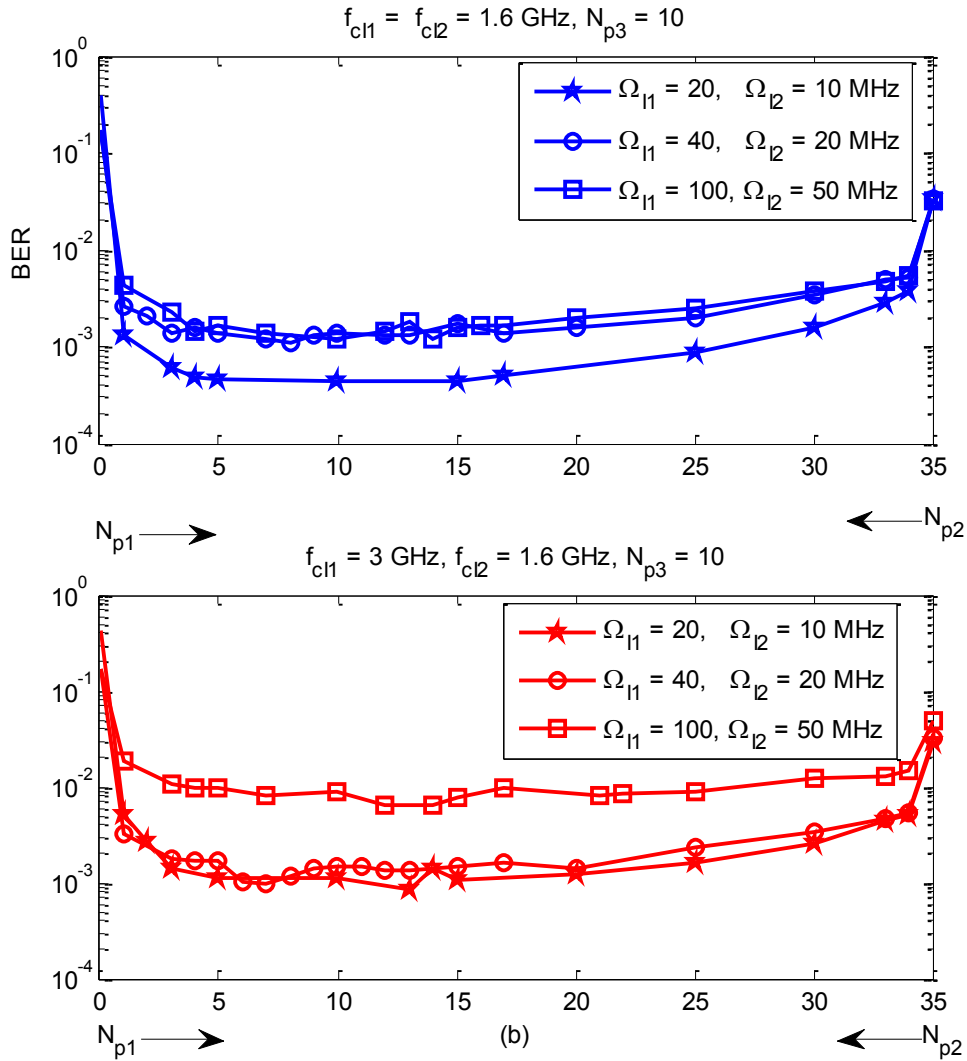


Figure 3-6 The BER as a function of N_{p1} and N_{p2}

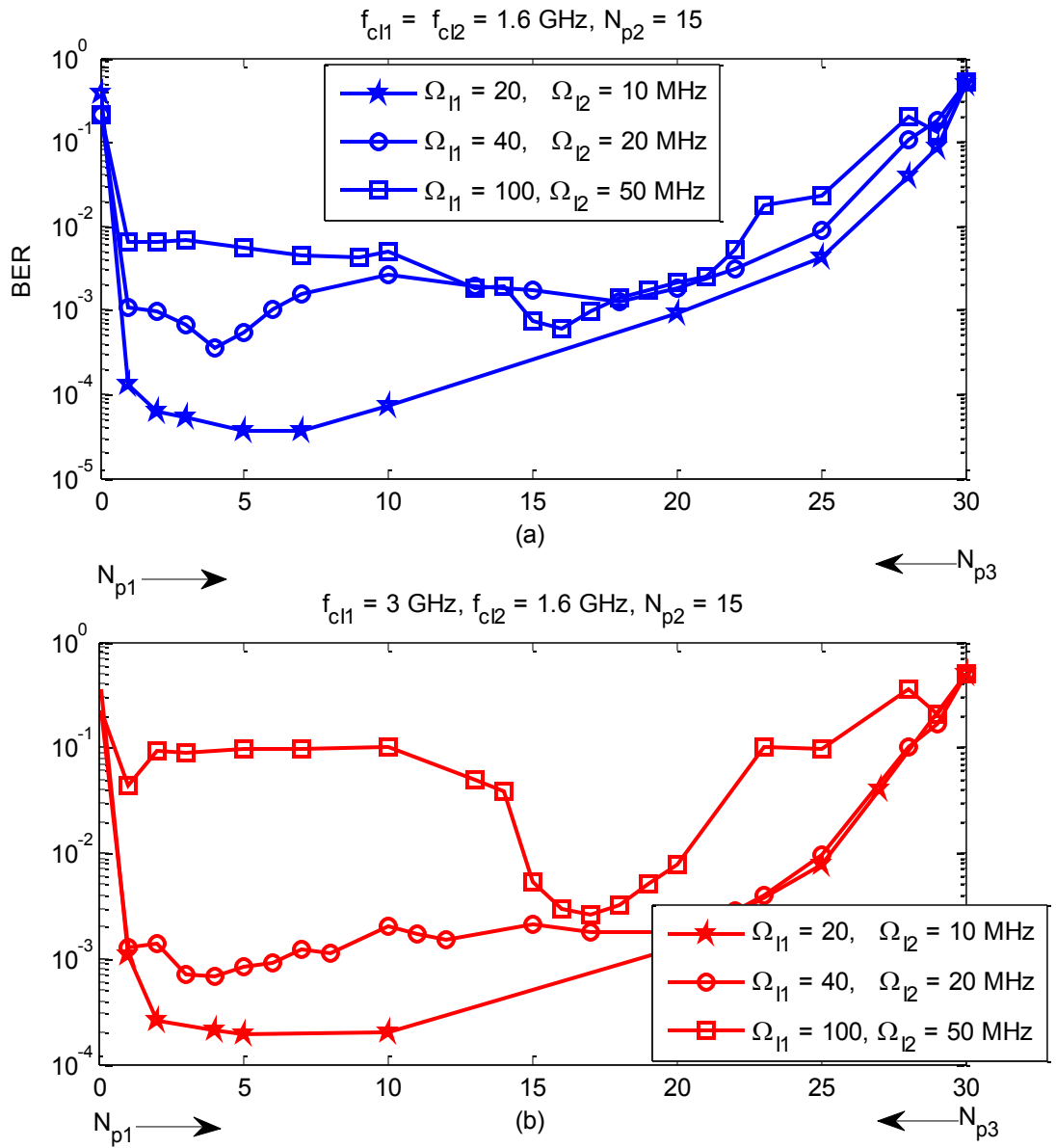


Figure 3-7 The BER as a function of N_{p1} and N_{p3}

In the second case, the NBI signal subspace estimation and the acquired channel information are investigated by fixing $N_{p2} = 15$. Figure 3-7 indicates that no communication is possible when neither NBI signal subspace estimation nor channel

information is being used. The NBI that has large bandwidth ($\Omega_{11} = 100$ MHz $\Omega_{12} = 50$ MHz) becomes less sparse since more coefficients appear in the DCT domain. Consequently, more symbols are required in N_{p1} to optimize the BER as the two subplots demonstrate. The situation is even worse when the two frequencies are unequal. Increasing N_{p3} results in a gradual reduction in the BER provided that N_{p1} is not less than the minimum requirements. For the simulated scenarios, a minimum of $N_{p1} = 5$ is required.

Finally, the UWB signal subspace estimation and the channel information are studied when N_{p1} is fixed as depicted in Figure 3-8. The third group, N_{p3} , must not be zero in order to know the channel characteristics and consequently have an acceptable system performance. On the other hand, communications can be established at $N_{p2} = 0$ in all bandwidth combinations. For the simulated scenarios, the BER decreases as we increase N_{p2} until $N_{p2} = 15$, and $N_{p3} = 25$.

From the previous simulations, the optimal distribution is a weak function of the center frequency or bandwidth of the NBI. The system performance is a strong function of N_{p3} as Figure 3-7 and Figure 3-8 illustrate. For limited power interference, the BER degrades as we shift the center frequency of the NBI to $f_{c11} = f_{cU}$. The BER degrades as we shift the center frequency of the NBI to $f_{c11} = f_{cU}$. However, the degradation due to increasing the NBI's bandwidth together with shifting the NBI's center frequency is larger because it results in more significant coefficients of the NBI in the DCT domain. The sparsity is also affected and subsequently, the mitigation of NBI won't be the same.

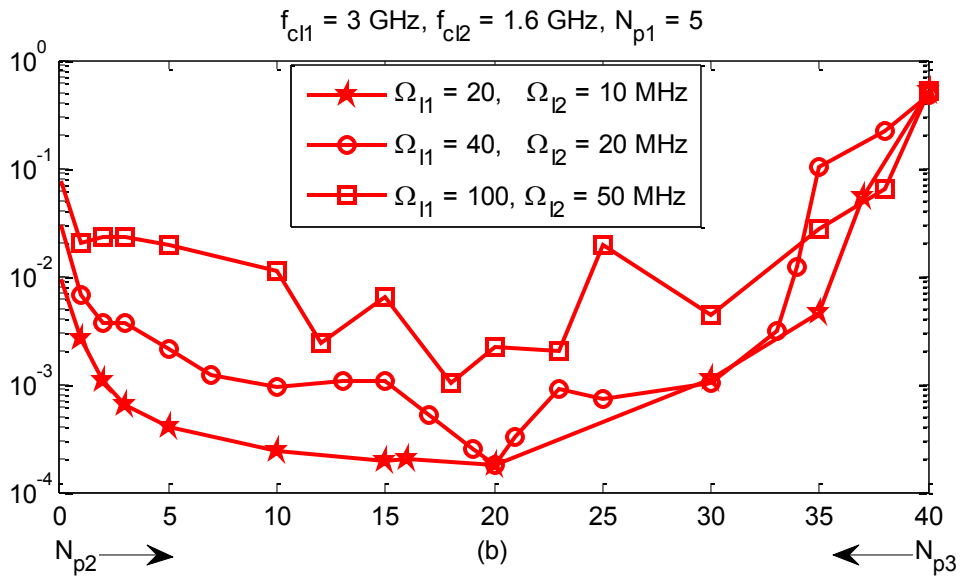
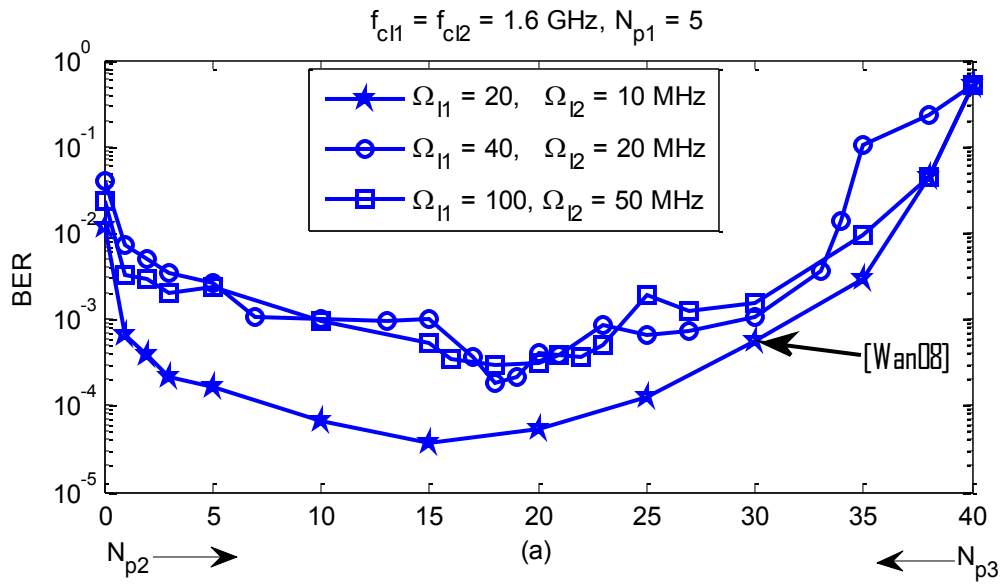


Figure 3-8 The BER as a function of N_{p2} and N_{p3}

The distribution of the pilot symbols in [Wan08] for the NBI that has $f_{c11} = f_{c12} = 1.6 \text{ GHz}$ and $(\Omega_{11} = 20 \text{ MHz}, \Omega_{12} = 10 \text{ MHz})$, was $N_{p1} = 5, N_{p2} = 30$ and $N_{p3} = 10$ which isn't optimal as Figure 3-6 shows. Based on the simulations, the distribution at

$N_{p1} = 5, N_{p2} = 15$ and $N_{p3} = 25$ leads to better performance as shown in Figure 3-7 and Figure 3-8.

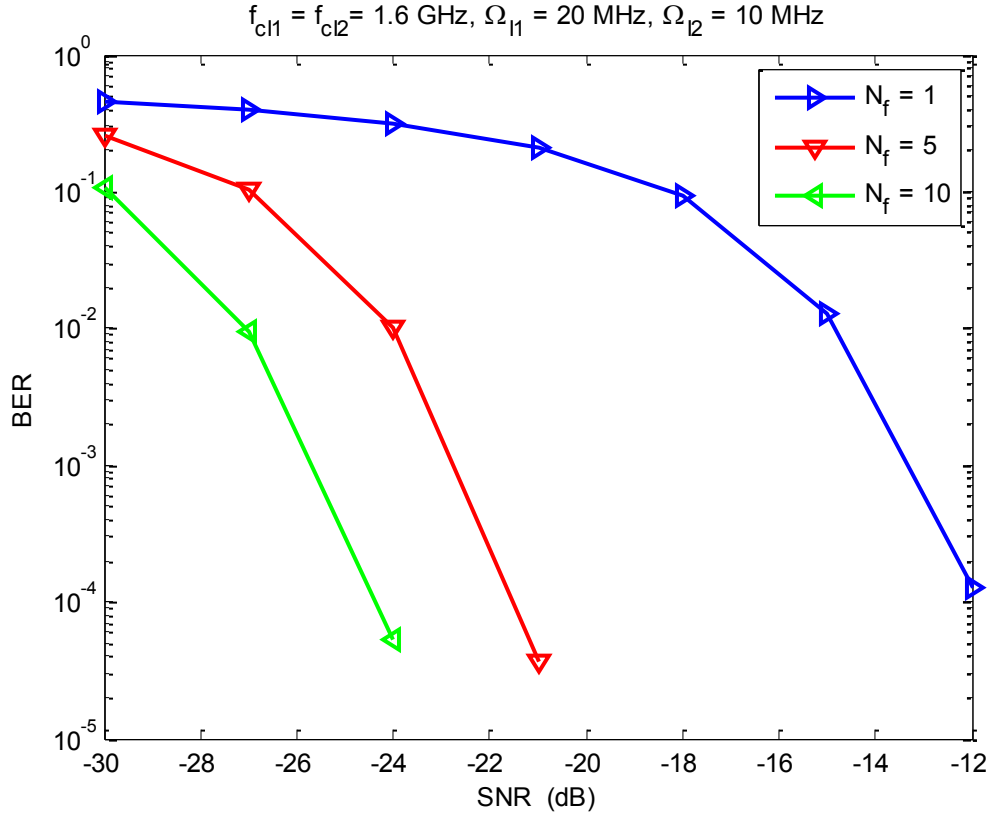


Figure 3-9 BER with different frame number

In the remaining simulations, we fix the pilot symbols distribution according to our previous investigations as: $N_{p1} = 5, N_{p2} = 15$ and $N_{p3} = 25$. The effect of the frame repetition, N_f , is examined in Figure 3-9. The performance is evaluated for $f_{cl1} = f_{cl2} = 1.6$ GHz with ($\Omega_{I1} = 20$ MHz and $\Omega_{I2} = 10$ MHz). Similar behavior is expected for the other combinations of interferers. The BER is reduced as more frames being used to represent one symbol. With no repetition, we need around 9 dB more to have similar performance of $N_f = 5$. The simulation shows that, increasing N_f from 5 to 10 saves

around 3 dB at very low BER. Note that this is not affair comparison as the rate is reduced by a factor of 2.

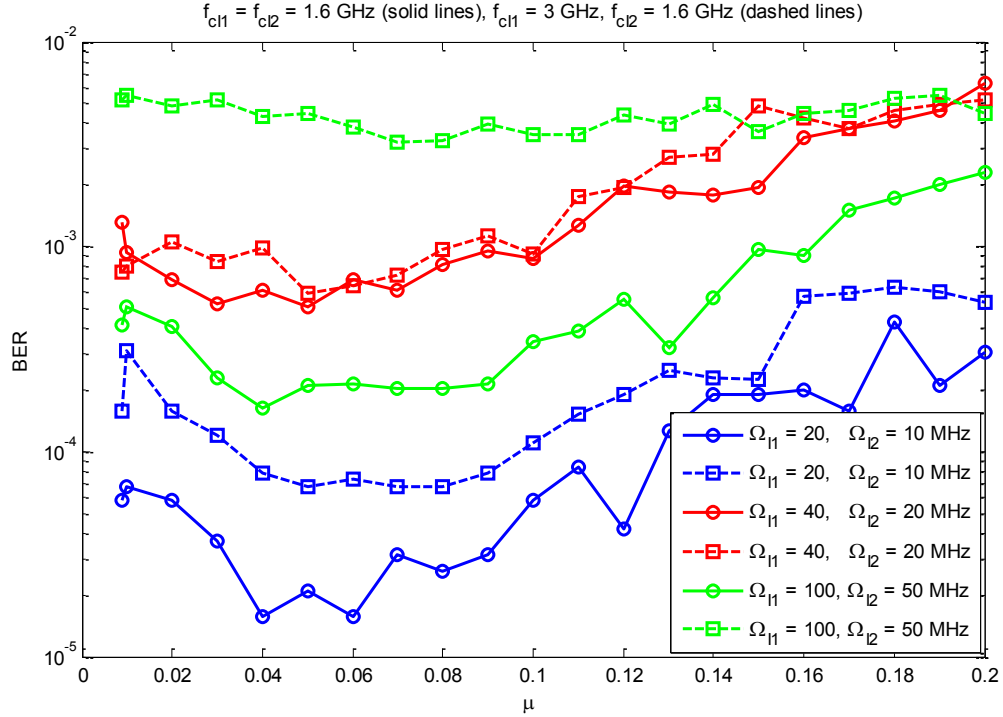


Figure 3-10 The BER as a function of the interference threshold

In the preceding simulations, the interference threshold, $\mu = 10^{-2}$, was fixed. The effect of this factor on the system performance is plotted in Figure 3-10. For the region where $0 < \mu < 0.04$, the performance improves as we increase μ . The small improvement is because the suppressed coefficients used to construct the NBI subspace is decreased. Few columns are being involved in the construction of the estimated NBI subspace, the performance enhances. Herein we eliminate the noisy coefficients and consequently the noise level is reduced. This is equivalent to avoid picking up the non-significant coefficients and avoid collecting more noise. For $\mu > 0.1$, the performance starts to

degrade. In those range, the constructed NBI subspace is not enough to suppress the interference effect. In other words, few NBI's coefficients are involved in the construction process.

The third part of the simulation addresses different NBI types that might jam the UWB systems. Different NBIs are studied under the same distribution of the pilot symbol. The unlicensed NBIs to be investigated are considered as the sum of two QPSK signals. The effect of the center frequency of the NBI and its bandwidth are studied.

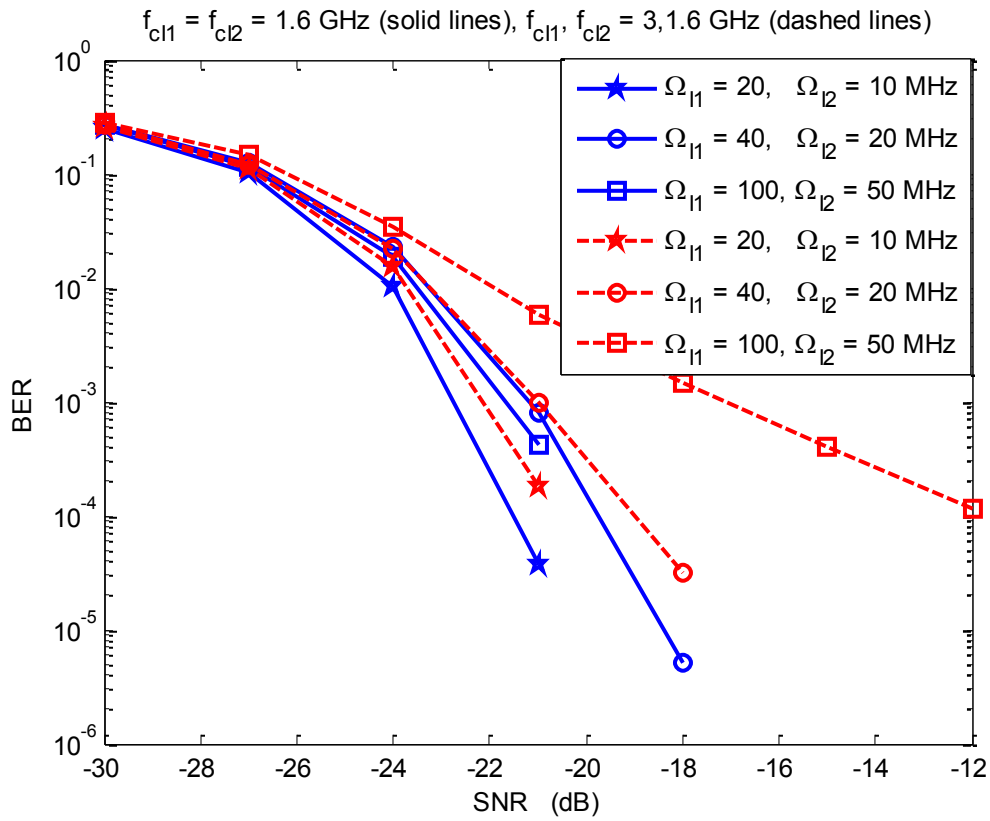


Figure 3-11 System performance for different NBI

Figure 3-11 demonstrates six different scenarios. Solid lines are used to represent the three traces where the center frequencies of the two QPSK jammers are $f_{c11} = f_{c12} = 1.6$ GHz, while dashed lines are used when the center frequencies are 3, and 1.6 GHz. When one center frequency of the NBI ($\Omega_{11} = 20$ MHz, $\Omega_{12} = 10$ MHz) matches f_{cU} , this results in a loss of 1 dB at $\text{BER} = 1 \times 10^{-4}$. For the $f_{c11} = f_{c12} = 1.6$ GHz NBI, we need no more than 2 dB to work at $\text{BER} = 10^{-4}$ if the bandwidth of the NBI increases from ($\Omega_{11} = 20$ MHz, $\Omega_{12} = 10$ MHz) to ($\Omega_{11} = 100$ MHz, $\Omega_{12} = 50$ MHz). However, we need more than 8 dB if the bandwidth of the NBI increases from ($\Omega_{11} = 20$ MHz, $\Omega_{12} = 10$ MHz) to ($\Omega_{11} = 100$ MHz, $\Omega_{12} = 50$ MHz) and at the same time f_{c11} changes to match f_{cU} . The considered distribution of the pilot symbols isn't optimal for the last case; hence we get such huge difference.

Next, we investigate the system performance for different licensed NBIs. In Figure 3-12, we consider WiMAX, IEEE802.11a WLAN (WLANa), IEEE802.11b WLAN (WLANb), and Bluetooth. Those NBIs have fixed center frequencies and bandwidths according to the regulation as discussed in Section 2.4.2.

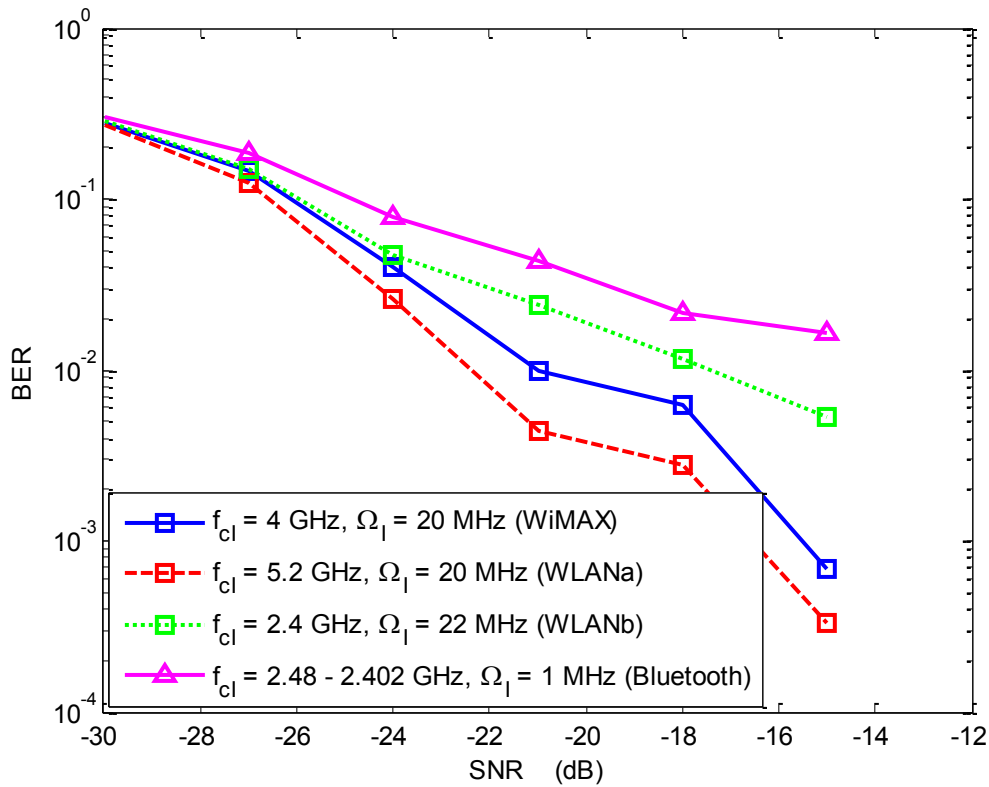


Figure 3-12 The performance for licensed NBIs

WLANa signal has the least effect in system performance because it operates at 5.2 GHz away from the center frequency of the transmitted pulse at $f_{CU} = 3$ GHz, see Figure 3-12. On the other hand, the performance degradation due to WLANb at 2.4 GHz is large which is very close to our transmitted pulse at 3 GHz. Although Bluetooth signal has very low bandwidth, the randomness of the center frequency of the Bluetooth signal causes large degradation in the performance. We want to point out that Bluetooth and the estimation process of its subspace are changed in every transmission.

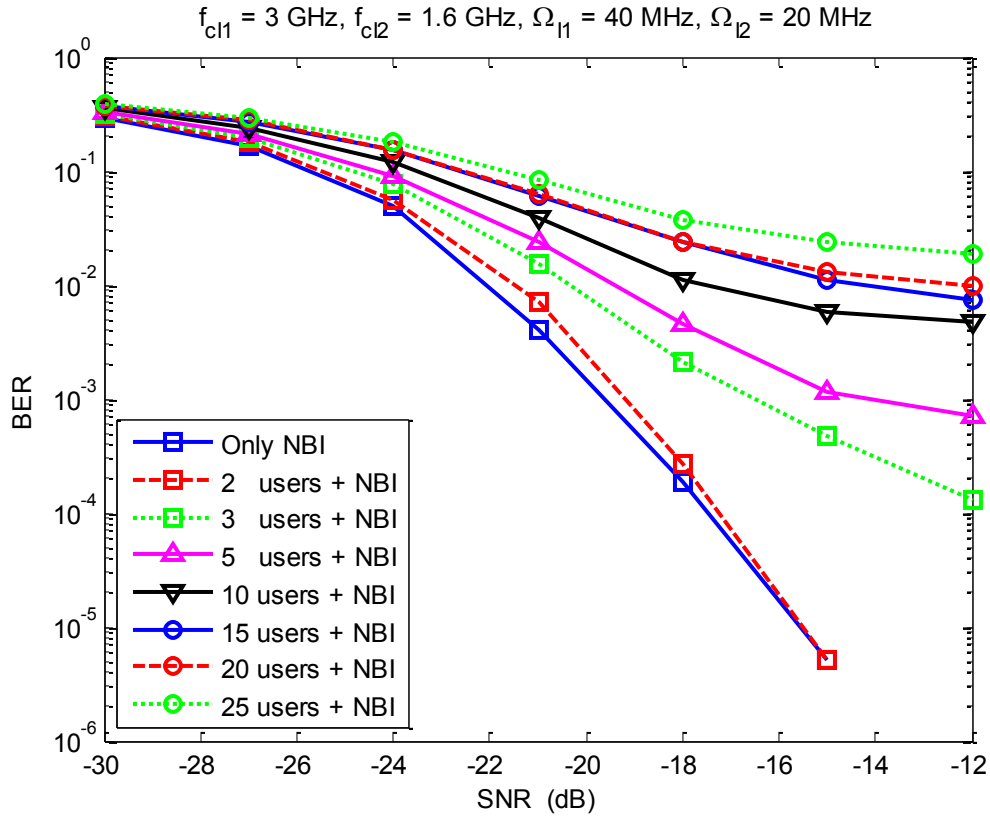


Figure 3-13 System performance when 0, 2, 3, 5, 10, 15, 20 and 25 users are active

In the last part, we evaluate the system in the presence of multiuser interference in addition to the NBI. The utilized signaling scheme for the multiuser system is DS-TH coding. Synchronized data transmission is assumed for the intended and the secondary user(s). The NBI has center frequencies of $f_{c1} = f_{cU} = 3$ GHz, $f_{c2} = 1.6$ GHz with bandwidth ($\Omega_{11} = 40$ MHz and $\Omega_{12} = 20$ MHz). Figure 3-13 shows that the system performance degrades as more users are present together with the NBI. For the given system parameters, two secondary users resulted in a minimal effect on the BER. This indicates the ability of the DS-TH code to reduce the interference. This is a direct function of the system's spreading gain.

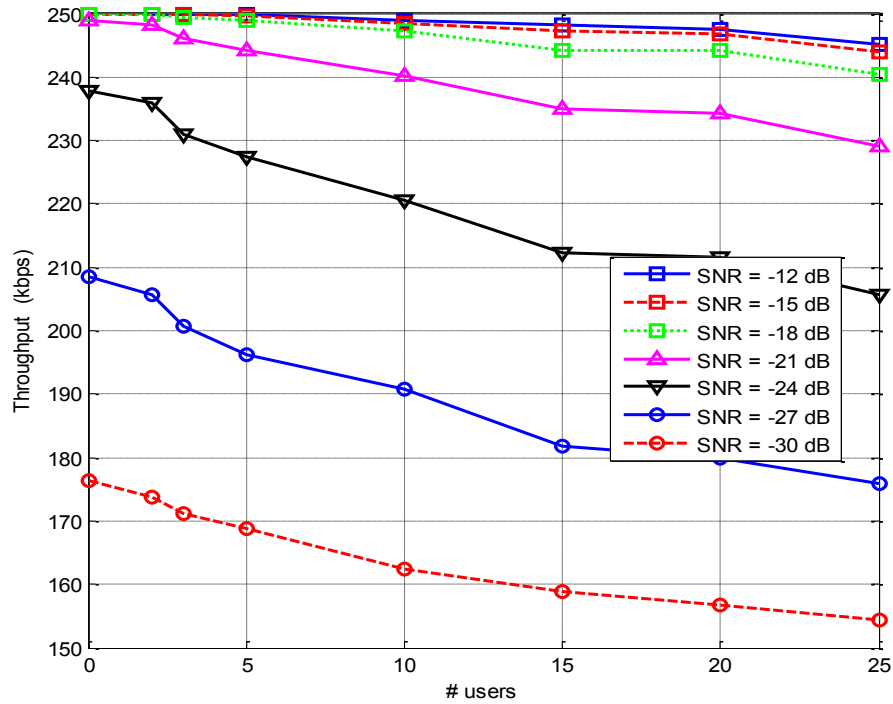


Figure 3-14 Throughput of DS-TH coding for different number of interfering users

Finally, throughput versus the SNR is plotted in Figure 3-14 as the number of the interfering user changes. As expected, throughput decreases when more users jam the intended one and vice-versa. At large SNR, throughput is almost constant as we have up to five secondary users. Moreover, the reduction in the throughput at such SNR is lower than 10 kbps as the number of users increases up to 25 users. At very low SNR, the effect of the multi user interference becomes large and clear. This multiuser study quantifies the amount of degradation due to the presence of other users. It also serves as a motive for future study where the entire compressive sensing algorithm is redesigned to possible reject other users. The challenge is in the similarity between the intended dictionary and the one to be nullified.

3.6 Chapter Summary

In this chapter the mitigation of NBI in trained UWB systems is investigated based on CS. The speeds of the ADC as well as the NBI effects are reduced through CS. The chapter first investigates the optimum pilot symbols distribution as well as the effect of each pilot group symbols. We conclude that there are a minimum required number of symbols in the first group N_{p1} after which the performance saturates. For the considered scenarios, $N_{p1} = 5$ was enough to achieve good system performance at low SIR and low NBI's bandwidth, this value is satisfied for weaker NBIs i.e. $SIR > -20$ dB. Communications can be achieved with $N_{p2} = 0$. However, the performance can be enhanced if the UWB signal structure is employed in the construction of the projection matrix, i.e. $N_{p2} > 0$. The number of pilot symbols in the third group N_{p3} is directly proportional to the performance.

We've studied different parameters that may affect the system performance such as the number of frame per symbol and the interference threshold, μ . The BER is reduced as more frames are being used to represent one symbol. Simulations also show that we should choose the value of the interference threshold carefully. The performance improves as μ increases over a certain range where the number of the suppressed coefficients used to construct the NBI subspace is decreased. Herein we eliminate the noisy coefficients and consequently the noise level is reduced.

The mitigation process was also applied when licensed NB services are present. Based on the simulation, the performance of the system degrades as the NBI's center frequency

locates closer to that of the transmitted pulse. Generally, increasing the NBI's bandwidth will reduce the sparsity of the NBI signal. More than one NBI with unequal center frequencies also results on a reduction in the sparsity of their equivalent NBI signal. Therefore, the interference threshold should be changed or the system needs to redistribute the pilot symbols to have acceptable performance.

Furthermore, the system behavior is studied in the presence of multiuser interference besides the NBI. As expected, simulation shows that when more users being active the system performance degrades and vice-versa. This also causes a reduction in the system throughput. Future optimization for CS in the presence of multiusers is motivated.

CHAPTER 4 MITIGATION OF NARROWBAND INTERFERENCE IN BLIND SYSTEMS

4.1 Introduction

Channel estimation is an important element that determines the performance of a given communications system especially in the presence of interference. Channel estimation can be done by training the system with a priori known data or it can be done blindly. Communication systems that don't use training sequences are known as blind systems. They are capable to do several processes blindly such as channel estimation, synchronization, and demodulation. The effect of the NBI on UWB systems can be eliminated using CS in two different systems; trained systems and blind systems. In this chapter, we concentrate on blind systems. The utilized system model is the one proposed by [Oka09a], [Oka09b], [Oka09c].

The main objective of this chapter is to study the performance of CS in blind UWB systems in the presence of NBI. Specifically, we study the performance for different licensed and unlicensed NBIs and we extend the mitigation technique in [Oka09b] for two NBIs. The speeds of the ADC as well as the NBI effects are reduced through CS. The channel models in [Oka09b] for the UWB signal and the NBI were fixed with only two different realizations. In this work, the channels are randomly selected from different UWB channel realizations in every burst transmission. We evaluate the effect of the burst size, the type of the modulated window and the baud rate. The work also goes over the

parameters that are related to the mitigation process such as the NBI's bandwidth and bandwidth of the transmitted pulse.

The chapter addresses the problem of utilizing CS to blind UWB system in the presence of NBI. The configuration of UWB transmitter is explained first. The interference source follows next with some details. More details about NBI modeling are mentioned in Section 2.4. The receiver has two main parts, analog-front-end and DSP-back-end which are clarified in details. Since the major processes are done in the receiver, we elaborate on all functions and explain the construction of the related blocks. Simulation and some results are given at the end of the chapter.

4.2 UWB Transmitter Configuration

The proposed system contains two main transmission paths, UWB signal path and interference path as shown in Figure 4-1. The UWB signal's transmitter consists of UWB symbol generator, UWB pulse shaper, UWB channel, and signal attenuator. The interfering signal has a similar path. The received signal is corrupted by NBI signal and thermal noise. The corrupted signal goes through an ideal BPF that has bandwidth and center frequency matched to those of the intended signal to be received.

The transmitter sends burst of data represented by a burst of pulses. The transmitter comprises three blocks, including baud clock, payload bits, and IR pulse generator as shown in Figure 4-1. The baud clock generates a clock signal at frequency $f_{baud} = 1/T_{baud}$. It determines the timing of the pulse within the same burst. Moreover, the start of every burst is also set by this clock through down-conversion of its frequency to f_{burst} .

The payload bits block produces information bits, B^k . In every burst, the transmitter sends K pulses after that it remains silent till the start of the next burst. The supplied bits, drawn equally probable from $\{+1, -1\}$, amplitude modulate an IR pulse, $\phi_U(t)$. The pulse shape of UWB signal is generated by modulating a Hanning window with an RF carrier at the desired center frequency. Thus, the pulse $\phi_U(t)$ will have a center frequency f_{cU} , bandwidth Ω_U and interval T_{pulse} .

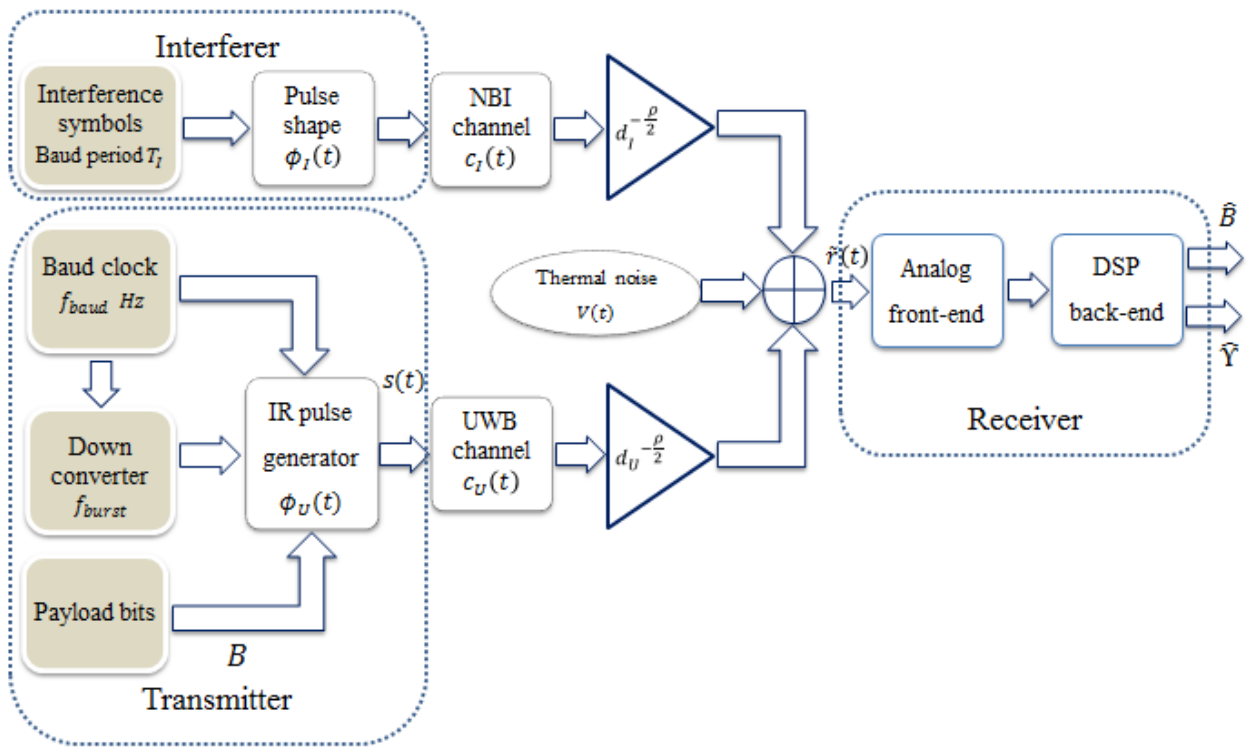


Figure 4-1 Signal paths taken by the UWB-IR and the NBI signals

The time and the frequency domain of the modulated pulse is plotted in Figure 4-3. The pulse has pulse duration, $T_{pulse} = 1$ ns, center frequency, $f_{cU} = 4$ GHz, and a 6-dB bandwidth of about $\Omega_U = 2$ GHz.

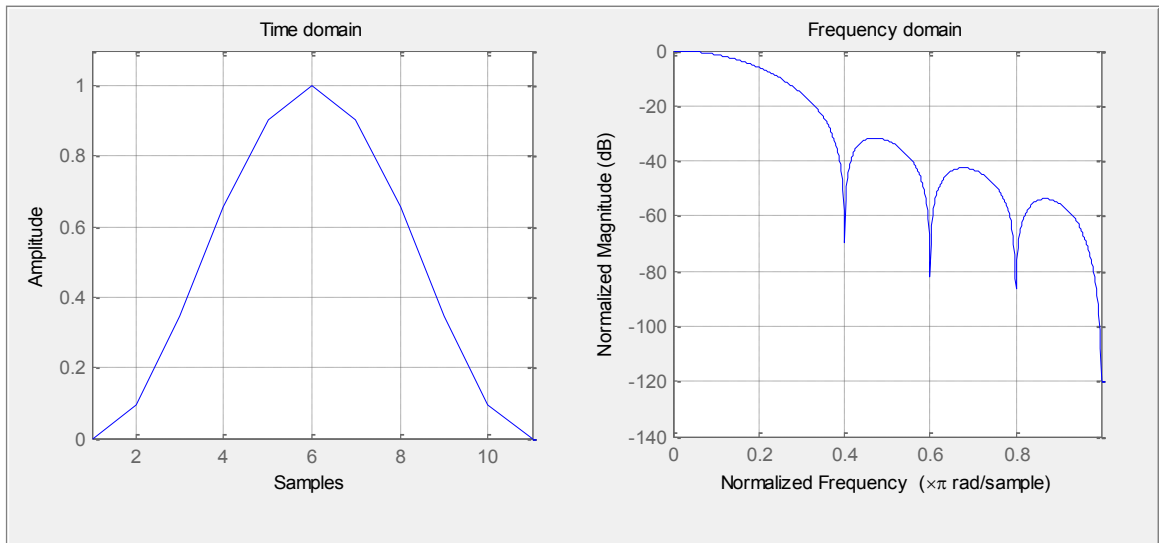


Figure 4-2 Hanning window in time and frequency domain

The correct TOA, T_d , for each burst is uniformly distributed in the interval $[0, \gamma]$. The transmitter sends K pulses per burst per transmission. Then it keeps silent during a period of T_{burst} . After that, it sends K pulses, followed by the silent period. The process continues till the transmitter completes sending all the information.

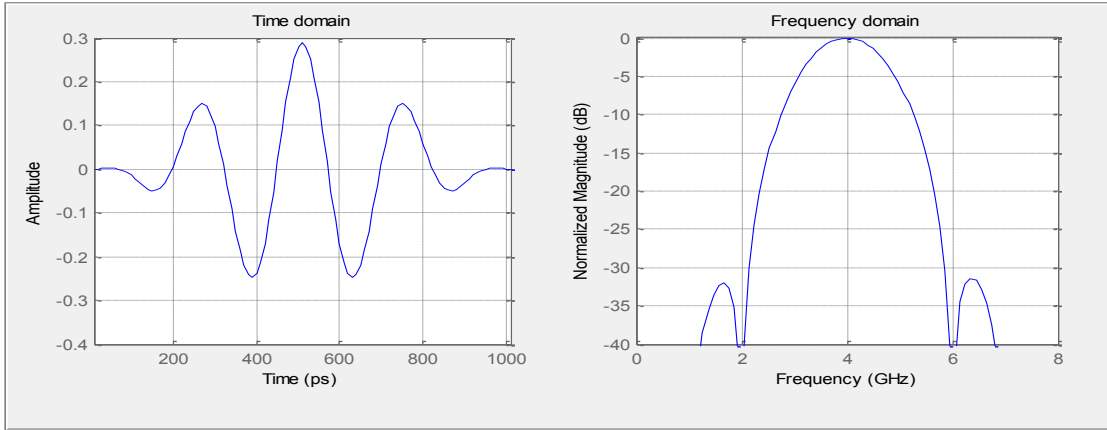


Figure 4-3 Hanning modulated pulse and its power spectrum

In Figure 4-4, illustration for three burst transmission is sketched where there are four bits per burst. The transmitted waveform for a burst of data transmission can be written as:

$$s(t) = \sum_{k=0}^{K-1} B^k \phi_U(t - k T_{baud} - T_d) \quad (4-1)$$

The UWB waveform is then passed through an UWB channel, $c_U(t)$, according to IEEE802.15.4a channel model CM1 presented in Chapter 2. The impact of path-loss due to distance between the UWB transmitter and the UWB receiver, d_U , is represented by $d_U^{-\rho}$ where ρ is the path-loss exponent.

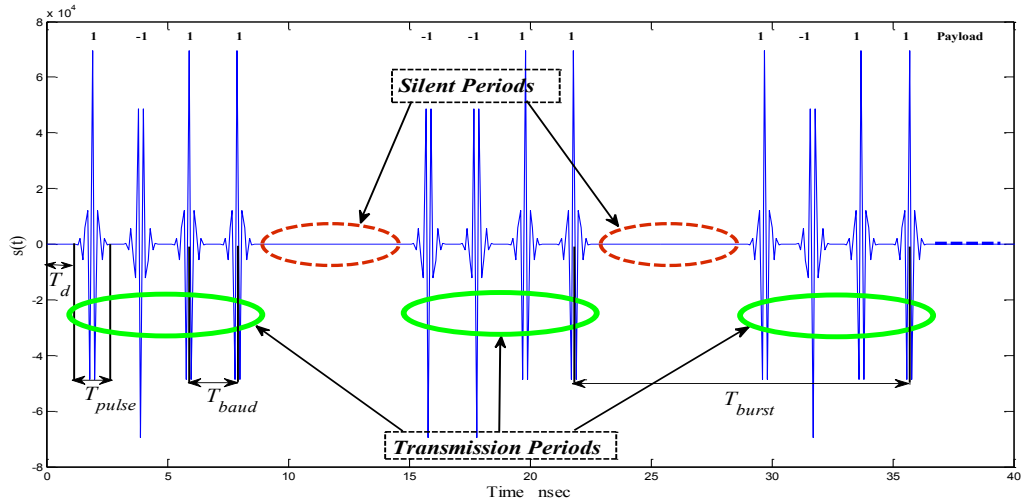


Figure 4-4 Frame format for the bursty data transmission

4.3 Interference Configuration

The interfering symbols are generated at rate $1/T_I$, where T_I is the baud rate of the NBI. As for UWB signal, the symbols are shaped first using $\phi_I(t)$. Then the interfering signal, $v(t)$, is passed through channel $c_I(t)$. The channel of the NBI might be an IEEE802.11.4a channel model as used for the UWB signal but with different realization [Oka09b]. Alternatively, it may be other channel model as Figure 2-1 shows that perfect channel can be also used. The impact of path-loss due to the distance between the NBI and the UWB receiver, d_I , is represented by $d_I^{-\rho}$.

4.4 UWB Receiver Configuration

The received signal is contaminated by both two sided PSD, $\frac{N_0}{2}$, additive White Gaussian Noise (AWGN), $w(t)$, and narrowband interference, $v(t)$; see Figure 4-1. A

correlator receiver with digital notch filter is employed to detect the transmitted signal and mitigate the NBI. The receiver in Figure 4-5 has two main parts, analog front-end and DSP back-end. Those parts are presented with more details in the coming subsections. The DSP back-end applies simple quadratic problem optimization. Quadratic programs can be easily solved by optimization techniques like interior-point-methods.

In blind systems, CS is used to achieve two main things. The first one is reducing the speed of the ADC or the sampling rate. The other is the utilization of a sparse signal to detect a certain waveform's structure. As we'll see later in this chapter, when the length of a signal is N samples, according to Nyquist theorem it requires at least M mixer-integrators to reconstruct the original shape of the signal being transmitted where $M \geq N$. However, with $M \ll N$ the original signal can be –with high probability– estimated perfectly without degradation using CS. Hence the speed of the ADC is reduced to by a factor of M/N . The transmitted signal contains K nonzero samples and the test functions are also sparse in the frequency domain. The sparsity of the transmitted signal helps in the demodulation process, while the sparsity of the test functions emphasis that the NBI has only small effect in the measurements being taken. Subsequently the location of the NBI is detected as well as its effect is effectively eliminated.

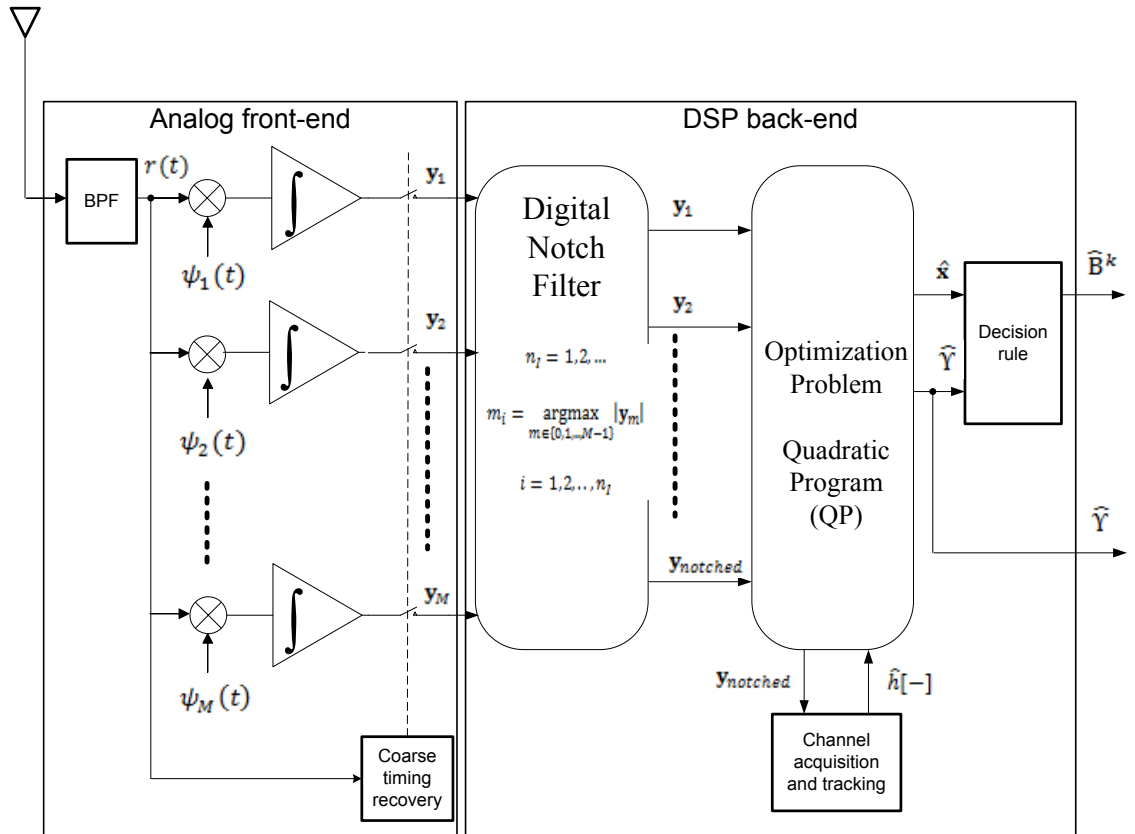


Figure 4-5 Correlator receiver with digital notch filter

4.4.1 Analog Front-End

The analog front end part contains a BPF and M mixer-integrators. Each mixer compares the signal with one of the basis. The receiver first utilizes BPF, $g(t)$, to capture the intended UWB signal and limit the noise. The BPF should have a center frequency which coincides with the frequency of the desirable UWB signal f_c and bandwidth equal to the bandwidth of the transmitted UWB signal Ω [Oka09c], i.e. $\Omega = \Omega_U$ and $f_c = f_{cU}$. Figure 4-6 demonstrates the time and the frequency domain of a BPF with a center

frequency of 4 GHz and almost a flat bandwidth around 2 GHz. The design of the filter should ensure that the desired UWB signal passes the filter without distortion.

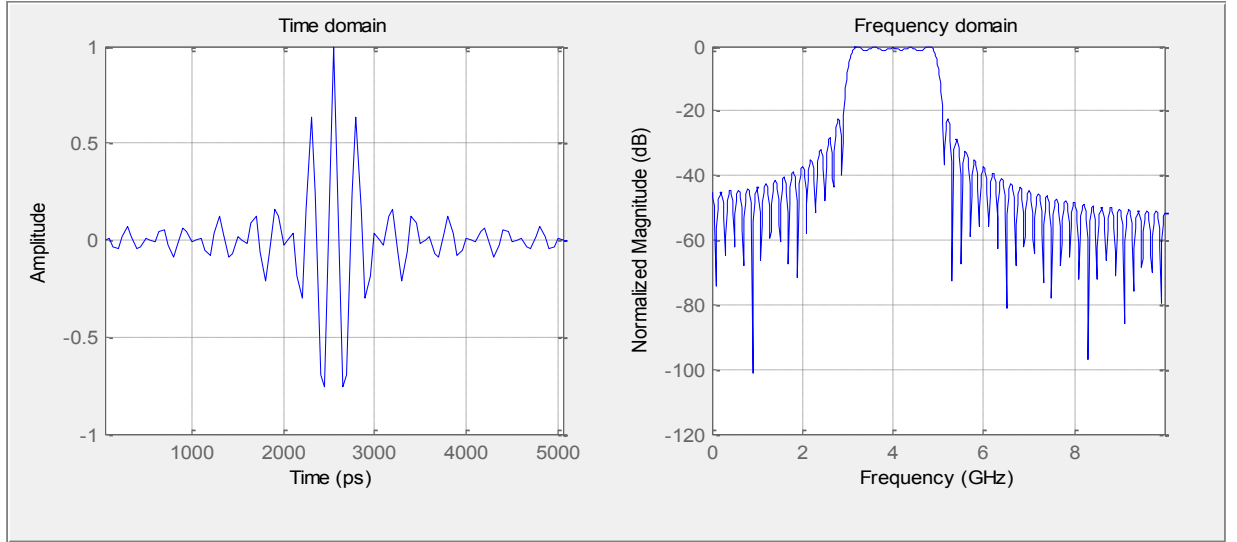


Figure 4-6 Time and frequency domain representations of the BPF

Ignoring the path-loss, the signal at the output of the BPF can be written as:

$$r(t) = \sum_{k=0}^{K-1} B^k h(t - k T_{baud} - T_d) + w(t) + i(t) \quad (4-2)$$

where $h(t) = \phi_U(t) * c_U(t) * g(t)$ is the total impulse response of length denoted by λ_h second. The last two terms are the response of the filter to the noise and to the interference respectively. M mixer-integrators follow the BPF with highly frequency selective test functions. The number of correlators is smaller than required by Shannon-Nyquist sampling theorem. The output from those mixers is taken simultaneously at $t = \lambda_h + (K - 1)T_{baud}$.

The test functions $\Psi \in \mathbb{R}^{M \times N}$ are sinusoidal waveforms of amplitude $1/\sqrt{N}$ designed to have a rapid decay through windowing technique. In addition, their frequencies are deterministically and uniformly distributed in the interval $[f_c - \frac{\Omega}{2}, f_c + \frac{\Omega}{2}]$, so they are sparse in the frequency domain. Tukey window or tapered cosine, $w[n]$, is used here, to be compared with [Oka09b], where the equation for computing its coefficients is given by:

$$w[n] = \begin{cases} \frac{1}{2} \left[1 + \cos \left(\frac{2\pi}{\alpha'} \left[n - \frac{\alpha'}{2} \right] \right) \right], & 0 \leq n < \frac{\alpha'}{2} \\ 1, & \frac{\alpha'}{2} \leq n < 1 - \frac{\alpha'}{2} \\ \frac{1}{2} \left[1 + \cos \left(\frac{2\pi}{\alpha'} \left[n - 1 + \frac{\alpha'}{2} \right] \right) \right], & 1 - \frac{\alpha'}{2} \leq n \leq 1 \end{cases} \quad (4-3)$$

The sampled m^{th} test function multiplied by the window can be written as:

$$\psi_i = \frac{1}{\sqrt{N}} \sin \left(\frac{2\pi f_i n}{f_s} \right) w[n], n = 0, 1, \dots, N - 1, \forall i = 0, 1, \dots, M - 1 \quad (4-4)$$

The shape of this window is controlled by a factor $0 \leq \alpha' \leq 1$. The window becomes a rectangle window when $\alpha' \leq 0$ and resembles a Hanning window if $\alpha' \geq 1$. Hence the shape of function approximately doesn't change if the controlled factor is greater than one or lower than zero. Figure 4-7 represents the frequency domain for three basis functions designed for three values of $\alpha' = 0.1, 0.5$ and 0.9 . By making use of Tukey window, the functions get narrower as α' increased. The basis functions must be known at the DSP back-end; however they are simple because they don't require any tuning.

Beside the sinusoidal waveforms, the basis functions can be other signals [Oka09c]. This thesis focuses on the sinusoidal signals explained previously. Unless otherwise stated, the controlled factor is fixed to be $\alpha' = 0.9$.

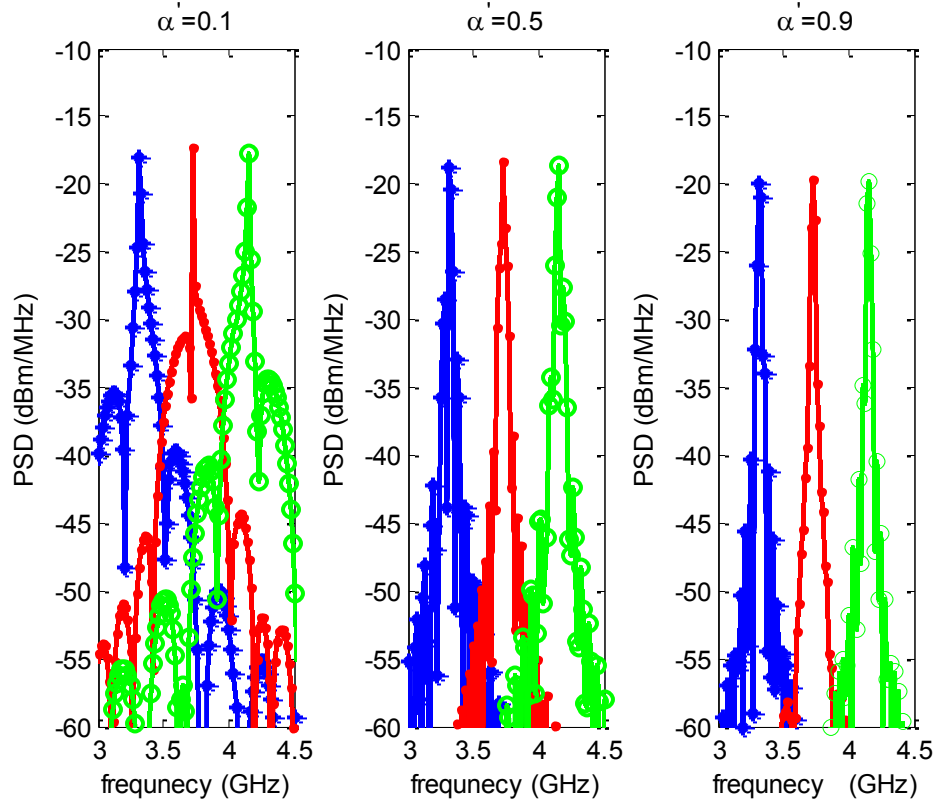


Figure 4-7 Frequency domain for different test functions selected randomly

For the quantity $\frac{M}{N} \frac{f_s}{2\Omega}$, if we sample at the Nyquist frequency, f_s should equal to 2Ω .

When $M = N$, there is no loss and we achieve the Nyquist rate. While the bandwidth is calculated at the 3 dB point, a factor, α , is injected to the quantity to be $\frac{Mf_s}{2\alpha\Omega N}$. This factor

is included to enhance and support practical pulses because there are no ideal band-limited pulses. The factor $\frac{Mf_s}{2\alpha\Omega N}$ is called the sampling-factor with $\alpha = 1.5$. Perfect

sampling will occur when $\frac{Mf_s}{2\alpha\Omega N} = 1$, while $\frac{Mf_s}{2\alpha\Omega N} < 1$ represents the under-sampling case.

In the last case where $M \ll N$, the sampling rate at the receiver side is reduced further and the receiver complexity is reduced.

The output of the m^{th} mixer is given as [Oka09a]:

$$y_m = \int_0^{\lambda_h + \gamma + (K-1)T_{baud}} r(t)\psi_m(t)dt \quad (4-5)$$

The measurement vector $\mathbf{y} = [y_0, y_1, \dots, y_{M-1}]$ is used in the DSP back-end to demodulate the payload, B^k , via QP algorithm.

4.4.2 DSP Back-End

The main objective of the DSP back-end is to estimate the payload transmitted information vector $\mathbf{B} = [B^0, B^1, \dots, B^{K-1}]$ and actual TOA uncertainty \hat{Y} . When an NBI(s) signal is presented in the band of interest, correlating the test functions with the received signal gives a vector with large value(s) whenever the NBI and any one of the test functions have the same frequency. The first task is to find the position of this value. The location of the interferer is detected then its effect is reduced by a digital notch filter. Since we drop the affected measurements, we may lose small amount of the UWB signal's energy. However, using such rapidly decaying basis will ensure that the loss is limited.

Suppose that the number of interferers is denoted by n_I . An algorithm searches for the index or the indices of the maximum absolute measurement value(s) in the measurement vector \mathbf{y} using the relation:

$$\hat{m}_i = \operatorname{argmax}_{m \in \{0,1,\dots,M-1\}} |\mathbf{y}_m|, i = 1, 2, \dots, n_I \quad (4-6)$$

When $n_I = 1$, let D be an even number, the notch filter drops $D + 1$ measurements around the index \hat{m} resulting in $\mathbf{y}_{notched} \in \mathbb{R}^{M-(D+1)}$, with the proper sub-matrix of Ψ .

$$\mathbf{y}_{notched} = \left[y_0, y_1, \dots, y_{\hat{m}-\frac{D}{2}-1}, y_{\hat{m}+\frac{D}{2}+1}, \dots, y_{M-2}, y_{M-1} \right] \quad (4-7)$$

$$\Psi = \begin{bmatrix} \psi_{11} & \psi_{12}, \dots & \psi_{1N} \\ \vdots & \vdots & \vdots \\ \psi_{(\hat{m}-\frac{D}{2}-1)1} & \psi_{(\hat{m}-\frac{D}{2}-1)2}, \dots & \psi_{(\hat{m}-\frac{D}{2}-1)N} \\ \psi_{(\hat{m}+\frac{D}{2}+1)1} & \psi_{(\hat{m}+\frac{D}{2}+1)2}, \dots & \psi_{(\hat{m}+\frac{D}{2}+1)N} \\ \vdots & \vdots & \vdots \\ \psi_{M1} & \psi_{M2}, \dots & \psi_{MN} \end{bmatrix} \quad (4-8)$$

A major issue is how to set the value of D ? The value of D is related to the bandwidth of UWB signal, Ω_U , bandwidth of NBI signal, Ω_I , and the number of measurements, M . It can be also related to Δ which is the frequency band that separates any two successive test functions, $\Delta = \frac{\Omega_U}{M}$. Hence, we may write $D = \beta \frac{\Omega_I}{\Delta}$, where β is a safety factor to account for leakage into adjacent measurements. The value of β is set to 4 as in [Oka09b].

Depending on the indices of the maximum absolute values in the measurement vector, there might be an overlapping between the notched measurements when $n_I = 2$ for

example. Consequently the notched vector may not be $\mathbf{y}_{notched} \in \mathbb{R}^{M-(D_1+1+D_2+1)}$. Let the index or the location of the second maximum absolute measurement value be greater than the index of the first maximum absolute measurement value, mathematically $\hat{m}_2 > \hat{m}_1$. If there is no overlapping, the notched measurement vector is written as:

$$\mathbf{y}_{notched} = \left[y_0, y_1, \dots, y_{\hat{m}_1 - \frac{D_1}{2} - 1}, y_{\hat{m}_1 + \frac{D_1}{2} + 1}, \dots, y_{\hat{m}_2 - \frac{D_2}{2} - 1}, y_{\hat{m}_2 + \frac{D_2}{2} + 1}, \dots, y_{M-1} \right] \quad (4-9)$$

In this case, because of the first interferer the measurements $\hat{m}_1 - \frac{D_1}{2}, \hat{m}_1 - \frac{D_1}{2} + 1, \dots, \hat{m}_1 + \frac{D_1}{2} - 1, \hat{m}_1 + \frac{D_1}{2}$ are notched. Additionally, the measurements $\hat{m}_2 - \frac{D_2}{2}, \hat{m}_2 - \frac{D_2}{2} + 1, \dots, \hat{m}_2 + \frac{D_2}{2} - 1, \hat{m}_2 + \frac{D_2}{2}$ are dropped because of second the interferer. It is clear that no overlapping occurs when $\hat{m}_2 - \frac{D_2}{2} > \hat{m}_1 + \frac{D_1}{2}$. Although, there is an overlapping if $\hat{m}_2 - \frac{D_2}{2} \leq \hat{m}_1 + \frac{D_1}{2}$.

Through either knowing the number of the presented interferers or finding the magnitudes which are larger than a specified threshold (the number of the active interferers), n_I can be determined. The affected points are then subtracted and removed by digital notch filter employed in the DSP back-end. Therefore the interference signal is effectively mitigated [Oka09b].

Let f_s be a virtual sampling rate that is large enough, and the sampling time $T_s = 1/f_s$. Since the length of the channel impulse response is λ_h seconds, the number of samples in the response will be $\Lambda_h = \lceil \lambda_h f_s \rceil$ samples. The discrete time representation of the channel

can be written as $h[n] = [h[0], h[1], \dots, h[\Lambda_h - 1]]^T$. The maximum TOA uncertainty, γ , and the baud interval, T_{baud} , are constructed to be multiple of T_s . Hence the number of samples in the maximum possible TOA uncertainty becomes $\Gamma = \gamma f_s$ samples, and the samples between two consecutive bits will be $N_{baud} = f_s T_{baud}$ samples. While each transmission includes K bits and Γ maximum possible TOA uncertainty, the maximum length of the payload is $\Lambda_X = \Gamma + (K - 1)N_{baud}$ samples. Because of the convolution process, the maximum number of samples in each burst including the channel is $N = \Lambda_h + \Lambda_X - 1$.

Additionally, the actual TOA uncertainty quantization is $Y = \text{round}(T_d f_s)$ samples. Small quantization error occurs which can be ignored when the sampling rate is large enough.

The received sampled waveform, $\mathbf{r} \in \mathbb{R}^N$, becomes:

$$\mathbf{r} = \mathcal{H}\mathbf{x} + \mathbf{w} + \mathbf{i} \quad (4-10)$$

where $\mathbf{i}, \mathbf{w} \in \mathbb{R}^N$ are the sampled forms of $i(t)$ and $w(t)$, respectively. $\mathcal{H} \in \mathbb{R}^{N \times \Lambda_X}$ is the convolutional matrix (Toeplitz form) of $h[n]$ as in [Oka09c]. $\mathbf{x} \in \mathbb{R}^{\Lambda_X}$ is the virtual discrete time representation of the payload with K nonzero samples (K -sparse). Each sample has a random amplitude of $\{+1, -1\}$, and has a random position separated by N_{baud} samples; mathematically $\Lambda^k = Y + kN_{baud}$, $k = 0, 1, \dots, K - 1$. Since the samples are spaced equally by N_{baud} knowing the location of the first bit handles the locations of the remaining ones provided N_{baud} . Hence the effective sparsity of the signal is only one

rather than K . The sampled measurement vector, \mathbf{y} , is the simultaneous sampling of the output of all correlators after multiplying the received signal by test functions which can be written as:

$$\mathbf{y} = \Psi \mathbf{r} = \Psi \mathcal{H} \mathbf{x} + \Psi \mathbf{w} + \Psi \mathbf{i} \quad (4-11)$$

Assume that all transmitted signals $x \in \mathbb{R}^{\Lambda x}$ are equiprobable and are contained in the set χ . This set has burst length of $\|x\|_0 = K$. The K nonzero entries of level $\{-1, +1\}$ are equally spaced by N_{baud} samples. The locations of those nonzero samples are calculated based on the relation: $l^k = l^0 + kN_{baud}$ where $k = 0, 1, \dots, K - 1$ and $l^0 \in [0, \Gamma]$, as Figure 4-8 depicts that. There is a one-to-one mapping [Oka09a], [Oka09b], [Oka09c]. To sum up, any possible transmitted signal, $\{-1, +1\}^K$, has its own payload and random TOA uncertainty (\mathbf{B}, Y) which is mapped in the set χ to the corresponding vector $\mathbf{x}(\mathbf{B}, Y)$. Therefore, the ML algorithm can be used to estimate the received discretized signal $\hat{\mathbf{x}}$ first. Then the result is mapped to estimate the payload $\hat{\mathbf{B}}(\hat{\mathbf{x}})$ and TOA $\hat{Y}(\hat{\mathbf{x}})$, in other words $P(\mathbf{y}|\mathbf{B}, Y) = P(\mathbf{y}|\mathbf{x})$.

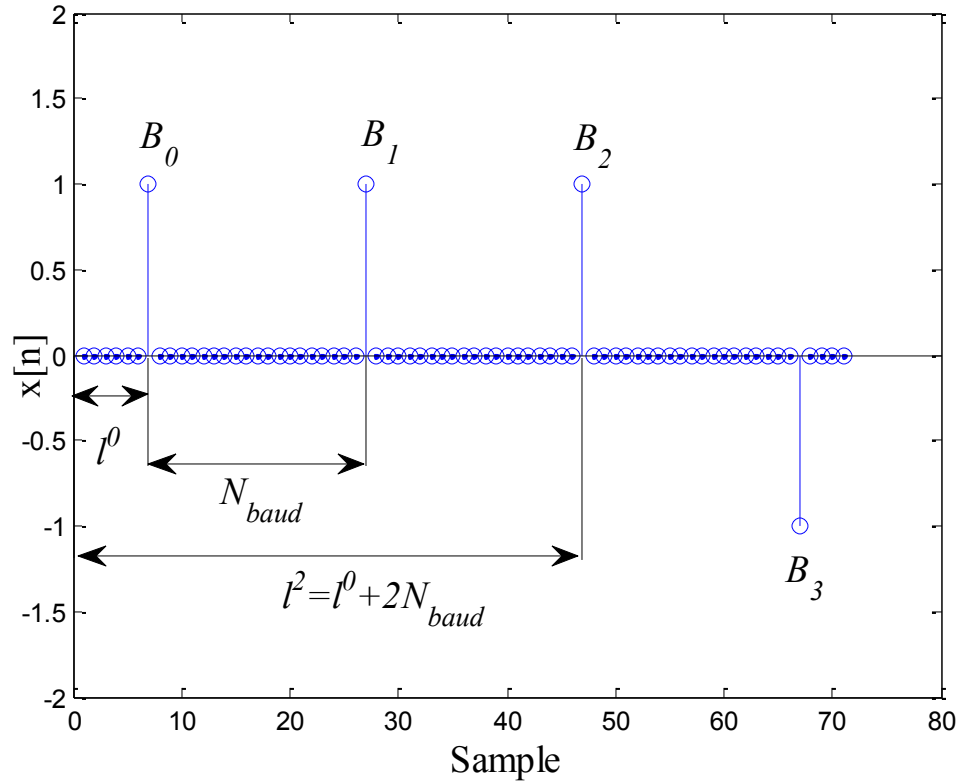


Figure 4-8 The location of the k^{th} nonzero samples

Let us ignore the interference term in equation above for the time being. Given x was transmitted, the ML demodulator used to detect the intended signal will be [Oka09a]:

$$\hat{\mathbf{x}} = \underset{x \in \mathcal{X}}{\operatorname{argmin}} (\mathbf{y} - \Psi \mathcal{H} x)^T (\Psi \mathbf{G} \mathbf{G}^T \Psi^T)^{-1} (\mathbf{y} - \Psi \mathcal{H} x) \quad (4-12)$$

where \mathbf{G} is the convolutional matrix (Toeplitz form) of $g(t)$. Let $\xi[n]$ be a vector that represents one of the possible transmitted signals $x \in \mathbb{R}^{\Lambda_x}$. This candidate vector has very large values \mathcal{U} in positions where it's unlikely to include nonzero samples in the original transmitted signal [Jin11], [Oka09a], [Oka09b], [Oka09c] and equals one in the remaining positions. For $n = 0, 1, \dots, \Lambda_x - 1$, the vector $\xi[n]$ is defined as:

$$\xi(a, l_1, l_2)[n] = \begin{cases} 1, & \begin{array}{l} n = l + kN_{\text{baud}}, \\ l \in \{a + l_1, a + l_2\} \\ k \in \{0, 1, \dots, K - 1\} \end{array} \\ 0, & \text{otherwise} \end{cases} \quad (4-13)$$

The ML demodulation problem equation can be rewritten as:

$$\tilde{\mathbf{x}} = \operatorname{argmin}_{\mathbf{x} \in \mathbb{R}^{\Lambda_X} \|\Xi(a, l_1, l_2)\mathbf{x}\|_1 = K} (\mathbf{y} - \Psi\mathcal{H}\mathbf{x})^T (\Psi\mathcal{G}\mathcal{G}^T\Psi^T)^{-1} (\mathbf{y} - \Psi\mathcal{H}\mathbf{x}) \quad (4-14)$$

where $\Xi(a, l_1, l_2) = \operatorname{diag}\{\xi(a, l_1, l_2)\}$. Consequently, the previous equation can be simplified more and more to be a QP problem with two constraints as [Oka09a], [Oka09b], [Oka09c]:

$$\tilde{\mathbf{z}} = \min \mathbf{f}^T \mathbf{z} + \frac{1}{2} \mathbf{z}^T \mathbf{Q} \mathbf{z}, \text{ Subject to: } \mathbf{z} \in \mathbb{R}^{2\Lambda_X} : \mathbf{z} \geq 0, [\xi(a, l_1, l_2)^T, \xi(a, l_1, l_2)^T] \mathbf{z} = K \quad (4-15)$$

$$\mathbf{Q} = \begin{pmatrix} \mathcal{H}^T \Psi^T (\Psi\mathcal{G}\mathcal{G}^T\Psi^T)^{-1} \Psi\mathcal{H} & -\mathcal{H}^T \Psi^T (\Psi\mathcal{G}\mathcal{G}^T\Psi^T)^{-1} \Psi\mathcal{H} \\ -\mathcal{H}^T \Psi^T (\Psi\mathcal{G}\mathcal{G}^T\Psi^T)^{-1} \Psi\mathcal{H} & \mathcal{H}^T \Psi^T (\Psi\mathcal{G}\mathcal{G}^T\Psi^T)^{-1} \Psi\mathcal{H} \end{pmatrix} \quad (4-16)$$

$$\mathbf{f} = [-\mathbf{y}_{\text{notched}}^T (\Psi\mathcal{G}\mathcal{G}^T\Psi^T)^{-1} \Psi\mathcal{H}, \mathbf{y}_{\text{notched}}^T (\Psi\mathcal{G}\mathcal{G}^T\Psi^T)^{-1} \Psi\mathcal{H}] \quad (4-17)$$

The following equation used to extracts $\tilde{\mathbf{x}} \in \mathbb{R}^{\Lambda_X}$ from $\tilde{\mathbf{z}} \in \mathbb{R}^{2\Lambda_X}$ calculated in (4-15) [Jin11], [Jin12]:

$$\tilde{\mathbf{x}}_n = \tilde{\mathbf{z}}_n - \tilde{\mathbf{z}}_{(n+\Lambda_X)}, \quad n = 0, 1, \dots, \Lambda_X - 1 \quad (4-18)$$

The fastest one among several algorithms used to solve the QP problems is the interior-point algorithm [Boy04]. Since the QP problem in hand has only equalities and lower

bounds, the problem is efficiently solved using medium-scale algorithm through Matlab in this thesis.

The detection process aims to estimate the signal $\hat{\mathbf{x}}$ first, map $\hat{\mathbf{x}}$ to estimate the payload $\hat{\mathbf{B}}(\hat{\mathbf{x}})$ and TOA $\hat{Y}(\hat{\mathbf{x}})$. Hence the DSP back-end accomplishes the demodulation process through two steps. Estimating the arrival of the burst \hat{Y} is the first one which is achieved by solving the QP problem using $\xi(a = 0, l_1 = 0, l_2 = \Gamma)$ to get $\tilde{\mathbf{x}}^{(1)}$. The TOA can be estimated by correlating $\tilde{\mathbf{x}}^{(1)}$ with the template $\xi(0,0,0)$ using the relation:

$$\hat{Y} = \operatorname{argmax}_{n' \in \{0,1,\dots,\Gamma\}} \sum_n |\tilde{\mathbf{x}}^{(1)}[n - n']| \xi(0,0,0)[n] \quad (4-19)$$

The second step is to solve the QP problem using $\xi(a = \hat{Y}, l_1 = 0, l_2 = 0)$. The result $\tilde{\mathbf{x}}^{(2)}$ and the first step's result \hat{Y} are used to detect the payload sequence using the following formula:

$$\hat{\mathbf{B}}^k = \operatorname{sign}(\tilde{\mathbf{x}}^{(2)}[\hat{Y} + kN_{baud}]), \quad k = 0, 1, \dots, K - 1 \quad (4-20)$$

The vector $\tilde{\mathbf{x}}^{(2)}$ should contain K nonzero samples, but because of the noise and incorrect estimation of \hat{Y} it may include more than K samples with different magnitudes. The estimated TOA \hat{Y} is used to determine the location of the first nonzero sample in $\tilde{\mathbf{x}}^{(2)}$. The remaining $K - 1$ are handled easily as they are equally spaced by N_{baud} samples. Finally the payload bits $\hat{\mathbf{B}}^k$ are detected by taking only the sign of the determined locations in $\tilde{\mathbf{x}}^{(2)}$.

4.5 Simulation and Results

In this section the mitigation of the NBI in blind UWB systems is evaluated. The diagram in Figure 4-9 summarizes the main steps that are used to simulate our system. To sum up, the UWB system generates K bits in the first step, and shapes them. Next, the resultant signal goes through an IEEE802.11.4a channel. The UWB signal amplitude is scaled based on the traveled distance if the path-loss is considered. The NBI system also generates its own symbols, shapes them, and finally sends them over the interference channel.

At the receiver side, the received UWB signal is captured using BPF. Then the measurement is taken using the test functions followed by an algorithm that determines the number of active interferers. Based on this number, a digital notch filter suppresses the effects of those NBIs. Finally, the QP performs a joint decoding through two stages. The arrival of the current burst is estimated first. The payload is then demodulated in the second stage based on the estimated arrival.

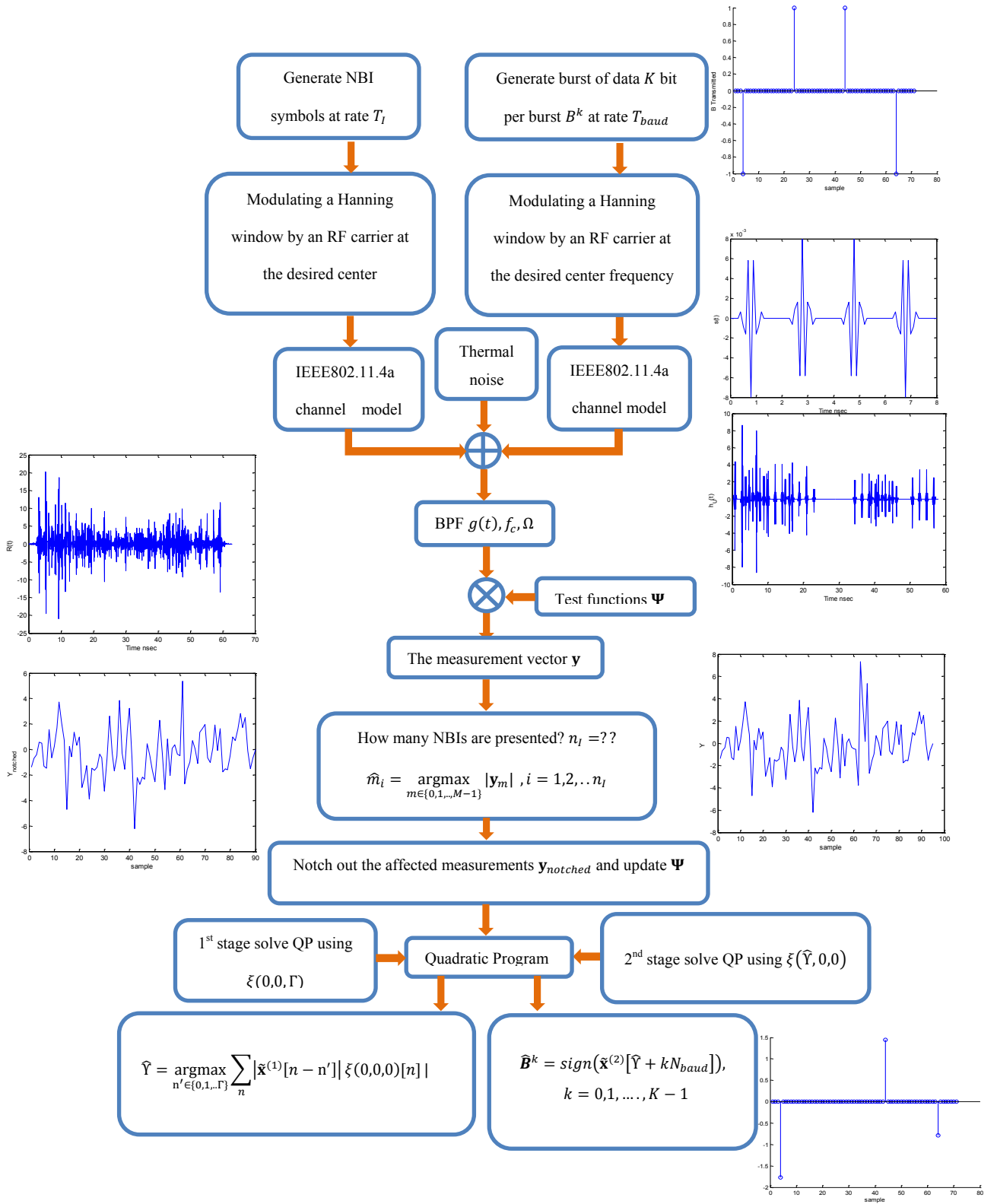


Figure 4-9 Flow chart for the main steps of the blind system

All simulations are accomplished with $f_s = 10$ GHz. For residential LOS environment, IEEE802.11.4a CM1 is used [Mol06]. The channel models for the UWB and the NBI signals are randomly selected from 100 realizations generated from CM1 that has a dispersion time around 50 nanosecond and normalized to have unit energy. A Hanning modulated pulse centered at frequency $f_{cU} = 4$ GHz is used to shape the UWB symbols with duration interval $T_{pulse} = 1$ ns, which yields $\Omega_U = 2$ GHz. Moreover, the transmission rate is $f_{baud} = \frac{f_{Nyquist}}{8} = \frac{2\Omega_U}{8} = 500$ Mbaud which causes an ISI to be extend over 25-50 pulses. The test functions are sinusoid waveforms generated to have frequencies that are deterministically selected from the band $\left[f_c + \frac{\Omega_U}{2}, f_c - \frac{\Omega_U}{2} \right]$. They are also designed to have a rapid decay using Tukey window. The maximum TOA is $\gamma = 1$ ns which yields $\Gamma = 10$ samples. Since one of our main objectives is to reduce the ADC through CS, the sampling-factor is adjusted to be 0.25 which implies 75% reductions in the sampling frequency. For the unlicensed NBI, the center frequency of the UWB pulse, the center frequency and the bandwidth of the jammers can be located anywhere in the UWB signal's spectrum. So we assume that we have a partial band jammer and 2 partial bands jammer with two equal bandwidths. The 2 partial bands jammer causes interference in two bands at specific center frequencies. The partial band is fixed such that it has a center frequency equal to that of the modulated UWB pulse in order to produce as much as possible interference for the intended system i.e. $f_{cI} = f_{cU} = 4$ GHz. The location of the 2 partial bands jammer is adjusted to be similar to one partial band which has bandwidth equal to summation of the two bands in the 2 partial bands jammer. In this case the center frequencies are located at $f_{cI1,2} = f_{cU} \pm \frac{\Omega_I}{2} = 4 \text{ GHz} \pm \frac{\Omega_I}{2}$

where Ω_I is the bandwidth of each band. While for the licensed NB services, the center frequencies and the bandwidth are fixed as illustrated in Section 2.4.2. All those parameters are fixed unless stated otherwise.

At the beginning, the impact of the number of bits per burst, K , is considered. For a specific NBI, the performance is evaluated from the BER point of view. The performance is evaluated for $K = 2, 4$, and 8 bit per burst and $\text{SNR} = 9 \text{ dB}$ which is fixed for the following simulations unless otherwise stated. Figure 4-10 shows the case of a partial band interferer that has $\Omega_I = 20 \text{ MHz}$ and $f_{cI} = f_{cU} = 4 \text{ GHz}$.

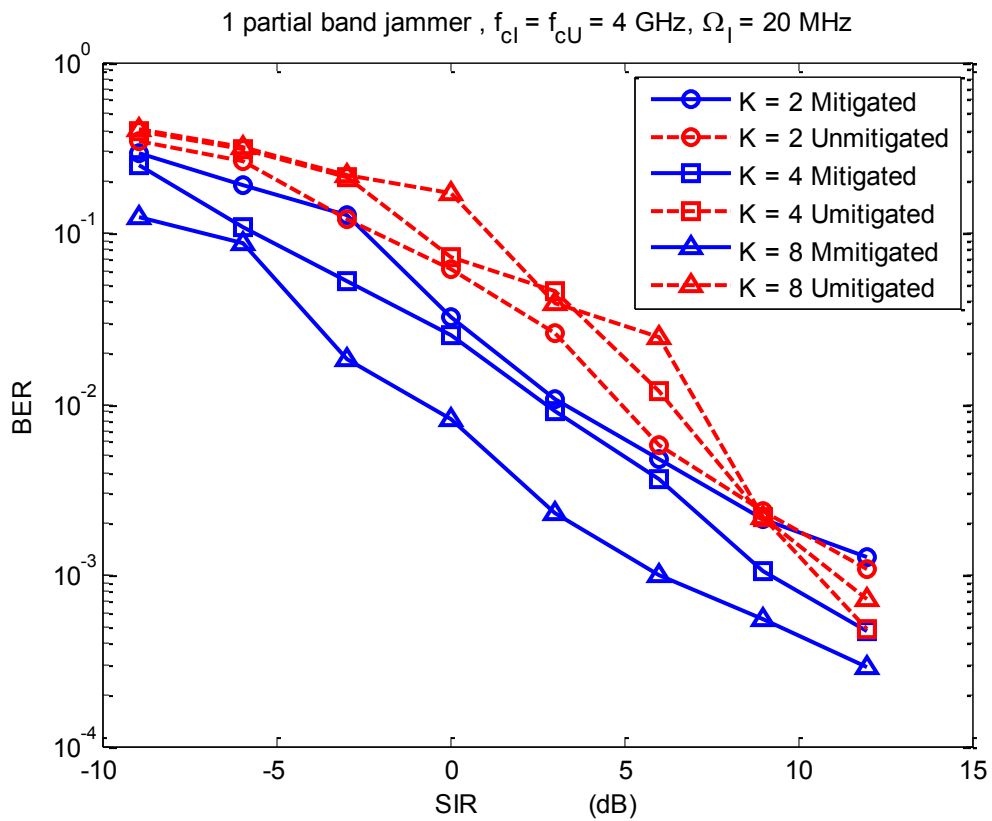


Figure 4-10 Performance of a partial band interferer for different burst size

If we compare the mitigated with the unmitigated case, it is clear that the performance is enhanced as K increases. Moreover, sending the information using large burst size outperforms sending it using small burst size. This is because of the equally spaced pulses and the low probability of error in arrival estimation which reduces the BER. At higher SIR, we expect that there will be no benefit from the mitigation process since the NBI becomes very weak and we actually notch out the desired measurements.

Before changing the type and the location of the NBI, the type of the UWB modulated pulse is investigated. Three different windows are chosen including Hanning, Gaussian, and Hamming modulated pulses. For fair comparison, they're adjusted to produce similar 6-dB bandwidth of $\Omega_U = 2$ GHz. The performance is discussed for the same NBI as shown in Figure 4-11. For $K = 2$, a partial band jammer is assumed with $f_{cl} = f_{cu} = 4$ GHz. The Hanning and Hamming modulated pulses exhibit almost the same performance. When the SIR becomes greater than 3 dB, the Gaussian modulated pulse needs to increase the SIR by around 3 dB to get the same BER compared with Hanning and Hamming. As a result, Hanning modulated pulse is chosen to be used in the remaining scenarios.

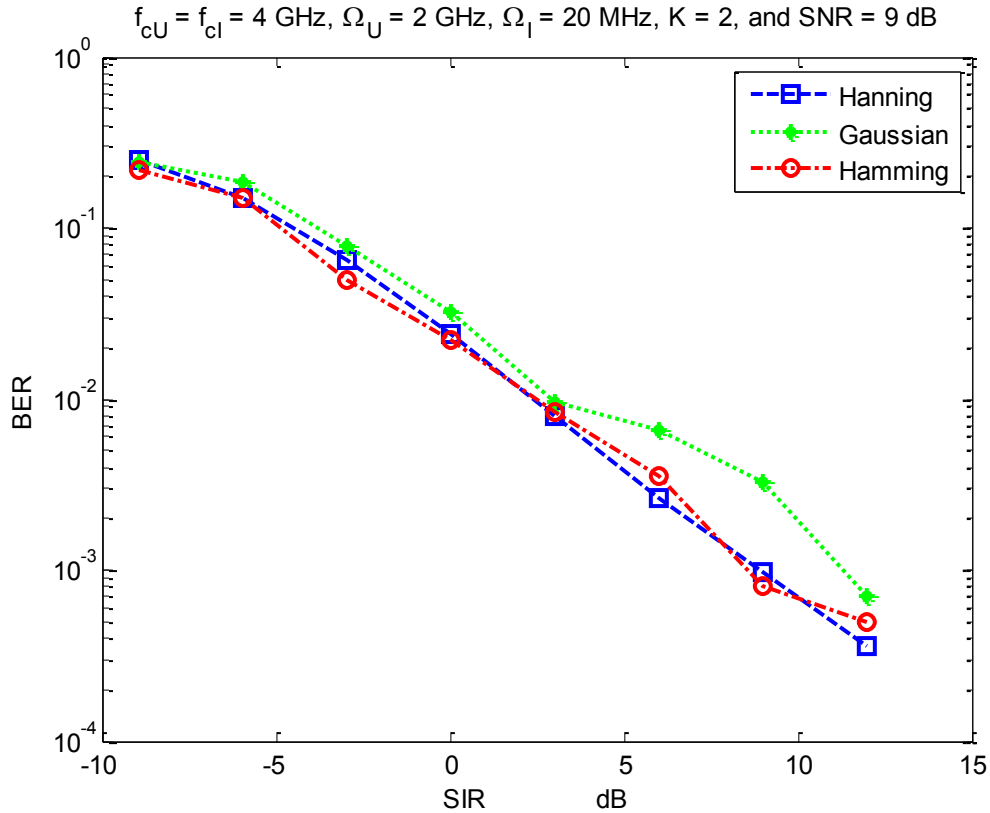


Figure 4-11 Performance for different UWB modulated pulses jammed by a partial band interferer

The interference can take different models according to Section 2.4. When an interferer jams a system, it won't affect the performance being evaluated provided that its center frequency is out of the band of interest. In other words, the received signal at the output of the BPF doesn't contain any NBI. In the NBI free case, the performance should be almost similar to the case when the NBI is located out of the band of interest. Again for the unlicensed NBIs, we assume that we have a partial band jammer and 2 partial bands jammer with two equal bandwidths. For the licensed NBIs, we study them two at a time. For example, WiMAX, IEEE802.11b WLAN are added together and considered as two jammers in the mitigation process.

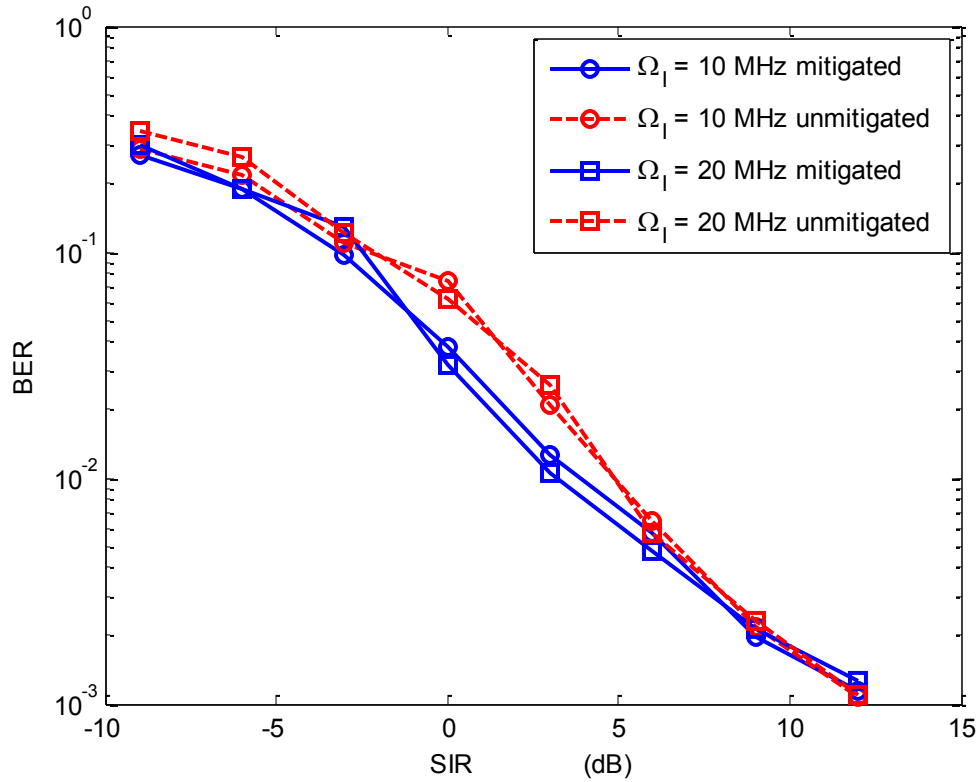


Figure 4-12 Performance of a partial band interferer with different bandwidth

In Figure 4-12 a partial band jammer is assumed to jam the UWB system with $K = 2$. Slight enhancement is achieved by doubling the bandwidth since the power spreads over large bandwidth (20 MHz) compared with the 10 MHz. If we mitigate the NBI, the performance enhances in the range of $-3 < \text{SIR} < 6$ dB. At higher SIR, we don't get any benefit since the NBI's power is very low where we actually drop the desired signal.

Similarly, the same system is evaluated in the presence of 2 partial bands jammer. The center frequencies for the two bands are adjusted at $f_{c11} = 4 \text{ GHz} + 5 \text{ MHz}$, $f_{c12} = 4 \text{ GHz} - 5 \text{ MHz}$, $\Omega_{I1} = \Omega_{I2} = 10 \text{ MHz}$, and for the other case $f_{c11} = 4 \text{ GHz} + 10 \text{ MHz}$, $f_{c12} = 4 \text{ GHz} - 10 \text{ MHz}$ and $\Omega_{I1} = \Omega_{I2} = 20 \text{ MHz}$. In this case,

the enhancement due to the mitigation against the jammers is large and clear as Figure 4-13 illustrates. We do such setting in the center frequencies of the jammers in order to make them equivalent to two different partial bands. Again we emphasize that the 2 partial bands jammer is one signal which contains two bands, leading two low power in the bands. For the considered SIR, the power in the band of a partial band jammer with $\Omega_l = 10$ MHz is greater than that of the 2 partial bands with $\Omega_{l1} = \Omega_{l2} = 10$ MHz. Therefore, the performance improves by increasing the bandwidth i.e. the NBI's effect decreases.

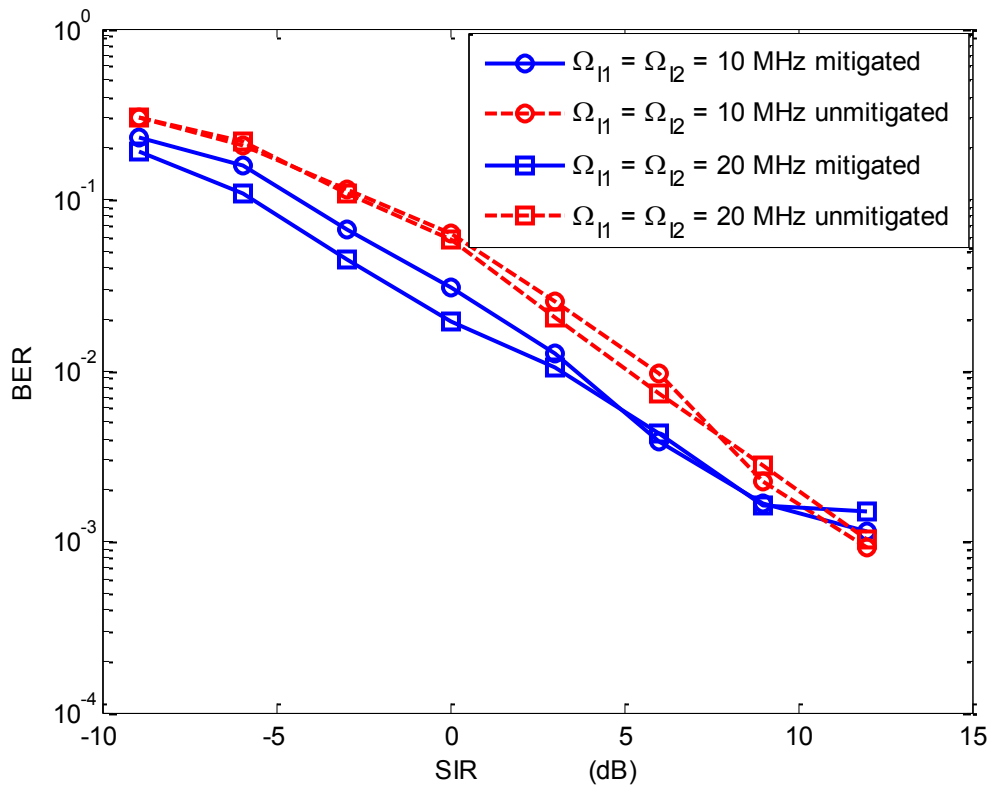


Figure 4-13 Performance of 2 partial bands interferer with different bandwidth

In the coming simulation, we want to see the behavior of the intended system as a function of the jammer's bandwidth. For the two types of the unlicensed interferers the BER is investigated versus the jammer bandwidth for $\Omega_I = \Omega_{I1} = \Omega_{I2}$, SNR = 9 dB, and SIR = -3 dB which implies that the interfering signal is double the UWB signal. As the NBI's power becomes very high, BER should decrease as the bandwidth of the jammer increases since the power spreads over large band.

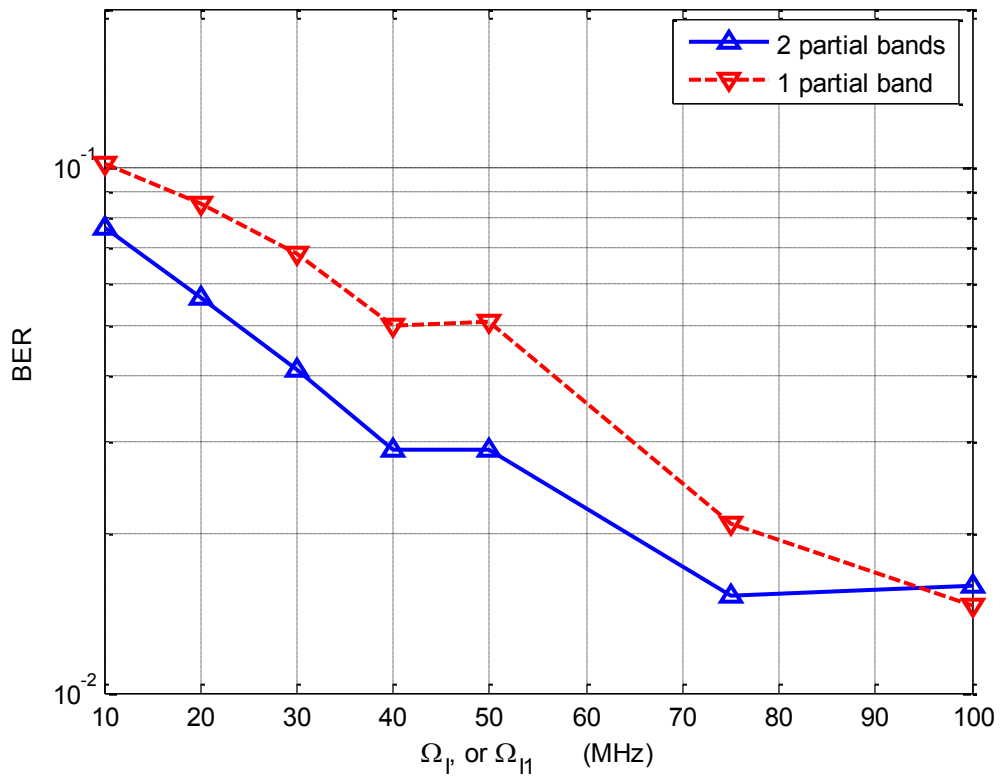


Figure 4-14 BER Performance as a function of the NBI's bandwidth

An UWB system that uses two bit per burst transmission is used ($K = 2$) to send 100,000 symbols. The performance is plotted in Figure 4-14. The dual-band interferer has less effect compared with the single-band case since the power at the effecting bands are so

low compared with that of the partial band NBI. At bandwidth between 75-to-100 MHz, the two cases have the same effect on the system performance.

The effect of the licensed NB services restricts the selected frequency band. For WiMAX the possible range is large, so it can be studied for example at 4 GHz together with IEEE802.11a WLAN (WLANa) operating at 5.2 GHz in order to have two licensed interferers to the intended system. The modulated UWB pulse is designed to have a center frequency at $f_{cU} = 4.5$ GHz and $\Omega_U = 2$ GHz. The two jammers are added together and consider as one signal when we calculate the SIR. Though, they are considered as two NBIs in the mitigation process.

Bluetooth and IEEE802.11b WLAN (WLANb), operating in the ISM band (2.4 GHz), need to change center frequency of the transmitted pulse. Coexistence of WiMAX interferer at 3.5 GHz with Bluetooth or with IEEE802.11b WLAN is also possible. Hence an UWB modulated pulse at $f_{cU} = 3$ GHz be subject to interference from those NB services. Bluetooth and IEEE802.11b WLAN interferers or WiMAX and Bluetooth interferers are two different cases which are evaluated. The UWB system sends the data with $K = 8$ and the SNR = 21 dB.

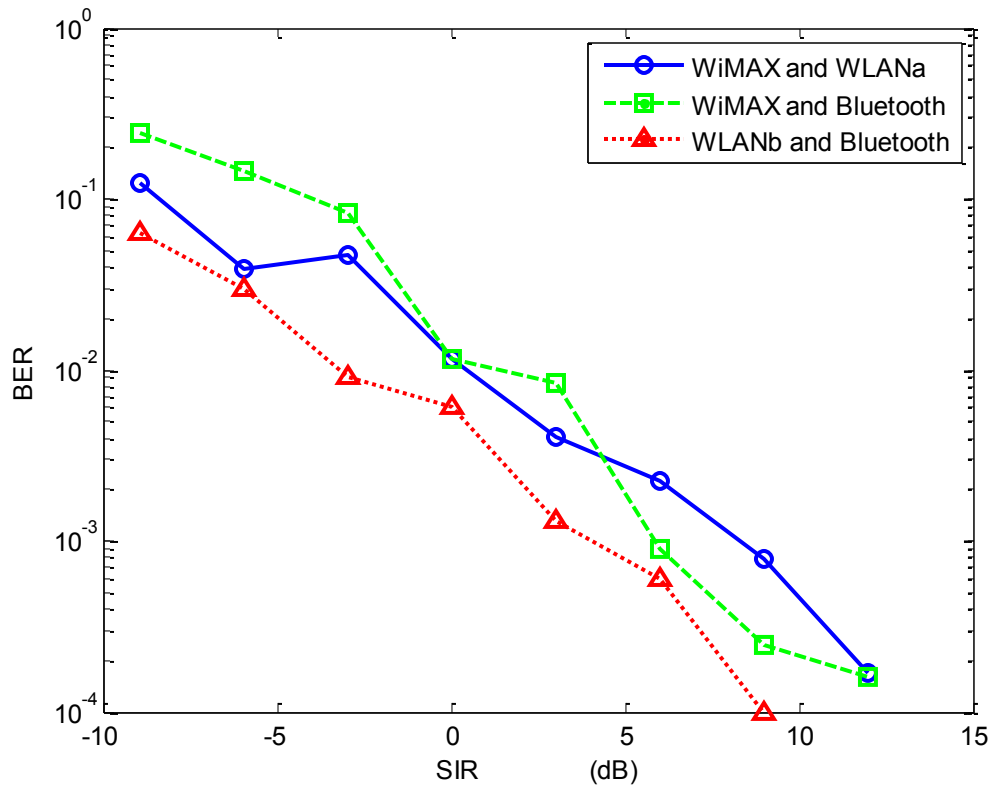


Figure 4-15 BER performance in the presence of licensed NBIs

The bandwidth of the WiMAX signal is set to its maximum ($\Omega_I = 20$ MHz). The maximum bandwidth equals 20 MHz, 1 MHz, 22 MHz for WLANa, Bluetooth, and WLANb, respectively. The performance in WLANb and Bluetooth case outperforms that of WiMAX and Bluetooth as shown in Figure 4-15. There are two main reasons for this; the bandwidth of the WiMAX is smaller than that for the WLANb by 2 MHz and its center frequency is closer to f_{cU} . Hence the affected band in the two cases is so different and consequently the corrupted and the notched measurements are also different. The center frequencies of WLANb and Bluetooth are the same which make them behave as

one NBI, though it is changing for the Bluetooth because of the frequency hopping. We can say that the performance is affected more as the interferer's bandwidth decreases.

The bandwidth of the UWB pulse also has an effect in the notched measurements. For Hanning window with pulse duration around 1 nanosecond the 6-dB bandwidth is $\Omega_U = 2$ GHz, see Figure 4-3. As the pulse duration increases to 2 nanosecond the 6-dB bandwidth decreases to $\Omega_U = 1$ GHz. In other words, the 6-dB bandwidth is $\Omega_U = 2/T_{pulse}$. This parameter is related to the number of corrupted measurements being dropped. Comparing two different bandwidth for the same modulated pulse, the performance is shown in Figure 4-16 for $K = 2$, and 4 bit per burst. Meanwhile this parameters has an effect on the baud rate, the ratio of transmission remains as before i.e.

$$f_{baud} = \frac{f_{Nyquist}}{8} \text{ where } f_{Nyquist} = 2\Omega_U.$$

When Ω_U increases the number of the notched measurements is reduced and we preserve the important information of the transmitted pulse. Therefore, the performance enhances as Figure 4-16 illustrates. When Ω_U decreases we notch out more of the measurements ($D \propto \frac{1}{\Omega_U}$). Consequently the performance degrades. Similar to our previous observation in Figure 4-10, as K increases the performance improves.

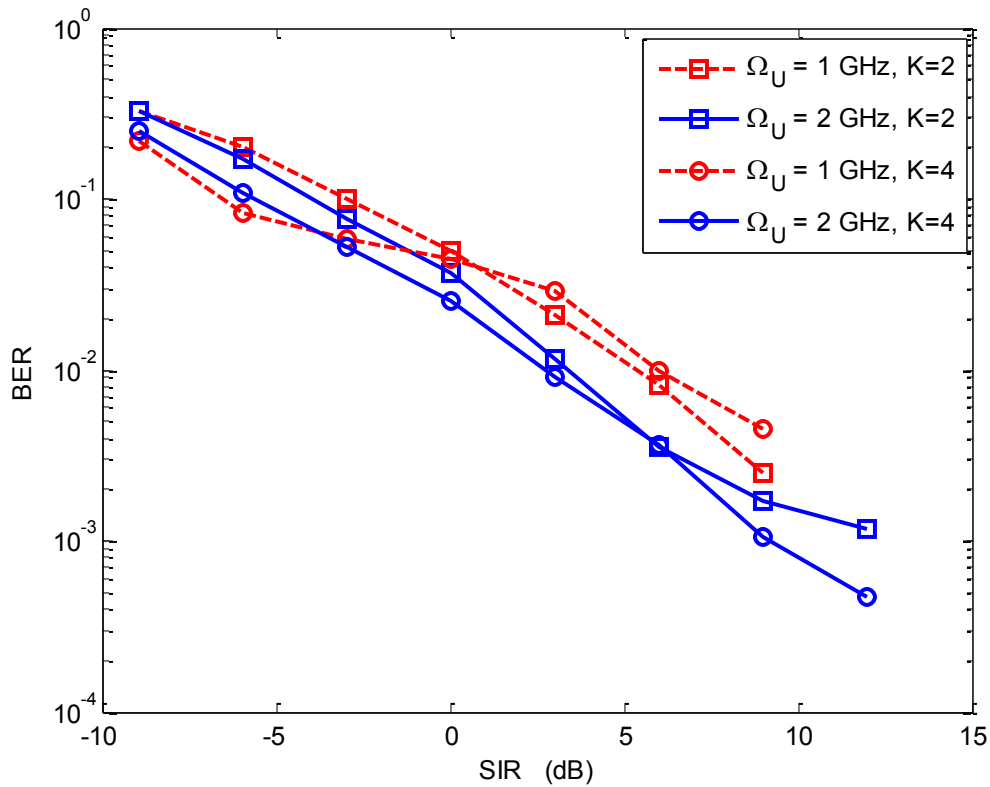


Figure 4-16 BER performance when changing the bandwidth of the UWB modulated pulse

The baud rate is also another important parameter. Here we want to know how much data can be transmitted compared to the Nyquist rate without degrade the system performance.

The system in [Oka09] was studied at baud rate $f_{baud} = \frac{f_{Nyquist}}{8}$, where $f_{Nyquist} = 2\Omega_U$.

Three different baud rates are compared in Figure 4-17 including $f_{baud} = \frac{f_{Nyquist}}{8} = 500$

Gbaud, $\frac{f_{Nyquist}}{4} = 1000$ Gbaud and $\frac{f_{Nyquist}}{2} = 2000$ Gbaud with $K = 2$. A partial band

NBI is present with bandwidth and center frequency of $\Omega_I = 20$ MHz, $f_{cI} = 4$ GHz, respectively.

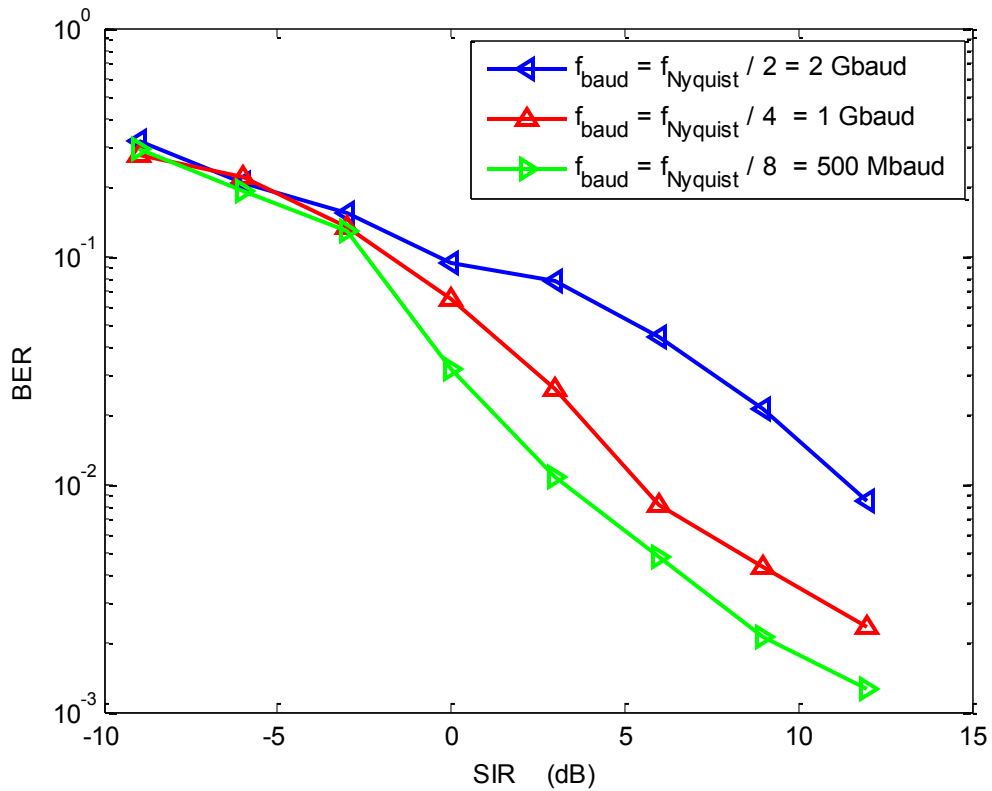


Figure 4-17 BER performance for one partial band interferer with different baud rate

The ISI is proportional to the transmission rate. Consequently, as the baud rate increases more pulses are being overlapped which degrade the system performance.

4.6 Chapter Summary

In this chapter, the mitigation of the NBI in blind UWB systems is evaluated. The speeds of the ADC as well as the NBI effects are reduced through CS. We extended the mitigation technique in [Oka09b] to consider the effect of two licensed or unlicensed NBIs. We've also studied different parameters that may affect the system performance such as the burst size, the type of the modulated window and the baud rate. In addition,

we examine the performance of the system in the presence of different licensed and unlicensed NBIs. The work also goes over the parameters that are related to the mitigation process such as the NBI's bandwidth and the bandwidth of the transmitted pulse.

As we use more bit per burst, the difference between the mitigated and the unmitigated case increases. Though, this difference becomes low as the SIR increases because the NBI becomes so weak. Moreover, sending the information using large burst size outperforms sending it using small burst size since the probability of making an error in one bit decreases as the burst size increases. The simulation shows that the BER is a weak function of the considered modulated widow. Additionally, the performance is highly affected when the NBI's center frequency is shifted to the center frequency of the transmitted pulse.

For a partial band jammer, slight enhancement is achieved by doubling the bandwidth since the power spreads over larger bandwidth. While in the dual-band jammer case, the enhancement due to the mitigation against the jammers is evident. At higher SIR, we don't get more benefit since the NBI's power is very low where we actually drop the desired signal. For the considered scenarios, we've demonstrated that the BER is a strong function of the NBI's bandwidth.

In the simulation, we've also considered different bandwidth of the transmitted pulse, Ω_U . When Ω_U increases the number of the notched measurements is reduced and we preserve the important information of the transmitted pulse. Therefore, the performance enhances.

When Ω_U decreases we notch out many of them. Consequently the performance degrades since the power of the NBI is now concentrated in a relatively larger band.

CHAPTER 5 CONCLUSION AND FUTURE WORK

The thesis mainly focuses on studying the mitigation of NBI in trained and blind UWB systems based on CS. The mitigation technique in the trained system needs to have some knowledge about the NBI signal's subspace, while in blind systems other parameters are more dominant such as the bandwidth of the NBI, the bandwidth of UWB transmitted pulse and the number of measurements (mixer-integrators). In both systems, CS is applied to reduce the speed of the ADC by using M mixer-integrators lower than the required by Shannon theorem. This chapter concludes the work of this thesis and discusses some ideas about the future work.

5.1 Summary of Conclusions

In this work, we've investigated the optimal pilot symbol distribution that optimizes the BER in trained UWB systems. In blind systems, we extend the mitigation process to mitigate the effect of two licensed and unlicensed NBIs. The main parts of the thesis are concluded in the following:

It was shown in Chapter 1 that due to the large bandwidth of the UWB signals, they require a very high speed ADC and they may interfere with other narrowband systems. Hence, an UWB receiver should handle those two problems in an efficient way. Chapter 2 provided the technical background needed for the work. The chapter gave brief explanations about the characteristics of the channel model and the MP algorithm.

Chapter 3 investigated the problem of NBI mitigation in UWB systems based on CS. Since narrowband signals have sparse representation in the DCT domain, they can be estimated using CS. The mitigation technique needs to have knowledge about the NBI signal's subspace. We estimated the sparse components of the interferer using MP and then we used our knowledge to suppress the most significant coefficients. This was achieved by adjusting the value of the interference threshold, μ . We have established that, this value shouldn't be very large in order to have a good NBI's subspace estimation and shouldn't be very low to avoid excessive noise level.

Moreover, we've evaluated pilot symbols distribution that optimizes the BER. We conclude that there is a minimum required number of symbols in the first group N_{p1} after which the performance saturates. Communications can be achieved with $N_{p2} = 0$, however, the performance can be enhanced if the UWB signal structure is employed in the construction of the projection matrix. The number of pilot symbols in the third group N_{p3} is directly proportional to the performance; hence more symbols should be assigned to get information about the channel.

In the presence of strong and different licensed and unlicensed NBIs, we conclude that, the location of the NBI relative to the center frequency of the transmitted pulse determines the amount of the degradation in the system performance. Additionally, we've evaluated the system in the presence of multiuser interference. As expected, simulations show that when more users being active the system performance degrades.

Chapter 4 considered the mitigation of narrowband interference in blind systems. The mitigation process needs to locate the center frequency of the NBI. Then a digital notch filter is employed to drop out the affected measurements around the estimated interferer based on some parameters such as the bandwidth of the NBI, the bandwidth of UWB transmitted pulse and the number of measurements (mixer-integrators). The main parameter in hand is the bandwidth of the NBI. Hence, it should be available at the intended receiver.

The performance is highly affected by the NBI's center frequency relative to the center frequency of the transmitted pulse. We've demonstrated that the BER is a strong function of the NBI's bandwidth. The performance enhances as the NBI's bandwidth increases since the power spreads over large bandwidth. As the UWB signal's bandwidth increases the number of the notched measurements reduces and we preserve the important information of the transmitted pulse. Moreover, simulation shows that the BER is a weak function of the considered modulated windows.

To sum up, the mitigation process in the blind and trained systems is totally different since it depends on various parameters. The inverse DCT transformation matrix of interferer should be known; in this case the trained system is used. On the other hand, the blind system can be effectively used, if the NBI's bandwidth is known.

5.2 Future Work

The work in this thesis considered NBI mitigation in UWB systems based on CS. There are still several open problems whose solution could add a great benefit in the field of interest. We may summarize them in the following points:

- Extend the trained CS based UWB system to perform Multiuser Detection (MUD). Therefore, we have to mitigate both the NBI and the multiuser interference. Before NBI mitigation, the receiver should jointly decode all users first. Then it subtracts the decoded information from the received noisy signal.
- In Multiuser systems the dictionary must be redesigned to nullify the other users. A novel technique is needed. This could be achieved by using different waveforms for the different users. Future work may need to compare and study different signaling schemes that can be used for multiuser techniques.
- This multiuser study quantifies the amount of degradation due to the presence of other users. It also serves as a motive for future study where the entire compressive sensing algorithm is redesigned to possibly reject other users. The challenge is in the similarity between the intended dictionary and the one to be nullified.
- Propose a receiver that changes the interference threshold, γ , adaptively in order to enhance the BER. The same receiver may adaptively select the best pilot symbols distribution that optimizes the system performance.

- In our research we assume a perfect NBI channel model. Future studies may consider the effect of different NBI channel models and how the mitigation process will be accomplished.
- Evaluate the blind UWB system for multiuser signal detection.
- Since the receiver has to know the NBI's bandwidth, the receiver needs to develop a way to approximate it. An algorithm used to estimate the number of the active NBIs is another concern. Putting a threshold and handle the NBI as a random signal can be used to detect weather the NBI is active or not.

APPENDIX

Table I-1 Abbreviations

Abbreviation	Stand for
AcR	Auto-Correlation Receiver
ADC	Analog-to-Digital Converter
AWGN	Additive White Gaussian Noise
BER	Bit Error Rate
BP	Basis Pursuit
BPDN	Basis Pursuit Denoising
BPF	Band-Pass Filter
CCK	Complementary Code Keying
CM1-9	Channel Model 1-9
CS	Compressive Sensing
DCT	Discrete Cosine Transform
DFT	Discrete Fourier Transform
DS	Direct Sequence
DSP	Digital Signal Processing
DSSS	Direct Sequence Spread Spectrum
DS-TH	Direct Sequence spread spectrum coding and Time-Hopping
EIRP	Effective Isotropic Radiated Power
FCC	Federal Communication Committee

FHSS	Frequency Hopping Spread Spectrum
GFSK	Gaussian frequency shift keying
GLRT	Generalized Likelihood Ratio Test
i.i.d.	Independent and Identically Distributed
IR	Impulse Radio
ISI	Inter-Symbol Interference
ISM	Industrial, Scientific, and Medical band
MB-OFDM	Multi-Band Orthogonal Frequency Division Multiplexing
MIMO	Multiple-Input-Multiple-Output
MLSE	Maximum Likelihood Sequence Estimation
MP	Matching Pursuit
NBI	NarrowBand Interference
OMP	Orthogonal Matching Pursuit
PCS	Personal Communications Service
PSD	Power Spectral Density
QP	Quadratic Program
SD	Selection Diversity
SIMO	Single-Input-Multiple-Output
SIR	Signal-to-Interference Ratio
SISO	Single-Input-Single-Output
SVD	Singular Value Decomposition
TOA	Time Of Arrival

TR	Transmitted-Reference
UWB	Ultra Wide-Band

Table I-2 List of Variables

Variable	Indication
α'	Factor to control Tukey window
α_l	Attenuation of the l^{th} path
a_n	PN DS code
B	Bandwidth of BPF
B_f	Fractional bandwidth
B^k	Payload data
β	Safety factor to account for leakage into adjacent measurements
BW	Bandwidth
$c_I(t)$	NBI channel
$c_U(t)$	UWB channel
c_n	PN TH code
\mathbf{C}	DCT transformation matrix
\mathbf{C}_v	NBI subspace
χ	Set that contain all the possible transmitted signals
d_I	The distance from interferer to receiver UWB
$d_I^{-\rho}$	Path-loss due to the transmission over distance d_I
d_U	The distance from transmitter to receiver UWB
$d_U^{-\rho}$	Path-loss due to the transmission over distance d_U
$D + 1$	The notched measurements

Δ	Frequency band that separates any two successive test functions
E	Energy of the transmitted signal
f_{baud}	Baud clock
f_{burst}	Burst rate
f_c	Center frequency of BPF
f_{cl}	Center frequency of NBI signal
f_{cU}	Center frequency of UWB signal
f_H	The upper band in the frequency spectrum at -10 dB points
f_I	Frequency of a single tone jammer
f_L	The lower band in the frequency spectrum at -10 dB points
f_s	Sampling frequency
\mathbf{G}	An i.i.d. Random matrix of dimension $M \times N$
\mathcal{G}	Convolutional matrix (Toeplitz form) of $g(t)$
$g(t)$	BPF pulse
Γ	Maximum possible TOA uncertainty in samples
γ	Maximum possible TOA in second
H_u	UWB signal subspace
$h(t)$	Channel impulse response
\mathcal{H}	Convolutional matrix (Toeplitz Form) Of $h[n]$
$i(t)$	BPF response to narrowband interference signal
\mathbf{i}	Sampled waveform of $I(t)$

K	Number of bits per burst
L	Number of propagation paths
Λ^k	Position Of The k^{th} Nonzero Sample
Λ_h	Length of channel impulse response in samples
Λ_X	Length of discretized payload in samples
λ_h	The length of total channel impulse response in second
M	Number of mixers or test functions
\mathcal{U}	Large number
\hat{m}	The index of the maximum measurement value
μ	Interference threshold
N	Number of samples in each burst
N_0	Two sided noise PSD
N_{baud}	Number of samples between two consecutive bits
N_c	Number of chips
N_d	Total burst symbols
N_f	Number of frames
N_p	Total pilot symbols
N_{p1}	First pilot group symbols
N_{p2}	Second pilot group symbols
N_{p3}	Third pilot group symbols
N_s	Data modulated symbols

N_v	Number of interferers
n_I	Number of interferers
Ω	Bandwidth of BPF
Ω_I	NBI bandwidth
Ω_U	Bandwidth of UWB signal
$p(t)$	Gaussian pulse
\mathbf{P}_v^\perp	The projection matrix of the estimated null space of NBI
Φ_1	1 st measurement matrix with i. I. D. Bernoulli distribution
Φ_2	2 nd measurement matrix $\Phi_2 = \Phi_1 \mathbf{P}_v^\perp$
Φ_3	3 rd $M \times N$ measurement matrix $\Phi_3 = \mathbf{G}(\tilde{\mathbf{H}}_u^T \tilde{\mathbf{H}}_u)^{-1} \tilde{\mathbf{H}}_u^T$
Φ_i	The i^{th} Measurement matrix
$\phi_I(t)$	NBI pulse
$\phi_U(t)$	UWB pulse
$r(t)$	The received signal
\mathbf{r}	Received sampled waveform
ρ	Path-loss exponent
$s(t)$	Transmitted signal
$S_v(f)$	PSD of a jammer
Ψ_u	Sampled version of a specific dictionary
$\psi_m(t)$	The m^{th} Test Functions
T_{baud}	Baud interval

T_c	Chip duration
T_d	Actual TOA uncertainty in second
T_f	Frame duration
T_g	Pulse duration
T_{med}	Maximum excess delay time
T_{prj}	Integration period of the integrator
T_s	Sampling time
τ_l	Delay of the l^{th} Path
Y	Actual TOA uncertainty in samples
$\mathbf{V} = \Phi\Psi$	Combined dictionary
$\mathbf{v}[n]$	The digitized NBI within the measurement interval of the n^{th} Frame of length $N \times 1$
$V(t)$	Thermal noise
$v(t)$	Narrowband interference signal
$w(t)$	BPF response to thermal noise signal
$w[n]$	Tukey window
$\mathbf{w}[n]$	The digitized noise within the measurement interval of the n^{th} frame of length $N \times 1$
\mathbf{w}	Sampled waveform of $W(t)$
\mathbf{x}	Virtual discrete time representation of the payload
$y_1[n]$	The 1 st compressive measurement

$y_2[n]$	The 2 nd compressive measurement
$y_3[n]$	The 3 rd compressive measurement
$y_{a j}[n]$	The compressive measurement for data modulated symbols
y	Measurement vector
\bar{y}_2	Averaging $y_2[n]$ to reduce the noise
$y_{notched}$	The notched measurement vector
y_m	The m^{th} Measurement value
$\zeta[n]$	The DCT representation of $\mathbf{v}[n]$
$\xi[n]$	Candidate vector

REFERENCES

- [Ale07] Y. D. Alemseged and K. Witrisal, "Two Stage Narrowband Interference Mitigation for Transmitted Reference UWB Systems," in *IEEE International Symposium on Personal, Indoor and Mobile Radio Communications, PIMRC*, Athens, Greek, Sept. 2007.
- [Ale09] Y. D. Alemseged, H. Harada, and K. Witrisal, "Detection and Identification of NBI for Multichannel UWB Autocorrelation Receivers," in *IEEE Wireless Communications and Networking*, May, 2009.
- [Bel03] J. Bellorado, S. S. Ghassemzadeh, L. J. Greenstein, T. Sveinsson, V. Tarokh, "Coexistence of ultra-wideband systems with IEEE-802.11 a wireless LANs," *Proc. IEEE Global Telec. Conf. (GLOBECOM '03)*, Vol. 1, pp. 410–414, 1-5 Dec. 2003.
- [Boy04] S. Boyd and L. Vandenberghe. *Convex Optimization*. Cambridge University Press, 2004.
- [Can06] E. J. Candes, "Compressed Sampling," European Mathematical Society, 2006.
- [Che09] Si Chen; Bang-ning Zhang; Daoshen Guo; Qin-yu Zhang, "Jammer cancellation in time-hopping impulse radio using independent component analysis," in *International Conference on Wireless Communications & Signal Processing, WCSP*, Vol., no., pp.1-4, 13-15 Nov. 2009.

- [Dan06] Q. Dang and A. van der Veen, "Narrowband Interference Mitigation for a Transmit-Reference Ultra-Wideband Receiver," in *14th European Signal Processing Conference*, 2006.
- [Dow04] F. Dowla F. Nekoogar , and A.Spiridon, "Interference Mitigation in Transmitted-Reference Ultra-Wideband Receivers," in *IEEE Antennas and Propagation Society*, Vol.4,pp.1307-1310, Jun., 2004.
- [Gom10] A. Gomaa and N. Al-Dhahir, "A Compressive Sensing Approach to NBI Cancellation in Mobile OFDM Systems," in *IEEE Communications Society*, Dec., 2010.
- [Gom11] A. Gomaa and N. Al-Dhahir, "A Sparsity-Aware Approach for NBI Estimation in MIMO-OFDM," in *IEEE Transactions on Wireless Communications*, Vol. 10, No. 6, pp. 1854 - 1862 Jun.,2011.
- [Ibr07] J. Ibrahim, R. M. Buehrer, "NBI Mitigation for UWB Systems Using Multiple Antenna Selection Diversity," in *IEEE Transactions on Vehicular Technology*, Vol. 56, No. 4, pp. 2363-2374, July 2007.
- [Jin11] B. Jin, S. Zhang, J. Pan, and K. Lin, "Serial compressed sensing communication system for UWB impulse radio in bursty applications," *Electronics Letters*, Vol.47, no.6, pp.412-414, March 17 2011.

- [Jin12] B. Jin, S. Zhang, J. Pan, and K. Lin, "Sub-Nyquist sampling based narrowband interference mitigation in UWB impulse radio," *Electronics Letters*, Vol.48, no.15, pp.963-964, July 19 2012.
- [Lan01] I. Lensford, A. Stephens, and U. Nevo, "Wi-Fi (802.11b) and Bluetooth: Enabling Coexistence?" in *IEEE Network Magazine*, Vol. 15, pp. 20-27, Sep/Oct. 2001.
- [Li09] X. Li and K. Kwak, "NBI Suppression UWB System Based on Novel Nonlinear Chirp Pulses," in *IEEE Communications and Information Technology*, pp. 1167 - 1170 Sept., 2009.
- [Mol06] A. F. Molisch, K. Balakrishnan, C. Chong, S. Emami, A. Fort, J. Karedal, J. Kunisch, H. Schantz, U. Schuster, and K. Siwiak, "Ieee 802.15.4a channel model - final report," Tech. Rep., IEEE 802.15 TG4a, 2006.
- [Nik09] H. Nikookar and R. Prasad, *Introduction to Ultra Wideband for Wireless Communications*, Springer, 2009.
- [Oka09a] A. Oka and L. Lampe, "A Compressed Sensing Receiver for Bursty Communication with UWB Impulse Radio," in *Intl. Conf. on Ultra-Wideband*, pp. 279 – 284, Sept. 2009.
- [Oka09b] A. Oka and L. Lampe, "Compressed Sensing Reception of Bursty UWB Impulse Radio is Robust to Narrow-Band Interference," in *IEEE Global Telecommunications*, Dec., 2009.

- [Oka09c] A. Oka and L. Lampe, “Compressed Sensing Reception of Bursty UWB Impulse Radio is Robust to Narrowband Interference,” in *IEEE GLOBECOM*, Nov.-Dec. 2009.
- [Ovt09] M. Ovtcharov, V. Poulkov, G. Iliev and Z. Nikolova, “Narrowband interference suppression for IEEE UWB channels,” *The Fourth Intern. Conf. on Digital Telecommunications (ICDT 2009)*, pp. 43–47, Colmar, France, July 20-25, 2009.
- [Poo97] H. V. Poor and X. Wang, “Code-aided Interference Suppression for DS/CDMA Communications—Part I: Interference Suppression Capability,” in *IEEE Trans. Commun.*, Vol. 45, No. 9, pp. 1101–1111, Sep.1997.
- [Sal87] A. Saleh and R. A. Valenzuela, “A statistical model for indoor multipath propagation,” in *IEEE J. Selected Areas Comm.*, Vol. 5, pp. 138–137, Feb. 1987.
- [Sti06] T. H. Stitz, T. Ihalainen, M. Renfors, ”Mitigation of Narrowband Interference in Filter Bank Based Multicarrier Systems,” in *IEEE Communications Society*, Vol.7, pp. 3241 – 3246, 2006.
- [Syd02] L. Sydanheimo, M. Keskilammi and M. Kivikoski, “Performance Issues on the Wireless 2.4 GHz ISM Band in a Multisystem Environment”, in *IEEE Trans. Consumer Electronics*, Vol. 48, No. 3, pp. 638-643, Aug. 2002.

- [Wan06] Y. Wang, X. Dong, and I.J. Fair, "A method for spectrum shaping and NBI suppression in UWB communications," *Proc. in IEEE Int. Conf. Commun. (ICC'06)*, Istanbul, Turkey, June 2006.
- [Wan07a] Z. Wang, G. R. Arce, J. L. Paredes, and B. M. Sadler, "Compressed Detection for Ultra-Wideband Impulse Radio," in *Proc. 8th IEEE Intl. Workshop SPAWC*, Jun. 2007.
- [Wan07b] Z. Wang, G. R. Arce, B. M. Sadler, J. L. Paredes, and X. Ma, "Compressed Detection for Pilot Assisted Ultra-Wideband Impulse Radio," in *Proc. IEEE Int. Conf. on Ultra-Wideband*, Singapore, Sep. 2007.
- [Wan07] Y. Wang, X. Dong, I. J. Fair, "Spectrum Shaping and NBI Suppression in UWB Communications," in *IEEE transactions on wireless communications*, Vol. 6, issue 5, pp. 1944-1952, May 2007.
- [Wan08] Z. Wang, G. R. Arce, B. M. Sadler, J. L. Paredes, S. Hoyos, and Z. Yu, "Compressed UWB Signal Detection with Narrowband Interference Mitigation," in *IEEE Int. Conf. on UWB*, Vol. 2 pp.157–160, Sep.,2008.
- [Wan10a] C. Wang, M. Ma, R. Ying, and Y. Yang," Narrowband Interference Mitigation in DS-UWB Systems," in *IEEE Signal Processing*, Vol. 17 pp. 429-432, 2010.
- [Wan10b] C. Wang, R. Ying, Y. Wei, and Y. Yang, ," Spreading Sequence Selection Scheme For NBI Suppression in DS-UWB System," in *IEEE Ultra wideband and Ultra short Impulse Signals*, pp. 186-188, Sep., 2010.

- [Wit05] K. Witrisal and Y. D. Alemseged, "Narrowband interference mitigation for Differential UWB systems," in *IEEE Asilomar Conference on Signals, Systems, and Computers*, Monterey, CA, Nov. 2005.
- [Zha06] G. Zhao, M. Jin, W. Fan, "A Low-complexity NBI Suppression Algorithm in UWB Systems," in *IEEE Communication Technology*, Nov., 2006.
- [Zha09] P. Zhang, Z. Hu, R. Qiu, and B. Sadler, "A compressed Sensing Based Ultra-Wideband Communication System," in *Proc. IEEE International Conference on Communications ICC*, pp. 1–5, 2009.
- [Zha10] P. Zhang and R. C. Qiu, "Wireless Tomography, Part III: Compressed Sensing for Ultra-Wideband Signals," in *IEEE Waveform Diversity and Design*, pp. 35 – 39, Aug. 2010.
- [Zha11] G. Zhang, Y. Dai, X. Zhang, Y. Lv and L. Chen, "Design and Implementation of UWB Pulse with Multiple Narrow-Band Interferences Mitigation," in *IEEE Consumer Electronics, Communications and Networks*, pp. 1154 – 1157, April 2011.

VITAE

Name ::Saleh Ahmed Yaslam Alawsh |

Nationality ::Yemeni |

Date of Birth ::4/1/1981|

Email ::alawsh21@gmail.com|

Address ::KFUPM main Campus Bld. 834 Room 211|

Academic Background ::Received Bachelor's Degree in Electronics and Communication Engineering (No.1) from Hadramout University of Science and Technology, Mukalla, Yemen in 2007. Completed Master's degree requirements at in Telecommunication at the Electrical Engineering Department in King Fahd University of Petroleum and Minerals, Dhahran, Saudi Arabia in April, 2013.|